NASA CR-165,869

NASA-CR-165869
19820015078

NASA CONTRACTOR REPORT 165869

Analytical Prediction of the Interior Noise for Cylindrical Models of Aircraft Fuselages for Prescribed Exterior Noise Fields

PHASE II: MODELS FOR SIDEWALL TRIM, STIFFENED STRUCTURES, AND CABIN ACOUSTICS WITH FLOOR PARTITION

L. D. POPE
E. G. WILBY

BOLT BERANEK AND NEWMAN INC.
CANOGA PARK, CA. 91303

CONTRACT NAS1-15782
APRIL 1982

LIBRARY COPY

APR 27 1982

LANGLEY RESEARCH CENTER
LIBRARY, NASA
HAMPTON, VIRGINIA

NASA
National Aeronautics and
Space Administration

Langley Research Center
Hampton Virginia 23665

NF01348

NASA CONTRACTOR REPORT 165869

ANALYTICAL PREDICTION OF THE INTERIOR NOISE FOR CYLINDRICAL MODELS OF AIRCRAFT FUSELAGES FOR PRESCRIBED EXTERIOR NOISE FIELDS

Phase II: Models for Sidewall Trim, Stiffened Structures, and Cabin Acoustics With Floor Partition

L.D. Pope

E. G. Wilby

Bolt Beranek and Newman Inc.
21120 Vanowen Street
Canoga Park, CA 91303

Contract NAS1-15782
April 1982

N82-21952#

TABLE OF CONTENTS

		Page
1.0	SUMMARY	1
2.0	INTRODUCTION	3
2.1	Analytical Model	4
2.2	Report Organization	4
2.3	Program Management	5
3.0	ANALYTICAL MODEL	6
3.1	Trim Dynamics	6
	Power Radiated into Cabin	21
	A Preliminary Comparison	30
	Band-Limited Power Absorbed on Cabin Wall (with trim)	34
	Noise Reduction Calculation	42
	High Frequencies	43
3.2	Influence of Internal Radiation Damping	47
3.3	Transmission of a Tone	52
3.4	Modal Properties of the Cabin Space (Cylinder with Floor)	55
	Finite Difference in Two Dimensions	56
	Boundary Conditions	58
	Details of Calculation	60
	Normalization	68
3.5	Fuselage Structural Model	69
	Model for a Curved Orthotropic Panel	71
3.6	Calculation of the Structure/Acoustic Coupling Term f'(n,r) (Cylinder with Floor)	73
3.7	Calculation of the Acoustic Loss Factor	75
3.8	Noise Reduction in the Volume Stiffness Controlled Region	77
3.9	End Cap Transmission	99
3.10	Status of the Interior Noise Program (Phase II)	102

TABLE OF CONTENTS (continued)

Page

4.0 EXPERIMENTS 103
4.1 NASA Tests 103
Description of Models 104
Instrumentation and Apparatus 105
Test Procedure 106
Application of Trim 108
4.2 BBN Test 109
4.3 Noise Reduction Data Analysis 109
5.0 RESULTS AND COMPARISONS 111
5.1 Cavity Modes (Cabin with Floor) 111
5.2 Noise Reduction Measurements, Predictions, and Comparisons 113
Noise Reduction Measurements 114
5.2.1 Predictions for the Bare 0.020 in. Ring-Stringer Stiffened Cylinder . 114
Structural Model 115
Noise Reduction Prediction 117
Discussion of Results 121
5.2.2 Predictions for the 0.063 in. Unstiffened Cylinder with Floor and Insulation 122
Discussion of Results 128
5.2.3 Predictions for the 0.020 in. Ring-Stringer Stiffened Cylinder with Floor and Trim 129
Acoustic Loss Factors and Trim Transfer Coefficients 129
Structural Loss Factors 130
Influence of Stringer Exposure 130
Discussion of Results 136

TABLE OF CONTENTS (continued)

Page

5.3 Statistical Analysis of Prediction Error 137

REFERENCES 141

APPENDICES:

A: Transfer Matrix for Trim Insulation 143

B: Photographs of Test Articles 148

C: Finite Difference Results -- Acoustic Modal Patterns and Resonance Frequencies, $\theta_o = 49°$, a = 1m, q = 0. 153

FIGURES

LIST OF FIGURES

Figure No.

1. Trim Model - Insulation and Lining
2. Typical Wide Body Trim Installation
3. Acoustical Parameters for Owens-Corning Fiberglas Type PF105. Fiber Diameter is 1 Micron and Bulk Density is 9.6 kg/m^3 (0.6 lb/ft^3) [4]
4. Comparison of Trim Transfer Coefficient Prediction with Measurement
5. Fuselage Model - Cylinder with Floor Partition
6. Finite Difference Grid Nomenclature
7. Grid Coordinate Specification
8. Fuselage Structural Models
9. Cylinder Subpanel Dimensions (Skin Only)
10. Cylinder Imperfection Model
11. Ratio of the Integral Θ_1 to Interval θ_1, versus $\bar{e}$
12. Approximate Criteria for Relief of Membrane Stresses
13. Status of Cylinder Noise Reduction Program (Phase II)
14. Unstiffened Cylinder - Model Details and Microphone Locations (Dimensions in centimeters)
15. Stiffened Cylinder (Dimensions in cm.)
16. Cross Section of Stiffened Cylinder with Floor and Trim Installed (Dimensions in cm.)
17. Noise Reduction Test Instrumentation
18. Arrangement of Apparatus (Dimensions in cm.)
19. Modal Pattern for the (0,0,2) Mode
20. Modal Pattern for a 15° Floor
21. Modal Pattern for a 30° Floor
22. Details of the 30° Floor Measurement
23. Finite Difference Calculation (40° Floor)
24. Equal Volume Sampling Scheme
25. Measured Noise Reduction of the Bare 0.020 in. Ring-Stringer Stiffened Cylinder

LIST OF FIGURES (continued)

Figure No.

26. Measured Noise Reduction of the 0.063 in. Unstiffened Cylinder with Floor and Insulation
27. Measured Noise Reduction of the 0.020 in. Ring-Stringer Stiffened Cylinder with Floor and Trim
28. Structural Loss Factors of the Stiffened Cylinder Without Floor
29. Acoustic Loss Factors of the Stiffened Cylinder Without Floor
30. Modes of the Stiffened Cylinder Computed with the Mikulas and McElman Equation
31. Response of the Cylinder Skin to Broad Band Shaker Input
32. Comparison of Predicted and Measured Noise Reductions, 0.020 in. Stiffened Cylinder Without Floor or Trim
33. Structural Loss Factors of the Unstiffened Cylinder with Floor and Insulation
34. Acoustic Loss Factors of the Unstiffened Cylinder with Floor and Insulation
35. Trim Transfer Coefficient for the Unstiffened Cylinder with Floor and Insulation
36. Comparison of Predicted and Measured Noise Reductions, 0.063 in. Unstiffened Cylinder with Floor and Insulation
37. Acoustic Loss Factors of the Stiffened Cylinder with Floor and Trim
38. Transfer Coefficient for the Stiffened Cylinder with Floor and Trim
39. Structural Loss Factors for the Stiffened Cylinder with Floor and Trim
40. Comparison of Predicted and Measured Noise Reductions, 0.020 in. Stiffened Cylinder with Floor and Trim (Stringers Exposed)

LIST OF TABLES

Table No.		Page
1.	Modal Pairs Having Highest Contributions to Interior Level	118
2.	Modal Pairs Having Highest Contributions to Interior Level	125
3.	Modal Pairs Having Highest Contributions to Interior Level	132
4.	Effect of Stringer Exposure	136
5.	Predicted versus Measured Noise Reductions	138

1.0 SUMMARY

As a part of the NASA Langley Research Center program to identify the important parameters governing sound transmission into airplane interiors, and to determine noise control methods, an aircraft interior noise prediction model is being developed by Bolt Beranek and Newman Inc. (BBN) of Los Angeles. The work includes analytical modeling and integration of information and technologies needed to understand sound transmission through a fuselage wall into an aircraft cabin. A three phase program has been defined for accomplishing the goal.

In the first phase (now concluded), the basic analytical modeling of the transmission problem (interaction of the structure with the exterior and interior acoustic fields) was undertaken and preliminary validation studies were conducted using an unpressurized, unstiffened cylinder as a test article. Results of that work were presented in Reference [1].

The second phase of work, reported in this document, includes the development of the general aircraft interior noise model and the laying out of the basic master computer program. Validation studies are considered using more advanced test articles (one being a stiffened cylinder with a floor partition and interior trim, i.e., insulation and lining).

The third phase, now underway, involves completion of the analytical models (including propeller excitation) and software development with application to an actual (or simulated) aircraft fuselage, along with validation tests, comparisons, refinements, and documentation of the finalized model and software.

As stated, this report presents the results of the Phase II studies. The theoretical developments of Phase I that describe the interaction of the structure and the interior acoustic field

are generalized to include the effects of sidewall insulation and lining (trim). The new analysis leads to a transmission coefficient that multiplies the previously derived expression for the power inflow to the cavity for the case where the trim is absent and an additive term giving an increase in the damping of the sidewall structure by the trim. Also a more precise calculation of the power flow from a structural mode closely coupled (in frequency) to an acoustic mode is developed to account for the influence of the radiation damping of the structural mode by the highly receptive acoustic mode.

A major addition is the generalization of the geometry of the acoustic space to include a floor (partition). The complex cross-section's modal properties are computed using a finite difference approach. Appropriate normalizations and use of the data for calculating the acoustic/structural coupling terms and the cavity loss factors (using predicted wall admittances) are also detailed.

Comparisons of noise reduction predictions with measurements are presented for three test articles:

1) a ring-stringer stiffened cylinder without floor or trim; wall thickness of 0.000508m (0.020 inches).

2) a 0.0016m (0.064 in.) thick unstiffened cylinder (the Phase I test article) modified with a floor partition and lined with a 0.0127m (0.50 in.) thick layer of PF-105 fiberglass that is covered with a 0.0000508m (0.002 in.) vinyl film.

3) a 0.000508m (0.020 in.) ring-stringer stiffened cylinder (same as (1) above) with floor partition lined with a simulated trim consisting of a 0.0127m (0.50 in.) thick

layer of PF-105 fiberglass covered with a 0.00119m (0.047 in.) thick layer of lead vinyl weighing 2.44 kg/m^2 (0.50 lb/ft^2), with a 0.0127m (0.50 in.) layer of PF-105 fiberglass on the inside of each end cap and exposed directly to the interior.

To our knowledge no attempt has ever previously been made to compute noise reductions for configurations as complex as cases (2) and (3) above.

2.0 INTRODUCTION

The present study has the specific goal of developing an analytical model that can be used to predict the sound levels in a ring-stringer stiffened cylinder that has a partition simulating a cabin floor and insulation and lining on the inside of the cylinder wall simulating a basic cabin sidewall trim. Theoretical developments for harmonic (tonal) excitation and for excitation by a reverberant acoustic field are given. Predictions of the noise reduction for three different test articles are compared to measurements for purposes of model validation. No calculations are presented for tonal excitation in this report (some have already been given in [1]). Tone prediction capability is to be brought to a practical level in Phase III, when the propeller induced exterior pressure field description is to be incorporated into the model and the modal forcing functions derived.

2.1 Analytical Model

In Reference 1, a basic discussion of the power flow technique adopted for this project is given. To a large extent, the concepts used for the predictions of concern here have been developed in References [2] and [3]. However, in the Phase I report, results from [2] and [3] were specialized to include the case of harmonic (tonal) excitation. In this report, the concepts previously developed in [1], [2] and [3] are extended, mainly by including the trim dynamics. Also, although including such information does not represent an advance in the concepts of Phase I, much more complex structural and acoustic properties are considered. Most notable is the use of finite-difference modal data for the cavity. Also the structural (modal) properties of the orthotropic cylinder (one stiffened by rings and stringers) are utilized.

2.2 Report Organization

A brief overview of the organization of this report is included here. Basically this report presents results of (1) analytical derivations, (2) experimental tests, and (3) validation studies.

In the analytical development, there is to begin with, one fundamental goal, that being to incorporate the trim dynamics. This has to be done for both the low and high frequency models. After that has been accomplished, consideration is given to improving the precision of calculations of power flow for certain coupled acoustic and structural modes by including the effect of radiation damping of a highly resonant structural mode when closely coupled to a highly resonant acoustic mode. Generalization of the tonal transmission calculation is then considered; however the question of exterior field for the propeller excitation remains for the Phase III study. After that the question of cavity modes for the cabin configuration (i.e., that formed by

the cylinder wall and floor partition) is addressed. The normalization and use of the finite difference data is then considered. Special problems in the volume stiffness controlled regions of the test articles are then discussed (this extreme low frequency regime will lie below the regions of concern when full scale fuselage structures are considered). Finally a brief overview of the basic master computer program is given.

The parts of the report concerned with the experimental work describe the tests, hardware, and data acquisition and reduction techniques.

Comparisons of predictions and measurements are presented for the noise reductions of the three test articles. The statistical analysis of the noise reduction data and comparison technique and philosophy are consistent with and identical to that of Ref [1].

2.3 Program Management

The work was accomplished in joint effort by BBN/Los Angeles and NASA Langley Research Center. The experimental work was done at NASA Langley by C. M. Willis and W. H. Mayes. Mr. Mayes acted as LaRC technical representative of the contracting officer (TRCO). L. D. Pope served as BBN program manager. Most of Section 4 of this report was provided by C. M. Willis. A. G. Piersol of BBN assisted with the statistical evaluation of the comparison data and M. D. Sneddon of BBN mapped the acoustic modal pattern in the cylinder with the various floor partitions.

3.0 ANALYTICAL MODEL

The purpose of the first part of this section is to incorporate the effects of sidewall trim (insulation and lining) in the transmission analysis. In the present case, the interaction of the exterior pressure field, fuselage structure, insulation and lining, and interior field is of concern. To integrate the trim dynamics into the analysis, the basic expressions that describe the response, transmission, and absorption characteristics of the various components of the sidewall system must be considered.

3.1 Trim Dynamics

The trim is assumed to be representable by a transfer matrix:

$$\left.\begin{matrix} p_1^i \\ w_1 \end{matrix}\right\} = \begin{bmatrix} \alpha_{11} & \alpha_{12} \\ \alpha_{21} & \alpha_{22} \end{bmatrix} \left.\begin{matrix} p_2^i \\ w_2 \end{matrix}\right\} ,$$

or

$$\left.\begin{matrix} p_2^i \\ w_2 \end{matrix}\right\} = \begin{bmatrix} a_{11} & a_{12} \\ a_{21} & a_{22} \end{bmatrix} \left.\begin{matrix} p_1^i \\ w_1 \end{matrix}\right\} ,$$

where referring to Figure 1,

w_1 is the displacement of the fuselage skin at $\bar{x}$
p_1^i is the pressure on the inner surface of the skin at $\bar{x}$
w_2 is the displacement of the trim panel at $\bar{x}$
p_2^i is the pressure on trim inside surface at $\bar{x}$ - (cavity side).

The coefficients are related as follows:

$$\alpha_{11} = a_{22} \; ; \quad \alpha_{12} = -a_{12} \; ; \quad \alpha_{21} = -a_{21} \; ; \quad \alpha_{22} = a_{11} .$$

The representation above is a simple one that will lead to a tractable problem. It is also felt to be a reasonable one because of a number of factors. Its simplicity lies in the fact that the pressures and displacements occurring at each location are assumed to be related (across the trim) on a point-by-point basis. This may seem to be a very restrictive model, but since the transmission of acoustic waves is to be considered, the pressures and displacements will vary rather slowly with $\bar{x}$.

One could argue that for oblique incidence the pressure at a point on the incident wave front would be felt by the outer and inner surfaces of the insulation at different coordinate positions, say $\bar{x}$ and $\bar{x}'$ as it passes through it and that the wave would travel a distance greater than the thickness of the insulation blanket as it did. However, the acoustic wave inside the blanket propagates in a direction that is much closer to the normal than does the wave outside the blanket because the speed of sound in the blanket is less than the speed of sound in air (Snell's Law). Because of this the blanket does not appear to be much thicker for oblique incidence than for normal incidence [4]. Thus there is justification for the simple model postulated. It is important to note that the transfer matrix representation given above applies only across the trim insulation and lining. The fuselage skin (sidewall) is not involved. The sidewall response obeys a much more complex dynamical relation.

The response of the sidewall (for harmonic excitation) is

$$w_1(\bar{x}) = \int G(\bar{x}|\bar{x}';\omega)\left[p^o(\bar{x}') - p_1^i(\bar{x}')\right] d\bar{x}', \qquad (1)$$

where $G(\bar{x}|\bar{x}';\omega)$ is the structure's Green's function, the form of which will be presented shortly. $p^o(\bar{x}')$ is the exciting exterior pressure field. The integral is performed over the excited structural area.

The interior acoustic field acting on the trim lining is

$$p_2^i(\bar{x}') = -\rho\omega^2 \int G_p(\bar{x}|\bar{x}';\omega)\, w_2(\bar{x})\, d\bar{x}, \tag{2}$$

where $G_p(\bar{x}|\bar{x}';\omega)$ is the Green's function for the cavity and ρ is the density in the cabin.

The exterior field is (ρ_o = exterior air density)

$$\begin{aligned} p^o(\bar{x}') &= p_{b1}(\bar{x}') + \rho_o\omega^2 \int G_p^o(\bar{x}|\bar{x}';\omega)\, w_1(\bar{x})\, d\bar{x} \\ &= p_{b1}(\bar{x}') + p_r(\bar{x}') , \end{aligned} \tag{3}$$

$G_p^o(\bar{x}|\bar{x}')$ is the exterior space Green's function,
$p_r(\bar{x}')$ is the radiated pressure field on the exterior surface,
$p_{b1}(\bar{x}')$ is the blocked pressure field on the exterior surface.

The three equations (1),(2), and (3) and the trim transfer matrix (which consists of two equations) forms a system of five equations in five unknowns: p_1^i , p_2^i, w_1, w_2, and p_r (or p^o). The blocked pressure field is determinable once the geometry of the structure is fixed. It is now necessary to solve the system of equations to determine the effects introduced by the presence of the trim. Before doing this, note that if the trim is removed from consideration, $p_1^i = p_2^i$ and $w_1 = w_2$ reducing Eqs. (1), (2), and (3) to the previous set solved in References [2] and [3].

To begin, p_1^i and w_2 are to be eliminated as variables. From the transfer matrix

$$\begin{aligned} p_1^i &= \alpha_{11} p_2^i + \alpha_{12} w_2 \\ &= \alpha_{11} p_2^i + \alpha_{12}(a_{21} p_1^i + a_{22} w_1). \end{aligned}$$

Therefore

$$p_1^i = c_p p_2^i + c_w w_1 , \tag{4}$$

where

$$c_p = \frac{a_{22}}{1+a_{12}a_{21}} ; \quad c_w = \frac{-a_{12}a_{22}}{1+a_{12}a_{21}} .$$

Also

$$w_1 = \alpha_{21} p_2^i + \alpha_{22} w_2$$

giving

$$w_2 = \frac{w_1}{\alpha_{22}} - \frac{\alpha_{21} p_2^i}{\alpha_{22}} ,$$

or

$$w_2 = c^p p_2^i + c^w w_1 , \tag{5}$$

where

$$c^p = \frac{a_{21}}{a_{11}} ; \quad c^w = \frac{1}{a_{11}} .$$

At this point, it is emphasized that in Eq.(4) the coefficients c_p and c_w are subscripted and in Eq.(5), the coefficients c^p and c^w are superscripted. These coefficients are found to play prominent roles in describing the trim effects.

Continuing now, Eqs.(4) and (5) are substituted into Eqs. (1) and (2), and after using the defining relations for the Dirac delta function, i.e., in the forms

$$w_1(\bar{x}) = \int w_1(\bar{x}') \, \delta(\bar{x}'-\bar{x}) \, d\bar{x}' ,$$

and

$$p_2^i(\bar{x}') = \int p_2^i(\bar{x}) \, \delta(\bar{x}-\bar{x}') \, d\bar{x} ,$$

it is found that Eqs. (1) and (2) become the following

$$\int \left[\delta(\bar{x}'-\bar{x}) + c_w\, G(\bar{x}|\bar{x}';\omega)\right] w_1(\bar{x}')\, d\bar{x}'$$
$$= \int G(\bar{x}|\bar{x}';\omega)\left[p^o(\bar{x}') - c_p\, p_2^i(\bar{x}')\right] d\bar{x}'. \qquad \text{(1a)}$$

$$\int \left[\delta(\bar{x}-\bar{x}') + \rho\omega^2 c^p\, G_p(\bar{x}|\bar{x}';\omega)\right] p_2^i(\bar{x})\, d\bar{x}$$
$$= -\rho\omega^2 c^w \int G_p(\bar{x}|\bar{x}';\omega)\, w_1(\bar{x})\, d\bar{x}\ . \qquad \text{(2a)}$$

Eqs.(1a), (2a), and (3) must be solved simultaneously for the modal displacements of the fuselage wall.

Consider the left hand side of Eq.(1a). Let

$$w_1(\bar{x}) = \sum_s \xi_s \psi^s(\bar{x})\ ,$$

where ξ_s is the modal coordinate and $\psi^s(\bar{x})$ the associated modal function of the fuselage wall. Then the left hand side is

$$\int \left[\delta(\bar{x}'-\bar{x}) + c_w\, G(\bar{x}|\bar{x}';\omega)\right] \cdot \sum_s \xi_s \psi^s(\bar{x}')\, d\bar{x}'$$
$$= \sum_s \xi_s \psi^s(\bar{x}) + c_w \sum_s \int \sum_r \frac{\psi^r(\bar{x})\,\psi^r(\bar{x}')}{M_r Y_r(\omega)}\, \xi_s \psi^s(\bar{x}')\, d\bar{x}',$$

where the structure's Green's function has been introduced

$$G(\bar{x}|\bar{x}';\omega) = \sum_r \frac{\psi^r(\bar{x})\ \psi^r(\bar{x}')}{M_r Y_r(\omega)}\ ,$$

with modal mass

$$M_r = \int m\, \psi^{r\,2}(\bar{x})\ d\bar{x}\ ,$$

and receptance

$$Y_r(\omega) = \omega_r^2\left[\left(1 - \frac{\omega^2}{\omega_r^2}\right) - i\eta_r\right]\ ,$$

where ω_r is the resonance frequency, η_r the mode's loss factor, and m the surface mass per unit of area.

Using the property of the orthogonality of the modes, the left hand side of Eq.(1a) reduces to

$$\sum_s \left[1 + \frac{c_w}{m Y_s(\omega)} \right] \xi_s \psi^s(\bar{x}) \ .$$

$c_w / m Y_s(\omega)$ is a dimensionless quantity.

Therefore Eq.(1a) becomes

$$\sum_s \left[1 + \frac{c_w}{m Y_s(\omega)} \right] \psi^s(\bar{x}) \xi_s = \int G(\bar{x}|\bar{x}';\omega) \left[p^o(\bar{x}') - c_p p_2^i(\bar{x}') \right] d\bar{x}' .$$

The above is multiplied through by $m \psi^r(\bar{x})$, and integrated with respect to $\bar{x}$ to obtain

$$\left[1 + \frac{c_w}{m Y_r} \right] M_r \xi_r = \int m \psi^r(\bar{x}) \int \sum_s \frac{\psi^s(\bar{x}) \psi^s(\bar{x}')}{M_s Y_s} \left[p^o(\bar{x}') - c_p p_2^i(\bar{x}') \right] d\bar{x}' d\bar{x}$$

$$= \frac{1}{Y_r} \left[\int p^o(\bar{x}') \psi^r(\bar{x}') d\bar{x}' - c_p \int p_2^i(\bar{x}') \psi^r(\bar{x}') d\bar{x}' \right]$$

$$= \frac{1}{Y_r} \left[\Gamma^r_{p_o} - c_p \Gamma^r_{p_2^i} \right] .$$

But according to Eq.(3)

$$\Gamma^r_{p_o} = \Gamma^r_{p_{bl}} + \Gamma^r_{p_r} \ .$$

Therefore

$$-Y_r\left[1+\frac{c_w}{mY_r}\right]M_r\xi_r+\Gamma^r_{p_r}-c_p\Gamma^r_{p_2^i}=-\Gamma^r_{p_{bi}}\ . \tag{6}$$

Now consider Eq. (2a). The right hand side becomes

$$-\rho\omega^2c^w\int G_p(\bar{x}|\bar{x}';\omega)\sum_s\xi_s\psi^s(\bar{x})\,d\bar{x}.$$

Multiplying Eq.(2a) through by $\psi^r(\bar{x}')$ and integrating gives

$$\begin{aligned}\int\psi^r(\bar{x}')\int\left[\delta(\bar{x}-\bar{x}')+\rho\omega^2c^p G_p(\bar{x}|\bar{x}';\omega)\right]p_2^i(\bar{x})\,d\bar{x}\,d\bar{x}'\\ &= -\rho\omega^2c^w\int\psi^r(\bar{x}')\int G_p(\bar{x}|\bar{x}';\omega)\sum_s\xi_s\psi^s(\bar{x})\,d\bar{x}\,d\bar{x}'\\ &= -\rho\omega^2c^w\sum_s\xi_s\iint G_p(\bar{x}|\bar{x}';\omega)\,\psi^r(\bar{x}')\psi^r(\bar{x})\,d\bar{x}\,d\bar{x}'\\ &= -\rho\omega^2c^w\sum_s I^{rs}\xi_s\ ,\end{aligned}$$

where being consistent with previous definitions [2,3]

$$I^{rs}(\omega)=\iint G_p(\bar{x}|\bar{x}';\omega)\,\psi^r(\bar{x}')\psi^r(\bar{x})\,d\bar{x}\,d\bar{x}'.$$

The left hand side can be rewritten to yield

$$\begin{aligned}\Gamma^r_{p_2^i}+c^p\rho\omega^2\iint\psi^r(\bar{x}')\,G_p(\bar{x}|\bar{x}';\omega)\,p_2^i(\bar{x})\,d\bar{x}\,d\bar{x}'\\ =-\rho\omega^2c^w\sum_s I^{rs}\xi_s\ .\end{aligned} \tag{7}$$

Return now to Eq. (6) and consider $\Gamma^r_{p_r}$:

$$\Gamma^r_{p_r} = \int \psi^r(\bar{x})\, p_r(\bar{x})\, d\bar{x}$$

$$= \int \psi^r(\bar{x}) \left[\rho_o \omega^2 \int G^o_p(\bar{x}|\bar{x}';\omega) w_1(\bar{x}')\, d\bar{x}' \right] d\bar{x}$$

$$= \rho_o \omega^2 \sum_s \xi_s \iint G^o_p(\bar{x}|\bar{x}';\omega)\, \psi^r(\bar{x})\, \psi^s(\bar{x}')\, d\bar{x}' d\bar{x}\,,$$

or using the previous definition of $J^{rs}(\omega)$ as the integral appearing in the expression above [2,3]

$$\Gamma^r_{p_r} = \rho_o \omega^2 \sum_s J^{rs} \xi_s \,. \tag{8}$$

Now substitute Eqs. (7) and (8) into Eq. (6)

$$-\left[1 + \frac{c_w}{mY_r}\right] M_r \xi_r + \rho_o \omega^2 \sum_s J^{rs} \xi_s - c_p \left[-\rho \omega^2 c^w \sum_s I^{rs} \xi_s \right]$$

$$- c_p \left[-c^p \rho \omega^2 \iint \psi^r(\bar{x}')\, G_p(\bar{x}|\bar{x}';\omega)\, p^i_2(\bar{x})\, d\bar{x}\, d\bar{x}' \right] = -\Gamma^r_{p_{b1}} .$$

Collecting terms in ξ_r gives

$$\left\{ -M_r Y_r \left[1 + \frac{c_w}{mY_r} \right] + \omega^2 \left[\rho_o J^{rr} + \rho c_p c^w I^{rr} \right] \right\} \xi_r$$

$$+ \omega^2 \sum_{s \neq r} \left[\rho_o J^{rs} + \rho c_p c^w I^{rs} \right] \xi_s$$

$$+ c_p c^p \rho \omega^2 \iint \psi^r(\bar{x}')\, G_p(\bar{x}|\bar{x}';\omega)\, p^i_2(\bar{x})\, d\bar{x}\, d\bar{x}' = -\Gamma^r_{p_{b1}} . \tag{9}$$

Consider the integral in Eq.(9):

$$\iint \psi^r(\bar{x}')\, G_p(\bar{x}|\bar{x}';\omega)\, p_2^i(\bar{x})\, d\bar{x}\, d\bar{x}' ,$$

with the cavity Green's function being given by

$$G_p(\bar{x}|\bar{x}';\omega) = \sum_n \frac{\phi_n(\bar{x})\,\phi_n(\bar{x}')}{\iiint \phi_n^2\, d\bar{v}\,(\bar{\lambda}_n^2 - k^2)} ,$$

where $\phi_n(\bar{x})$ is the acoustic modal function for the nth mode of the cavity and $\bar{\lambda}_n$ is the complex eigenvalue. According to the previous normalization [2,3]:

$$\iiint \phi_n^2\, d\bar{v} = \frac{V}{\epsilon_n} .$$

The integral therefore becomes

$$\iint \psi^r(\bar{x}') \sum_n \frac{\epsilon_n}{V} \frac{\phi_n(\bar{x})\,\phi_n(\bar{x}')}{(\bar{\lambda}_n^2 - k^2)} \left[\sum_m \pi_m \phi_m(\bar{x}) \right] d\bar{x}\, d\bar{x}' ,$$

where

$$p_2^i(\bar{x}) = \sum_m \pi_m \phi_m(\bar{x}) ,$$

with π_m = normal coordinate for interior pressure (dimensionally π_m is equal to pressure).

Now the surface integral

$$\int \phi_n(\bar{x})\, \phi_m(\bar{x})\, d\bar{x} ,$$

is identically zero in almost all cases when $m \neq n$. However, the surface area over which this integral is evaluated may not extend

completely around the periphery of the cavity since that area is the transmitting surface. In such a case, for a few acoustic modes, the above integral will not be identically zero. However it will be small in magnitude relative to

$$\int \phi_n^2(\bar{x})\, d\bar{x} .$$

Therefore, the following approximation is valid

$$\iint \psi^r(\bar{x})' \sum_n \frac{\epsilon_n}{V} \frac{\phi_n(\bar{x})\ \phi_n(\bar{x}')}{(\bar{\lambda}_n^2 - k^2)} \left[\sum_m \pi_m \phi_m(\bar{x})\right] d\bar{x}\, d\bar{x}'$$

$$= \sum_n \frac{\epsilon_n A \int \phi_n^2(\bar{x})\, d\bar{x}}{V(\bar{\lambda}_n^2 - k^2)}\ f'(n,r)\ \pi_n ,$$

where

$$f'(n,r) = \frac{1}{A} \int \phi_n(\bar{x})\ \psi^r(\bar{x})\, d\bar{x} ,$$

and A is the transmitting area.

Substituting into Eq.(9) gives

$$\left\{-M_r Y_r \left[1 + \frac{c_w}{m Y_r}\right] + \omega^2 \left[\rho_0 J^{rr} + c_p c^w \rho I^{rr}\right]\right\} \xi_r$$

$$+ \omega^2 \sum_{s \neq r} \left[\rho_0 J^{rs} + c_p c^w \rho I^{rs}\right] \xi_s$$

$$+ c_p c^p \rho \omega^2 \sum_n \frac{\epsilon_n A \int \phi_n^2\, d\bar{x}}{V(\bar{\lambda}_n^2 - k^2)}\ f'(n,r)\, \pi_n = -\Gamma^r_{p_{bl}} . \quad (10)$$

Now reconsider Eq.(6) which can be put in a similar form

$$\left\{-M_r Y_r\left[1+\frac{c_w}{mY_r}\right]+\rho_0\omega^2 J^{rr}\right\}\xi_r$$

$$+\rho_0\omega^2\sum_{s\neq r} J^{rs}\xi_s$$

$$-c_p\sum_n \pi_n A f'(n,r) = -\Gamma^r_{p_{bl}} . \qquad (11)$$

Note that in the above use has been made of the relation

$$\Gamma^r_{p_2^i} = \int \psi^r(\bar{x})\, p_2^i(\bar{x})\, d\bar{x} = \int \psi^r(\bar{x}) \sum_n \pi_n \phi_n(\bar{x})\, d\bar{x}$$

$$= \sum_n \pi_n A f'(n,r) .$$

It is now necessary to eliminate the π_n from Eqs.(10) and (11).

Let

$$a_{rr} = -M_r Y_r\left[1+\frac{c_w}{mY_r}\right]+\omega^2\left[\rho_0 J^{rr}+c_p c^w \rho I^{rr}\right]$$

$$a_{rs} = \omega^2\left[\rho_0 J^{rs}+c_p c^w \rho I^{rs}\right]$$

$$b_{rn} = c_p c^p \rho\omega^2 \frac{\epsilon_n A \int \phi_n^2 d\bar{x}\; f'(n,r)}{V(\bar{\lambda}_n^2-k^2)} .$$

Then Eq.(10) becomes

$$a_{rr}\xi_r+\sum_{s\neq r} a_{rs}\xi_s+\sum_n b_{rn}\pi_n = -\Gamma^r_{p_{bl}} ,$$

or

$$[a]\{\xi\}+[b]\{\pi\} = \{-\Gamma_{p_{bl}}\} . \qquad (12)$$

Let

$$c_{rr} = -M_r Y_r \left[1 + \frac{c_w}{m Y_r} \right] + \rho_0 \omega^2 J^{rr}$$

$$c_{rs} = \rho_0 \omega^2 J^{rs}$$

$$d_{rn} = -c_p A f'(n,r) \quad .$$

Then Eq.(11) becomes

$$[c]\{\xi\} + [d]\{\pi\} = \{-\Gamma_{Pbl}\} \quad . \tag{13}$$

From (13)

$$[d]^{-1}[c]\{\xi\} + [d]^{-1}[d]\{\pi\} = [d]^{-1}\{-\Gamma_{Pbl}\} ,$$

or

$$\{\pi\} = -[d]^{-1}[c]\{\xi\} - [d]^{-1}\{\Gamma_{Pbl}\} .$$

Substituting this into Eq.(12) gives

$$[a]\{\xi\} - [b][d]^{-1}[c]\{\xi\} - [b][d]^{-1}\{\Gamma_{Pbl}\} = \{-\Gamma_{Pbl}\} ,$$

$$[[a] - [b][d]^{-1}[c]]\{\xi\} = [[b][d]^{-1} - [I]]\{\Gamma_{Pbl}\} ,$$

or

$$\{\xi\} = [[a] - [b][d]^{-1}[c]]^{-1}[[b][d]^{-1} - [I]]\{\Gamma_{Pbl}\} . \tag{14}$$

From this form, it is not obvious as to the influence of the trim on the sidewall response. Thus, the terms composing the coefficient matrices [a], [b], [c], and [d] must be examined.

First consider things that are known. Since coupling of structural modes by the acoustics is negligible, generally

$$\left|M_r Y_r\right| \gg \left|\rho\omega^2 I^{rs}\right|, \left|\rho_0\omega^2 J^{rs}\right| .$$

Also the radiation damping term coming from J^{rr} can be included in the loss factor η_r. Thus it follows that

$$c_{rr} \cong -M_r Y_r\left[1 + \frac{c_w}{m Y_r}\right] ,$$

and

$$c_{rs} \cong 0 .$$

Therefore [c] is a diagonal matrix (very close) = $\lceil c \rfloor$.
Also I^{rr} and I^{rs} are so small that [a] is diagonal: $\lceil a \rfloor$

$$a_{rr} \cong -M_r Y_r\left[1 + \frac{c_w}{m Y_r}\right] ,$$

$$a_{rs} \cong 0 .$$

It follows that $\lceil a \rfloor \cong \lceil c \rfloor$ (very close).

Then

$$\{\xi\} \cong \left[\left[\lceil a \rfloor - [b][d]^{-1}\lceil a \rfloor\right]^{-1}\left[[b][d]^{-1} - \lceil I \rfloor\right]\right]\{\lceil p_{bl} \rfloor\}$$

$$\cong \left[\left[\lceil I \rfloor - [b][d]^{-1}\right]\lceil a \rfloor\right]^{-1}\left[\lceil I \rfloor - [b][d]^{-1}\right]\{-\lceil p_{bl} \rfloor\} .$$

But the inverse of the product of matrices is determined from the relation

$$(ABC)^{-1} = C^{-1}B^{-1}A^{-1}.$$

Therefore

$$\{\xi\} \cong \lceil a \rfloor^{-1}\left[\lceil I \rfloor - \lceil b \rfloor \lceil d \rfloor^{-1}\right]^{-1}\left[\lceil I \rfloor - \lceil b \rfloor \lceil d \rfloor^{-1}\right]\{-\Gamma_{p_{bl}}\}$$

$$= \lceil a \rfloor^{-1}\{-\Gamma_{p_{bl}}\} \equiv \lceil \alpha \rfloor \{-\Gamma_{p_{bl}}\}. \tag{15}$$

This form is quite similar to the case where trim is excluded.

Without trim

$$\alpha_{rr} = -\frac{1}{M_r Y_r}.$$

With trim

$$\alpha_{rr} = -\frac{1}{M_r Y_r\left[1 + c_w/m Y_r\right]},$$

where

$$c_w = \frac{-a_{12}a_{22}}{1 + a_{12}a_{21}}.$$

The solution is

$$\xi_r = -\sum_t \alpha_{rt}\,\Gamma^t_{p_{bl}}(\omega), \tag{16}$$

giving

$$w_1(\bar{x}) = -\sum_r \sum_t \psi^r(\bar{x})\,\alpha_{rt}\,\Gamma^t_{p_{bl}}(\omega),$$

which since $\alpha_{rt} = 0$ for $t \neq r$ reduces to

$$= -\sum_r \psi^r(\bar{x})\,\alpha_{rr}\,\Gamma^r_{p_{bl}}(\omega). \tag{17}$$

To get $p_2^i(\bar{x})$ from

$$p_2^i(\bar{x}) = \sum_n \pi_n \phi_n(\bar{x}),$$

Eqs. (12) and (13) have to be reconsidered. Either can be used to obtain the π_n. From Eq.(12)

$$[a]\{\xi\} + [b]\{\pi\} = \{-\Gamma_{pbl}\} ,$$

or

$$\lceil a \rfloor\{\xi\} + [b]\{\pi\} = \{-\Gamma_{pbl}\} .$$

But by Eq.(15)

$$\{\xi\} \cong \lceil a \rfloor^{-1}\{-\Gamma_{pbl}\} ,$$

that is,

$$\{\xi\} = \lceil a \rfloor^{-1}\{-\Gamma_{pbl}\} + \{\xi_\epsilon\} ,$$

where

$$|\xi_\epsilon^r| \ll |\alpha_{rr}\Gamma_{pbl}^r| .$$

This gives

$$\lceil a \rfloor[\lceil a \rfloor^{-1}\{-\Gamma_{pbl}\} + \{\xi_\epsilon\}] + [b]\{\pi\} = \{-\Gamma_{pbl}\} ,$$

or

$$[b]\{\pi\} = -\lceil a \rfloor\{\xi_\epsilon\} ,$$

i.e.

$$\{\pi\} = -[b]^{-1}\lceil a \rfloor\{\xi_\epsilon\} .$$

Now

$$p_2^i(\bar{x}) = \sum_n \pi_n \phi_n = \{\pi\}^T\{\phi\} = \{\phi\}^T\{\pi\} .$$

From Eq.(5),

$$W_2(\bar{x}) = c^p p_2^i(\bar{x}) + c^w w_1(\bar{x}).$$

Thus

$$\begin{aligned} W_2(\bar{x}) &= c^p\{\phi\}^T\{\pi\} + c^w\{\psi\}^T\{\xi\} \\ &= -c^p\{\phi\}^T[b]^{-1}[a]\{\xi_\epsilon\} + c^w\{\psi\}^T\{\xi\} \\ &\cong c^w W_1(\bar{x}), \end{aligned}$$

in the limit as acoustical coupling of structural modes is neglected, i.e., $\{\xi_\epsilon\} \rightarrow 0$.

The interpretation is this: while it is necessary to have a precise calculation of π_n for purposes of determining $p_2^i(\bar{x})$, the values of π_n have little bearing on the calculation of $W_2(\bar{x})$ and for all practical purposes can be set equal to zero for the $W_2(\bar{x})$ calculation.

This now allows a calculation of the power flow into the cabin using

$$W_2(\bar{x}) = c^w W_1(\bar{x}). \tag{18}$$

<u>Power Radiated into Cabin</u>

The cross power spectral density of pressure p_2^i at position $\bar{x}$ with trim lining velocity at $\bar{x}'$ is (for a one-sided spectrum)

$$S_{p_2^i v_2}(\bar{x}|\bar{x}';\omega) = \lim_{T\to\infty} \frac{2}{T}\left(\frac{1}{2\pi}\right) P_{2_T^i}(\bar{x};\omega) V_{2_T}^*(\bar{x}';\omega).$$

P^i_{2T} and V_{2T} are Fourier transforms of the truncated random quantities (* = conjugate).

Now

$$V^*_{2T}(\bar{x};\omega) = i\omega W^*_{2T}(\bar{x};\omega).$$

Here the definition of the Fourier transform is

$$\mathcal{F}(\ ) = \int_{-\infty}^{\infty} (\ )\, e^{i\omega t}\, dt.$$

Therefore

$$S_{P^i_2 V_2}(\bar{x}|\bar{x}';\omega) = \lim_{T\to\infty} \frac{2}{T}\frac{i\omega}{2\pi} P^i_{2T}(\bar{x};\omega) W^*_{2T}(\bar{x}';\omega).$$

But according to Eq.(2),

$$P^i_{2T}(\bar{x};\omega) = -\rho\omega^2 \int G_p(\bar{x}|\bar{x}'';\omega)\, W_{2T}(\bar{x}'';\omega)\, d\bar{x}''.$$

Thus

$$S_{P^i_2 V_2}(\bar{x}|\bar{x}';\omega) = -i\rho\omega^3 \left\{ \lim_{T\to\infty} \frac{2}{T}\frac{1}{2\pi} W^*_{2T}(\bar{x}',\omega) \right.$$

$$\left. \times \int G_p(\bar{x}|\bar{x}'';\omega)\, W_{2T}(\bar{x}'',\omega)\, d\bar{x}'' \right\}$$

$$= -i\rho\omega^3 \int G_p(\bar{x}|\bar{x}'') \left[\lim_{T\to\infty} \frac{1}{\pi T} W_{2T}(\bar{x}'',\omega)\, W^*_{2T}(\bar{x}',\omega) \right] d\bar{x}''$$

$$= -i\rho\omega^3 \int G_p(\bar{x}|\bar{x}'';\omega)\, S_{W_2}(\bar{x}''|\bar{x}';\omega)\, d\bar{x}''. \qquad (19)$$

Now let $\bar{x}' \to \bar{x}$. The spectral density of power radiated internally is obtained by integrating $S_{p_2^i v_2}(\bar{x},\omega)$ over the transmitting area.

$$W_{rad}^{int}(\omega) = \int_{\bar{x}} S_{p_2^i v_2}(\bar{x};\omega)\, d\bar{x} .$$

This quantity is complex. The real part is the real power (i.e., cospectrum of power).

Therefore

$$W_{rad}^{int}(\omega) = -i\rho\omega^3 \iint_{\bar{x}\,\bar{x}'} G_p(\bar{x}|\bar{x}';\omega)\, S_{w_2}(\bar{x}'|\bar{x};\omega)\, d\bar{x}'d\bar{x} .$$

But according to the previous finding

$$W_{2T}(\bar{x},\omega) \cong c^w W_{1T}(\bar{x},\omega).$$

Therefore

$$S_{w_2}(\bar{x}'|\bar{x};\omega) = \lim_{T\to\infty} \frac{2}{T}\left(\frac{1}{2\pi}\right) W_{2T}(\bar{x}';\omega)\, W_{2T}^*(\bar{x};\omega)$$

$$= \lim_{T\to\infty} \frac{2}{T}\left(\frac{1}{2\pi}\right) c^w W_{1T}(\bar{x}')(c^w)^* W_{1T}^*(\bar{x})$$

$$= \left|c^w\right|^2 S_{w_1}(\bar{x}'|\bar{x};\omega) , \qquad (20)$$

and

$$W_{rad}^{int}(\omega) = -i\rho\omega^3 \iint_{\bar{x}\,\bar{x}'} \left|C^w\right|^2 G_p(\bar{x}|\bar{x}';\omega)\, S_{w_1}(\bar{x}'|\bar{x};\omega)\, d\bar{x}\, d\bar{x}'.$$

But

$$W_{1T}(\bar{x},\omega) = -\sum_r \psi^r(\bar{x})\, \alpha_{rr}\, \Gamma^r_{p_{b1_T}}(\omega).$$

So

$$S_{w_1}(\bar{x}'|\bar{x};\omega) = \sum_{r,\ell} \alpha_{rr}\alpha^*_{\ell\ell}\, \psi^r(\bar{x}')\, \psi^\ell(\bar{x})$$
$$\times \iint S_{p_{b1}}(\bar{x}|\bar{x}';\omega)\, \psi^r(\bar{x})\, \psi^\ell(\bar{x}')\, d\bar{x}\, d\bar{x}',$$

giving, upon introduction of the joint and cross acceptances, $j^2_{r\ell}(\omega)$,

$$W_{rad}^{int}(\omega) = -i\rho\omega^3 \left|C^w\right|^2 \sum_{r,\ell} \alpha_{rr}\alpha^*_{\ell\ell} \Big[\iint_{\bar{x}\,\bar{x}'} G_p(\bar{x}|\bar{x}';\omega)$$
$$\times\, \psi^r(\bar{x}')\, \psi^\ell(\bar{x})\, d\bar{x}'\, d\bar{x} \Big]\, j^2_{r\ell}(\omega)\, S_{p_{b1}}(\omega)\, A^2$$

$$= -i\rho\omega^3 \left|C^w\right|^2 A^2 S_{p_{b1}}(\omega) \sum_{r,\ell} \alpha_{rr}\alpha^*_{\ell\ell}\, I^{r\ell}(\omega)\, j^2_{r\ell}(\omega).$$

Neglecting cross acceptances, this reduces to

$$W_{rad}^{int}(\omega) = -i\rho\omega^3 \left|C^w\right|^2 A^2 S_{p_{b1}}(\omega) \sum_r \left|\alpha_{rr}\right|^2 I^{rr}(\omega)\, j^2_r(\omega)$$

Now

$$I^{rr}(\omega) = \frac{A^2}{V} \sum_n \frac{\epsilon_n f'^2(n,r)}{(\bar{\lambda}^2_n - k^2)} = \mathrm{Re}\left[I^{rr}(\omega)\right] + i\,\mathrm{Im}\left[I^{rr}(\omega)\right]$$

Therefore

$$\mathrm{Re}\left[W_{rad}^{int}(\omega)\right] = \rho\omega^3 A^2 \left|c^w\right|^2 S_{p_{bl}}(\omega) \sum_r \frac{\mathcal{L}_m\left[I^{rr}\right] j_r^2(\omega)}{\left|M_r(Y_r + c_w/m)\right|^2},$$

$$= \rho\omega^3 A^2 S_{p_{bl}}(\omega) \left|c^w\right|^2 \sum_r \frac{A^2}{V} \sum_n \frac{\epsilon_n 2\lambda_n \Lambda_n}{\left|\bar{\lambda}_n^2 - k^2\right|^2} f'^2_{(n,r)}$$

$$\times \frac{j_r^2(\omega)}{\left|M_r(Y_r + \frac{c_w}{m}\right|^2},$$

$$= \frac{2\rho\omega^3 A^4}{V} \left|c^w\right|^2 \sum_n \frac{\epsilon_n \lambda_n \Lambda_n}{\left|\bar{\lambda}_n^2 - k^2\right|^2} \sum_r \frac{f'^2_{(n,r)}\, j_r^2(\omega)}{\left|M_r(Y_r + \frac{c_w}{m})\right|^2} S_{p_{bl}}(\omega).$$

It follows that the band-limited power flowing to the acoustic space is

$$\begin{aligned} W_{in} &= \int_{\Delta\omega} \mathrm{Re}\left[W_{rad}^{int}(\omega)\right] d\omega \\ &= \frac{\rho c_0^2 A^4}{V} \left|c^w\right|^2 S_{p_{bl}}(\omega) \sum_r \frac{j_r^2(\omega)}{M_r^2} \\ &\quad \times \sum_n \frac{\epsilon_n \eta_n f'^2_{(n,r)}}{\omega_n^2} \int_{\Delta\omega} \frac{\omega^3 d\omega}{\left\{\left[1-(\omega^2/\omega_n^2)\right]^2 + \eta_n^2\right\} \left|Y_r + \frac{c_w}{m}\right|^2}, \end{aligned} \tag{21}$$

where use has been made of the relations

$$\lambda_n = \omega_n / c_0 \;; \quad \Lambda_n = \omega_n \eta_n / 2c_0 ,$$

and

$$\bar{\lambda}_n = \lambda_n - i\Lambda_n .$$

Let

$$c_w = c_w^R + i\, c_w^I ,$$

Then

$$Y_r + \frac{c_w}{m} = \left\{ \omega_r^2 \left[1 - \frac{\omega^2}{\omega_r^2} \right] + \frac{c_w^R}{m} + i \left[\frac{c_w^I}{m} - \eta_r \omega_r^2 \right] \right\} ,$$

and

$$\left| Y_r + \frac{c_w}{m} \right|^2 = \omega_r^4 \left[1 - \frac{\omega^2}{\omega_r^2} \right]^2 + 2\omega_r^2 \left[1 - \frac{\omega^2}{\omega_r^2} \right] \frac{c_w^R}{m} + \frac{|c_w|^2}{m^2} - \frac{2c_w^I}{m} \eta_r \omega_r^2 + \eta_r^2 \omega_r^4 .$$

Since in general

$$\omega_r^2 \gg \frac{|c_w|}{m} ,$$

the above reduces to

$$\left| Y_r + \frac{c_w}{m} \right|^2 \cong \omega_r^4 \left\{ \left[1 - \frac{\omega^2}{\omega_r^2} \right]^2 + \left[\frac{|c_w|^2}{m^2 \omega_r^4} - \frac{2c_w^I}{m} \frac{\eta_r}{\omega_r^2} + \eta_r^2 \right] \right\}$$

Now set

$$\eta_r'^2 = \frac{|c_w|^2}{m^2 \omega_r^4} - \frac{2c_w^I}{m} \frac{\eta_r}{\omega_r^2} + \eta_r^2 .$$

This leads to the result

$$\left| Y_r + \frac{c_w}{m} \right|^2 \cong \omega_r^4 \left\{ \left[1 - \frac{\omega^2}{\omega_r^2} \right]^2 + (\eta_r')^2 \right\} ,$$

and Eq. (21) reduces identically to the form of Eq.(3), Section (1) of Reference [3] except for the presence of $|C^w|^2$. It follows that

$$W_{in} = \frac{\langle p_{bl}^2 \rangle}{c_\omega \omega} \frac{2\pi A^2}{\rho V} \left(\frac{mA}{4}\right)^2 \tau_{mL} |C^w|^2 \sum_n \epsilon_n \eta_n$$

$$\cdot \sum_r \frac{j_r^2(\omega) f'^2(n,r)}{M_r^2} \left\{ \frac{2}{\pi} \frac{\omega^2 \omega_n^2}{D_{nr}} \left[\left(\frac{c_r - c_n}{4}\right) \ln_n \right.\right.$$

$$+ \left(\frac{2c_n(b_r - b_n) - b_n(c_r - c_n)}{4\eta_n \omega_n^2}\right) \arctan_n + \left(\frac{c_n - c_r}{4}\right) \ln_r$$

$$\left.\left. + \left(\frac{2c_r(b_n - b_r) - b_r(c_n - c_r)}{4\eta_r' \omega_r^2}\right) \arctan_r \right] \right\}, \qquad (22)$$

where for n or $r = j$

$$\ln_j = \ln \left\{ \frac{|(1 + c_\omega/2)^4 \omega^4 + b_j (1 + c_\omega/2)^2 \omega^2 + c_j|}{|(1 - c_\omega/2)^4 \omega^4 + b_j (1 - c_\omega/2)^2 \omega^2 + c_j|} \right\},$$

$$\arctan_j = \tan^{-1} \frac{(2 + c_\omega)^2 \omega^2 - 4\omega_j^2}{4\eta_j \omega_j^2} - \tan^{-1} \frac{(2 - c_\omega)^2 \omega^2 - 4\omega_j^2}{4\eta_j \omega_j^2},$$

with

$$D_{nr} = (c_r - c_n)^2 + (b_n - b_r)(b_n c_r - b_r c_n),$$

$$b_n = -2\omega_n^2 \; ; \; b_r = -2\omega_r^2,$$

$$c_n = \omega_n^4 (1 + \eta_n^2) \; ; \; c_r = \omega_r^4 (1 + \eta_r'^2).$$

The above is identical to Eq.(5) of the Reference [3] except that $|C^w|^2$ multiplies the result and η_r' replaces η_r.

Now closer consideration needs to be given to C_w and C^w.

First consider the multiplying factor $|c^w|^2$. Suppose the trim is a simple model of insulation plus limp mass as shown in Figure 1. The transfer matrix for the insulation is [refer to transfer matrix derivation in Appendix A]

$$\left.\begin{matrix} p_2 \\ v_2 \end{matrix}\right\} = \begin{bmatrix} C & -WS \\ -\frac{S}{W} & C \end{bmatrix} \left.\begin{matrix} p_1 \\ v_1 \end{matrix}\right\} ,$$

where

C = cosh γL
S = sinh γL
γ = propagation constant of insulation
W = wave impedance of insulation.

The inverse of this is

$$\left.\begin{matrix} p_1 \\ v_1 \end{matrix}\right\} = \begin{bmatrix} C & WS \\ \frac{S}{W} & C \end{bmatrix} \left.\begin{matrix} p_2 \\ v_2 \end{matrix}\right\} .$$

The transfer matrix for the lining is

$$\left.\begin{matrix} p_2 \\ v_2 \end{matrix}\right\} = \begin{bmatrix} 1 & i\omega m_t \\ 0 & 1 \end{bmatrix} \left.\begin{matrix} p_1 \\ v_1 \end{matrix}\right\} ,$$

where m_t is the mass per unit of area of lining.

When coupled together, the transfer matrix across the trim is found using

$$\left.\begin{matrix} p_2 \\ v_2 \end{matrix}\right\}_{\substack{\text{insulation}\\ \text{output}}} = \left.\begin{matrix} p_1 \\ v_1 \end{matrix}\right\}_{\substack{\text{into trim}\\ \text{mass}}}$$

This gives

$$\left.\begin{matrix} p_2^i \\ v_2 \end{matrix}\right\} = \left.\begin{matrix} p_2 \\ v_2 \end{matrix}\right\}_{\substack{\text{trim mass}\\ \text{output}}} = \begin{bmatrix} 1 & i\omega m_t \\ 0 & 1 \end{bmatrix} \begin{bmatrix} C & -WS \\ -\frac{S}{W} & C \end{bmatrix} \left.\begin{matrix} p_1^i \\ v_1 \end{matrix}\right\}_{\substack{\text{into}\\ \text{insulation}}} \tag{23}$$

Also

$$v_1 = -i\omega w_1 \quad ; \quad v_2 = -i\omega w_2 \ .$$

The transfer matrix of concern here must be of the form including displacement. Thus

$$\left.\begin{matrix} p_2^i \\ w_2 \end{matrix}\right\} = \begin{bmatrix} a_{11} & a_{12} \\ a_{21} & a_{22} \end{bmatrix} \left.\begin{matrix} p_1^i \\ w_1 \end{matrix}\right\}$$

$$= \begin{bmatrix} 1 & \omega^2 m_t \\ 0 & 1 \end{bmatrix} \begin{bmatrix} C & i\omega WS \\ -\frac{iS}{\omega W} & C \end{bmatrix} \left.\begin{matrix} p_1^i \\ w_1 \end{matrix}\right\}$$

$$= \begin{bmatrix} (C - i\omega m_t \frac{S}{W}) & (i\omega WS + \omega^2 m_t C) \\ -\frac{iS}{\omega W} & C \end{bmatrix} \left.\begin{matrix} p_1^i \\ w_1 \end{matrix}\right\} . \tag{24}$$

Now according to the definition

$$c^w = \frac{1}{a_{11}} ,$$

or

$$c^w = \frac{W}{CW - i\omega m_t S} .$$

C, S and W are complex. This leads to

$$|c^w|^2 = \frac{W}{CW - i\omega m_t S} \frac{W^*}{C^* W^* + i\omega m_t S^*}$$
$$= \frac{|W|^2}{|C|^2|W|^2 + \omega^2 m_t^2 |S|^2 - i\omega m_t (SC^*W^* - S^*CW)} . \tag{25}$$

A Preliminary Comparison

At this point it is useful to make a comparison against some measured data. Consider a trim such as that of Figure 2 similar to that used in the 747 aircraft. In this case, the trim panel mass is m_t = 1.76 kg/m^2. It covers a 0.102m (4 in.) thick layer of Owens-Corning PF-105 fiberglass weighing 9.61 kg/m^3 (0.6 lb/ft^3).

From Appendix A

$$\gamma = \alpha - ik ,$$

where

$$k = 2\pi / \lambda_m .$$

λ_m is the acoustic wavenumber in the material. The attenuation constant is

$$\alpha(m^{-1}) = \alpha\,(dB/m)\,/\,8.69,$$

and the wave impedance is

$$W = Z_s \text{ mks rayls } (kg/m^2\text{-sec}).$$

At high frequencies,

$$|W| \longrightarrow \rho_0 c_0 \cong 420 \text{ kg}/m^2\text{-sec}.$$

Also

$$W = |W|\,e^{i\phi} = |Z_s|\,e^{-i\theta} = Z_s$$

The properties of the fiberglass are given in Figure 3.

The prediction for $|C^w|^2$ is shown in Figure 4. On the basis of these results the trim panel vibration isolation needs to be examined at high frequencies, otherwise, a reasonable prediction is afforded with the model.

Other trim configurations can be easily generated. Suppose the insulation is replaced by an airgap. Then

$$W = W_0 = \rho_0 c_0$$

$$\gamma = -ik \quad ; \quad k = \omega / c_0 .$$

$$|C^w|^2 = \frac{(\rho_0 c_0)^2}{(\rho_0 c_0)^2 |C|^2 + \omega^2 m_t^2 |S|^2 - \omega m_t \rho_0 c_0 \sin 2kL},$$

or

$$|c^w|^2 = \frac{1}{\left\{\frac{1}{2}\left[1+\left(\frac{\omega m_t}{\rho_0 c_0}\right)^2\right] + \frac{1}{2}\left[\cos 2kL - \left(\frac{\omega m_t}{\rho_0 c_0}\right)^2 \cos 2kL\right] \cdots - \left(\frac{\omega m_t}{\rho_0 c_0}\right) \sin 2kL\right\}}.$$

At low frequencies, $k \to 0$

$$|c^w|^2 \to \frac{1}{1+(\omega m_t/\rho_0 c_0)^2}.$$

This is simply the theoretical "weight (mass) law" attenuation spoken of in Beranek and Work [5].

At certain high frequencies,

$$\cos 2kL \to 0, \quad \sin 2kL \to 1$$

$$|c^w|^2 \to \frac{1}{\frac{1}{2}\left[1+\left(\frac{\omega m_t}{\rho_0 c_0}\right)^2\right] - \left(\frac{\omega m_t}{\rho_0 c_0}\right)}.$$

Since $\omega m_t/\rho_0 c_0 \gg 1$,

$$|c^w|^2 \to 2\left(\frac{\rho c_0}{\omega m_t}\right)^2,$$

which is mass law. This also looks good.

As has been shown then there is appearing in the theoretical results, a trim coefficient which will be called $\tau_t = |c^w|^2$,

$$\tau_t = \frac{1}{|a_{11}|^2}.$$

This is the "add-on" attenuation of the lining and insulation. It should be noted, however, that the multiplier τ_t is not the only effect of the trim. There also appears added damping due to $\eta_r \to \eta_r'$, as previously discussed.

There will be occasion to consider the lining dissipative (there being some flexure of the lining but with the lining stiffness small enough to ignore). Then the trim transfer matrix takes the form

$$\left.\begin{matrix} p_2^i \\ v_2 \end{matrix}\right\} = \begin{bmatrix} 1 & (i\omega m_t - \eta_t \omega m_t) \\ 0 & 1 \end{bmatrix} \begin{bmatrix} C & -WS \\ -\frac{S}{W} & C \end{bmatrix} \left.\begin{matrix} p_1^i \\ v_1 \end{matrix}\right\} ,$$

where η_t is the trim loss factor.

In terms of displacement, which is required in the present formulation, this becomes

$$\left.\begin{matrix} p_2^i \\ w_2 \end{matrix}\right\} = \begin{bmatrix} 1 & (\omega^2 m_t + i\omega^2 \eta_t m_t) \\ 0 & 1 \end{bmatrix} \begin{bmatrix} C & i\omega WS \\ -\frac{iS}{\omega W} & C \end{bmatrix} \left.\begin{matrix} p_1^i \\ w_1 \end{matrix}\right\}$$

$$= \begin{bmatrix} a_{11} & a_{12} \\ a_{21} & a_{22} \end{bmatrix} \left.\begin{matrix} p_1^i \\ w_1 \end{matrix}\right\} .$$

Therefore, for this case:

$$a_{11} = C + \omega m_t \eta_t \frac{S}{W} - i\omega m_t \frac{S}{W} \quad ,$$

$$a_{12} = \omega^2 m_t C + i(\omega W S + \omega^2 \eta_t m_t C) \ ,$$

$$a_{21} = -\frac{iS}{\omega W} \ ,$$

$$a_{22} = C \ .$$

The trim coefficient is always determined from the coefficient a_{11}. C_W is determined from the remaining three coefficients.

<u>Band Limited Power Absorbed on Cabin Wall (with trim)</u>

This result is taken directly from the previously cited reference [3]. The required expression is from the appendix of that paper, Eq.(A5). First the conductance, ξ , looking into the trim is considered to be independent of $\bar{x}$ (do not confuse the conductance ξ with the modal coordinate of the structure, i.e., ξ_r).

$$W_{diss} = \frac{\xi V}{\rho c_0} \sum_n \langle p_n^2 \rangle_{s,t} \int_{\bar{x}} \phi_n^2 \, d\bar{x} \left(\int_V \phi_n^2 \, dv \right)^{-1} , \qquad (26)$$

where $\langle p_n^2 \rangle_{s,t}$ is the space-time mean square modal pressure.

Thus

$$W_{diss} = \frac{\xi}{\rho c_0} \sum_n \epsilon_n \langle p_n^2 \rangle_{s,t} \int_{\bar{x}} \phi_n^2 \, d\bar{x} \ ,$$

when the normalization of the ϕ_n is taken into account.

In the case where ξ is a function of $\bar{x}$,

$$W_{diss} = \frac{1}{\rho c_o} \sum_n \epsilon_n < p_n^2 >_{s,t} \int_{\bar{x}} \xi(\bar{x}) \phi_n^2(\bar{x}) d\bar{x}, \quad (27)$$

where $\int_{\bar{x}}$ is always evaluated over the absorbing surface area.

The conductance can also be related to the imaginary part of the eigenvalue of the acoustic mode, or, alternately to the loss factor of the acoustic mode. From [3], if ξ is independent of $\bar{x}$

$$\Lambda_n \cong \frac{k}{2\lambda_n} \frac{\epsilon_n \xi}{V} \int_{\bar{x}} \phi_n^2 \, d\bar{x} \ ,$$

If not,

$$\Lambda_n \cong \frac{k}{2\lambda_n} \frac{\epsilon_n}{V} \int_{\bar{x}} \xi(\bar{x}) \phi_n^2(\bar{x}) \, d\bar{x} \ .$$

In terms of loss factor

$$\eta_n = \frac{\omega c_o}{\omega_n^2} \frac{\epsilon_n}{V} \int_{\bar{x}} \xi(\bar{x}) \phi_n^2(\bar{x}) d\bar{x}. \quad (28)$$

Thus substituting Eq.(28) into (27) gives

$$W_{diss} = \frac{V}{\rho c_o^2} \sum_n \frac{\eta_n \omega_n^2}{\omega} < p_n^2 >_{s,t} \cdot \quad (29)$$

In this report W_{in} is always used in the form of Eq.(22) and W_{diss} in the form of (29). The relation needed to determine the effects of the trim in terms of the absorption from the space will be Eq.(28). In other words, the acoustic loss factor of Eq.(28) will be calculated once $\xi(\bar{x})$ is determined. Alternately the loss factor can be measured. For the bare cylinder case (or a bare fuselage) measurements will usually be required. But for cases where trim is present the analytical determination of η_n is desired. Therefore, the calculation of the conductance ξ of the sidewall is needed.

By definition, the conductance is the real part of the admittance β.

$$\xi = \mathrm{Re}(\beta) = \mathrm{Re}(\xi - i\sigma)$$

$$\beta = z^{-1} = \left[\frac{p}{v}\left(\frac{1}{\rho c_0}\right)\right]^{-1}$$

$$= \rho c_0 v / p \ , \qquad (30)$$

where v and p are the trim velocity and the pressure on the inside (interior side) of the trim.

This can be written

$$\beta = -i\omega\rho c_0 w / p \ ,$$

where w is the trim displacement.

Suppose

$$v = V e^{-i\omega t}$$

$$p = P e^{-i(\omega t - \phi)} \ .$$

Then $v/p = V/P e^{-i\phi}$ where V and P are real amplitudes. If $\phi = 0, \beta = \text{real} = \xi = \rho c_0 (V/P)$. When p is maximum v is maximum in the direction of power flow. Be definition, v_2 is positive inward toward the interior (as is w_2) - refer to Figure 1. However the conductance desired is that looking into the panel. Therefore $v = -v_2$ (or $w = -w_2$). Thus β is determined with the relation (using $p = p_2^i$)

$$\beta = i\omega\rho c_0 w_2 / p_2^i . \tag{31}$$

Now

$$p_2^i = a_{11} p_1^i + a_{12} w_1 ,$$

and

$$w_2 = a_{21} p_1^i + a_{22} w_1 .$$

Define the impedance looking into the structure at $\bar{x}$ as

$$z_1 = -\frac{p_1^i}{v_1} = -\frac{p_1^i}{-i\omega w_1} = \frac{p_1^i}{i\omega w_1} . \tag{32}$$

Again the sign change is necessary to define an outward velocity.

Then

$$\beta = i\omega\rho c_0 \left[\frac{a_{21} p_1^i + a_{22} w_1}{a_{11} p_1^i + a_{12} w_1} \right]$$

$$= \rho c_0 \left[\frac{-\omega^2 a_{21} z_1 + i\omega a_{22}}{i\omega a_{11} z_1 + a_{12}} \right] . \tag{33}$$

This is the general result desired.

Before continuing, a check for correctness is needed. Let the impedance z' be calculated, where

$$z' = \rho c_0 \beta^{-1} = \frac{i\omega a_{11} z_1 + a_{12}}{-\omega^2 a_{21} z_1 + i\omega a_{22}} .$$

For the initial trim model it was found that

$$a_{11} = C - i\omega m_t \frac{S}{W}$$

$$a_{12} = i\omega W S + \omega^2 m_t C$$

$$a_{21} \doteq -\frac{iS}{\omega W}$$

$$a_{22} = C .$$

Therefore

$$z' = \frac{z_1 (i\omega C + \omega^2 m_t S/W) + (i\omega W S + \omega^2 m_t C)}{z_1 (i\omega S/W) + i\omega C} .$$

Dividing through by $i\omega$ (numerator and denominator) gives

$$z' = \frac{z_1 (C - i\omega m_t S/W) + (WS - i\omega m_t C)}{z_1 (S/W) + C}$$

$$= W \left[\frac{z_1 (C - i\omega m_t S/W) + (WS - i\omega m_t C)}{z_1 S + WC} \right] .$$

From this, it is seen that the impedance looking into the trim is of the correct form. For instance, if $m_t \to 0$,

$$z' = W\left[\frac{Cz_1 + WS}{Sz_1 + WC}\right],$$

which is the correct form for the insulation alone [6].

Now return to Eq.(33), repeated below

$$\beta = \rho c_0\left[\frac{-\omega^2 a_{21} z_1 + i\omega a_{22}}{i\omega a_{11} z_1 + a_{12}}\right], \tag{33}$$

$z_1 = p_1^i / i\omega w_1$ = impedance looking into structure.

In general $z_1 = z_1(\bar{x})$ = local, and therefore

$$\beta(\bar{x}) = \rho c_0\left[\frac{-\omega^2 a_{21} z_1(\bar{x}) + i\omega a_{22}}{i\omega a_{11} z_1(\bar{x}) + a_{12}}\right].$$

Now

$$w_1(\bar{x}) = \int G(\bar{x}|\bar{x}';\omega)\left[p^0(\bar{x}') - p_1^i(\bar{x}')\right] d\bar{x}'.$$

But since β is sought, one can for the present consider

$$p^0(\bar{x}') = p_r(\bar{x}'),$$

i.e., only the radiated pressure on the backside (outside) of the skin is of concern.

Recalling that

$$p_r(\bar{x}') = \rho\omega^2 \int G_p^o(\bar{x}|\bar{x}')\, w_1(\bar{x})\, d\bar{x},$$

and noting that the radiated pressure effect can be included in G as increased damping since the reactance of the air is negligible compared to that of the structure, for the present purposes

$$\begin{aligned} w_1(\bar{x}) &= -\int G(\bar{x}|\bar{x}';\omega)\, p_1^i(\bar{x}')\, d\bar{x}' \\ &= -\int \sum_s \frac{\psi^s(\bar{x})\,\psi^s(\bar{x}')}{M_s Y_s(\omega)}\, p_1^i(\bar{x}')\, d\bar{x}' \\ &= -\sum_s \int \frac{\psi^s(\bar{x})\,\psi^s(\bar{x}')}{M_s Y_s(\omega)}\, p_1^i(\bar{x}')\, d\bar{x}' \\ &= -\sum_s \frac{\psi^s(\bar{x})}{M_s Y_s(\omega)} \int p_1^i(\bar{x}')\,\psi^s(\bar{x}')\, d\bar{x}' . \end{aligned}$$

This leads to an approximation

$$z_1(\bar{x}) = \frac{p_1^i(\bar{x})}{-i\omega \sum_s \frac{\psi^s(\bar{x})}{M_s Y_s(\omega)} \int p_1^i(\bar{x}')\,\psi^s(\bar{x}')\, d\bar{x}'} .$$

One model is obtained by letting the pressure be uniform (constant)

$$p_1^i(\bar{x}) = p_1^i(\bar{x}') \ ,$$

leading to

$$Z_1(\bar{x}) = \left[-i\omega \sum_s \frac{\psi^s(\bar{x}) \int \psi^s(\bar{x}')\, d\bar{x}}{M_s Y_s(\omega)} \right]^{-1} . \tag{34}$$

Since for a given interior mode, p_1^i follows p_2^i , it is also possible to write

$$p_1^i(\bar{x}) = c_n \phi_n(\bar{x}) \ ,$$

where c_n is a constant. For such an approximation, another structure impedance model is found:

$$Z_1(\bar{x}) = \frac{c_n \phi_n(\bar{x})}{-i\omega \sum_s \frac{\psi^s(\bar{x})}{M_s Y_s} \int c_n \phi_n(\bar{x}') \psi^s(\bar{x}')\, d\bar{x}'}$$

$$= \phi_n(\bar{x}) \left[-i\omega \sum_r \frac{A\psi^r(\bar{x})}{M_r Y_r} f'(n,r) \right]^{-1} , \tag{35}$$

and the backing impedance depends not only on the structure, but on the prominent responding acoustic mode as well. Thus a precise calculation of β is a complex matter.

As will be seen, if the trim is fairly limp and absorptive, z_1 need not be very accurately determined to obtain β. In fact, in the present work, a simple model

$$z_1 = \rho c_0 - i\omega m$$

has been used.

Noise Reduction Calculation

This is obtained by setting $W_{in} = W_{diss}$ from Eqs.(22) and (29), solving for the mean square modal pressures $\langle p_n^2 \rangle_{s,t}$ one-by-one, and adding according to

$$\langle p_i^2 \rangle_{s,t} = \sum_n \langle p_n^2 \rangle_{s,t} \, .$$

The result is found to be

$$\begin{aligned}
\frac{\langle p_i^2 \rangle_{s,t}}{\langle p_e^2 \rangle_{s,t}} = \frac{8}{c_\omega \omega} \frac{A^2}{V^2} \left(\frac{mA}{4}\right)^2 \tau_{ML} \left| C^w \right|^2 c_0^2 \omega^3 \\
\cdot \sum_n \epsilon_n \sum_r \frac{j_r(\omega) \, f'^2(n,r)}{M_r^2 \, D_{nr}} \left\{ \left(\frac{c_r - c_n}{4}\right) \ln_n \right. \\
+ \left(\frac{2c_n(b_r - b_n) - b_n(c_r - c_n)}{4\eta_n \omega_n^2} \right) \arctan_n \\
\left. + \left(\frac{c_n - c_r}{4}\right) \ln_r + \left(\frac{2c_r(b_n - b_r) - b_r(c_n - c_r)}{4\eta_r' \omega_r^2} \right) \arctan_r \right\} ,
\end{aligned} \tag{36}$$

where the space average mean square pressure $\langle p_e^2 \rangle_{s,t}$ is (for the reverberant field) related to the mean square blocked pressure by

$$\langle p_e^2 \rangle_{s,t} = \langle p_{bl}^2 \rangle / 2 \, .$$

$|C^w|^2$ = trim addition transmission coefficient.

η_r' = modified structural loss factor.

The noise reduction is

$$NR = -10 \log \frac{\langle p_i^2 \rangle_{s,t}}{\langle p_e^2 \rangle_{s,t}} .$$

<u>High Frequencies</u>

Without trim, from the Phase I work

$$W_{in} = \left\{ \frac{A \tau_R}{4 \rho c_o} + \frac{8}{\pi} \frac{A^2}{m^2} \frac{\rho}{c_o} \sum_{r < \Delta\omega} \left[j_r^{2\,rev.}(\omega) \right]^2 \right\} \langle p_e^2 \rangle_{s,t}$$

$$- \left\{ \frac{\bar{\eta}_r}{\eta_{rad}^{ext}} \frac{A \tau_R}{4 \rho c_o} + \frac{8}{\pi} \frac{A^2}{m^2} \frac{\rho}{c_o} \sum_{r < \Delta\omega} \left[j_r^{2\,rev.}(\omega) \right]^2 \right\} \langle p_i^2 \rangle_{s,t} . \quad (37)$$

In the above expression, the second term represents a power flow through the panel (structure) outwardly. The transmitting area is A.

In the case of an added trim, there are three areas of concern: 1) the transmitting area with trim, which will be called A_t, 2) the absorbing surface area S, and 3) the transmitting area without trim A'. The total transmitting area is

$$A = A_t + A' ,$$

and the inflowing power takes the form

$$W_{in} = \left\{ \frac{A_t \tau_R}{4\rho c_o} + \frac{8AA_t}{\pi m^2} \frac{\rho}{c_o} \sum_{r<\Delta\omega} \left[j_r^{2\,rev.}(\omega) \right]^2 \right\} \tau_t \langle p_e^2 \rangle_{s,t}$$

$$+ \left\{ \frac{A' \tau_R}{4\rho c_o} + \frac{8AA'}{\pi m^2} \frac{\rho}{c_o} \sum_{r<\Delta\omega} \left[j_r^{2\,rev.}(\omega) \right]^2 \right\} \langle p_e^2 \rangle_{s,t}$$

$$- \left\{ \frac{\bar{\eta}_r A' \tau_R}{\eta_{rad}^{ext}(4\rho c_o)} + \frac{8AA'}{\pi m^2} \frac{\rho}{c_o} \sum_{r<\Delta\omega} \left[j_r^{2\,rev.}(\omega) \right]^2 \right\} \langle p_i^2 \rangle_{s,t} . \quad (38)$$

$\bar{\eta}_r$ is the sum of the average external radiation loss factor, i.e., η_{rad}^{ext} , and the average structural loss factor η_r'. τ_t is the trim transmission coefficient, and τ_R is the resonance transmission coefficient for the diffuse field case.

$$\tau_R = \left(2 n_r \pi^2 c_o \eta_{rad}^{ext} \eta_{rad}^{int} / \rho \omega \bar{\eta}_r \right) \cdot \left(4\rho c_o / A \right).$$

In this expression n_r is the modal density of the fuselage structure (modes/rad/sec).

The radiation loss factors for a diffuse field are given by

$$\eta_{rad}^{ext} = \frac{2\rho_0 \omega A}{\pi m c_0} < j_r^2(\omega) >_r$$

$$\eta_{rad}^{int} = \frac{2\rho \omega A}{\pi m c_0} < j_r^2(\omega) >_r \quad ,$$

where $< j_r^2 >_r$ is the joint acceptance averaged over the structural modes resonant in the band.

Let τ_f = field incidence transmission coefficient for mass controlled panels

$$\tau_f \equiv \frac{32}{\pi} \rho^2 \frac{A}{m^2} \sum_{r < \Delta\omega} \left[j_r^{2\,rev.}(\omega) \right]^2 ,$$

as defined in Phase I.[1] Then Eq. (38) becomes

$$\begin{aligned} W_{in} = & \left[\frac{\tau_t A_t}{4\rho c_0} (\tau_R + \tau_f) + \frac{A'}{4\rho c_0} (\tau_R + \tau_f) \right] < p_e^2 >_{s,t} \\ & - \left[\left(\frac{\bar{\eta}_r}{\eta_{rad}^{ext}} \tau_R + \tau_f \right) \frac{A'}{4\rho c_0} \right] < p_i^2 >_{s,t} \\ = & \frac{1}{4\rho c_0} \left[\tau_t (\tau_R + \tau_f) A_t + (\tau_R + \tau_f) A' \right] < p_e^2 >_{s,t} \\ & - \frac{A'}{4\rho c_0} \left[\frac{\bar{\eta}_r}{\eta_{rad}^{ext}} \tau_R + \tau_f \right] < p_i^2 >_{s,t} . \end{aligned} \quad (39)$$

[1] Eq.(16), Ref.[1], p. 20 is incorrectly typed. A should not be squared.

The power absorbed is

$$W_{diss} = \frac{\bar{\alpha} S}{4\rho c_o} < p_i^2 >_{s,t} . \tag{40}$$

S includes the area A covered with trim and any other absorbing surface area. Equating W_{in} to W_{diss} gives the desired high frequency result

$$\frac{< p_e^2 >_{s,t}}{< p_i^2 >_{s,t}} = \frac{\bar{\alpha} S + \left[\tau_f + \tau_R (\bar{\eta}_r / \eta_{rad}^{ext}) \right] A'}{\tau_t (\tau_f + \tau_R) A_t + (\tau_R + \tau_f) A'} .$$

Letting $\tau_f + \tau_R = \tau$ gives

$$\frac{< p_e^2 >_{s,t}}{< p_i^2 >_{s,t}} = \frac{\bar{\alpha} S + \left[\tau_f + \tau_R (\bar{\eta}_r / \eta_{rad}^{ext}) \right] A'}{\tau_t \tau A_t + \tau A'} . \tag{41}$$

This is the fundamental result with trim present. Note that if all transmitting surface is covered with trim, $A' = 0$, and

$$\frac{< p_e^2 >_{s,t}}{< p_i^2 >_{s,t}} = \frac{\bar{\alpha} S}{\tau_t \tau A_t} = \frac{\bar{\alpha} S}{\tau_t \tau A} .$$

On the other hand, if trim does not exist, $\tau_t = 1$, $A_t = 0$, and

$$\frac{< p_e^2 >_{s,t}}{< p_i^2 >_{s,t}} = \frac{\bar{\alpha} S + \left[\tau_f + \tau_R (\bar{\eta}_r / \eta_{rad}^{ext}) \right] A}{\tau A} ,$$

which is the Phase I result without trim.

Finally, $\bar{\alpha}$ is estimated with the relation

$$\bar{\alpha} = \frac{4\omega V}{c_o S} \bar{\eta}_n \; . \tag{42}$$

If $\bar{\eta}_n$ is calculated (say with trim only absorbing), Eq.(28) is applicable.

3.2 Influence of the Internal Radiation Damping

It has been found previously that, in the relation for the band-limited power flow to the cavity, there appears an integral

$$\int_{\Delta\omega} \frac{\omega^3 d\omega}{|\bar{\lambda}_n^2 - k^2|^2 \, |M_r Y_r - \rho\omega^2 (J^{rr} + I^{rr})|^2} \, .$$

In Ref.[1], this was evaluated after redefining η_r to be the sum of the structure's dissipative and external radiation loss factors and by neglecting the internal radiation losses. This allowed the term in the integral with J^{rr} to be incorporated into Y_r and the term with I^{rr} to be neglected. When this was done, the above was reduced to

$$\int_{\Delta\omega} \frac{\omega^3 d\omega}{|\bar{\lambda}_n^2 - k^2|^2 \, M_r^2 |Y_r|^2} \, ,$$

where

$$|\bar{\lambda}_n^2 - k^2|^2 = \frac{\omega_n^4}{c_o^4} \left[(1 - \omega^2/\omega_n^2)^2 + \eta_n^2 \right] ,$$

and

$$|Y_r|^2 = \omega_r^4 \left[(1 - \omega^2/\omega_r^2)^2 + \eta_r^2 \right] ,$$

with

$$\eta_r = \eta_r^{\text{structure}} + \eta_r^{\text{ext rad}} .$$

The integral becomes

$$\frac{c_0^4}{M_r^2 \omega_r^4 \omega_n^4} \int_{\Delta\omega} \frac{\omega^3 d\omega}{\left\{\left[1 - \frac{\omega^2}{\omega_n^2}\right]^2 + \eta_n^2\right\}\left\{\left[1 - \frac{\omega^2}{\omega_r^2}\right]^2 + \eta_r^2\right\}} ,$$

which appears in Eq.(3) of Reference [3]. It has just been shown in Section 3.1 that when trim is present the loss factor η_r above is replaced by η_r' where

$$\eta_r'^2 = \frac{|C_w|^2}{m\omega_r^4} - 2\frac{C_w^I}{m}\frac{\eta_r}{\omega_r^2} + \eta_r^2 .$$

Now for increased precision, the question must be asked: what if the term involving $I^{rr}(\omega)$ is <u>not</u> neglected? In this case, consider

$$\left| M_r Y_r - \rho\omega^2 I^{rr} \right|^2$$

$$= M_r^2 \left| Y_r(\omega) - \frac{\rho\omega^2}{M_r} I^{rr}(\omega) \right|^2 ,$$

where

$$I^{rr}(\omega) = \frac{A^2}{V} \sum_n \frac{\epsilon_n f'^2(n,r)}{(\bar{\lambda}_n^2 - k^2)} .$$

Consider a case where $\omega_n \in \Delta\omega$ and close to ω_r ; then consider a single acoustic mode, say mode n .

$$Y_r - \frac{\rho\omega^2}{M_r} I^{rr}$$

$$= Y_r - \frac{\rho\omega^2 A^2 \epsilon_n c_o^2 f'^2_{(n,r)} \left[\left(1 - \frac{\omega^2}{\omega_n^2}\right) + i\eta_n\right]}{M_r V \omega_n^2 \left[\left(1 - \frac{\omega^2}{\omega_n^2}\right)^2 + \eta_n^2\right]} .$$

This becomes

$$\omega_r^2 \left\{ \left(1 - \frac{\omega^2}{\omega_r^2}\right) - \frac{\rho\omega^2 A^2}{M_r V} \frac{\epsilon_n c_o^2 f'^2_{(n,r)}}{\omega_r^2 \omega_n^2} \frac{\left[1 - \frac{\omega^2}{\omega_n^2}\right]}{\left[\left(1 - \frac{\omega^2}{\omega_n^2}\right)^2 + \eta_n^2\right]} \right.$$

$$\left. - i \left[\eta_r + \frac{\rho\omega^2 A^2}{M_r V} \frac{\epsilon_n c_o^2 f'^2_{(n,r)}}{\omega_r^2 \omega_n^2} \frac{\eta_n}{\left[\left(1 - \frac{\omega^2}{\omega_n^2}\right)^2 + \eta_n^2\right]} \right] \right\} .$$

Now it can be shown that the non-dimensional form

$$\gamma = \frac{\rho\omega^2 A^2}{M_r V} \frac{\epsilon_n c_o^2 f'^2_{(n,r)}}{\omega_r^2 \omega_n^2} \ll 1 .$$

For instance, for the stiffened 0.020" cylinder of this study, for the two modes

$$n = (1,2,1) \; ; \quad r = (2,2) \text{ in 630 Hz band}$$

$$\epsilon_n = \epsilon_{1,2,1} = 29.59$$

$$f'(n,r) = 0.1023$$

$$\omega_n = 672 \times 2\pi \quad ; \quad \omega_r = 660 \times 2\pi$$
$$\rho = 1.204 \text{ kg/m}^3$$
$$\omega = 630 \times 2\pi \pm \Delta\omega/2 \quad ; \quad \Delta\omega = C_\omega \omega$$
$$M_r = mA/4 \quad ; \quad m = 4.29 \text{ kg/m}^2$$
$$c_o = 343 \text{ m/sec}$$
$$A = 1.89 \text{ m}^2 \text{ (surface of cylinder)}$$
$$V = 0.243 \text{ m}^3$$
and
$$\gamma = 0.016 \, .$$

As ω ranges across the band, the reactance term

$$\gamma \frac{\left[1 - \frac{\omega^2}{\omega_n^2}\right]}{\left[\left(1 - \frac{\omega^2}{\omega_n^2}\right)^2 + \eta_n^2\right]} \, ,$$

takes the following values:

If $\omega < \omega_n$; $\left[1 - \frac{\omega^2}{\omega_n^2}\right]^2 \gg \eta_n^2$ and

$$\simeq \frac{\gamma}{\left[1 - \omega^2/\omega_n^2\right]} \, .$$

If $\omega > \omega_n$; $\left[1 - \frac{\omega^2}{\omega_n^2}\right]^2 \gg \eta_n^2$ and again

$$\simeq \frac{\gamma}{\left[1 - \omega^2/\omega_n^2\right]} \, .$$

If $\omega \cong \omega_n$ (very close)

$$\approx \frac{\epsilon}{\eta_n} \Rightarrow 0.$$

Thus the reactance term is always small (in air). This gives the approximate result as

$$Y_r - \frac{\rho\omega^2}{M_r} I^{rr} = \omega_r^2 \left\{ \left(1 - \frac{\omega^2}{\omega_r^2}\right) - i \left[\frac{\gamma \eta_n}{\left(1 - \frac{\omega^2}{\omega_n^2}\right)^2 + \eta_n^2} + \eta_r \right] \right\}$$

Now the structural mode appears to be damped more heavily, by an amount η_r'' given by

$$\eta_r'' = \frac{\gamma \eta_n}{\left[\left(1 - \frac{\omega^2}{\omega_n^2}\right)^2 + \eta_n^2\right]} \cdot \tag{43}$$

For any given spectral component at frequency ω, we see that since η_r and η_r'' are small

$$Y_r - \frac{\rho\omega^2}{M_r} I^{rr},$$

is dominated by the reactance term $1 - \omega^2/\omega_r^2$, unless ω is very close to ω_r. When ω is close to ω_r, the resistance term

$$\eta_r + \eta_r''$$

becomes important. Moreover, if simultaneously ω_n lies close by, η_r'' can be significantly large. Thus, a frequency independent form of the resistance can be used and the following approximation is assumed to apply

$$Y_r - \frac{\rho\omega^2}{M_r} I^{rr} = \omega_r^2 \left[\left(1 - \frac{\omega^2}{\omega_r^2}\right) - i\left(\eta_r + \eta_r''\right) \right],$$

where

$$\eta_r'' = \frac{\gamma \eta_n}{\left[\left(1 - \frac{\omega_r^2}{\omega_n^2}\right)^2 + \eta_n^2\right]}.$$

When trim is present

$$\eta_r \rightarrow \eta_r'.$$

3.3 Transmission of a Tone

In the case where trim is present, assuming hereafter, that a floor will always be considered, the tone transmission calculation of Ref.[1] can be generalized to obtain the solution for the inflowing power to the cabin, i.e.,

$$W_{in} = \frac{2\pi}{\rho V}\left(\frac{mA}{4}\right)^2 \hat{T}_{ML}^{o} \hat{T}_{t}^{o} \frac{2}{\pi} \omega_o^2 \sum_n \frac{\epsilon_n \eta_n}{\omega_n^2}$$

$$\cdot \sum_r \frac{f'^2_{(n,r)}}{M_r^2 \omega_r^4} \iint_{\bar{x}\,\bar{x}'} C_{P_{bl}}(\bar{x}|\bar{x}')\, \psi^r(\bar{x})\, \psi^r(\bar{x}')\, d\bar{x}\, d\bar{x}'$$

$$\cdot \frac{\omega_o^3}{\left[\left(1 - \frac{\omega_o^2}{\omega_n^2}\right)^2 + \eta_n^2\right]\left[\left(1 - \frac{\omega_o^2}{\omega_r^2}\right)^2 + \left(\eta_r' + \eta_r''\right)^2\right]}. \qquad (44)$$

η_r' and τ_t^o are used to include the trim. The above result is consistent with Eq.(33)of Ref.[1]. To review ω_o is the frequency of the tone. In the case of propeller noise, this equation will hold for the blade passage frequency and also for each of its harmonics. The correlation function $C_{p_{bl}}(\bar{x}|\bar{x}')$ describes the blocked pressure field over the fuselage (cylinder) and is defined using the following relations:

$$C_{p_{bl}}(\bar{x}|\bar{x}')\,\delta(\omega-\omega_o) = C_{p_{bl}}(\bar{x}|\bar{x}';\omega)\,, \tag{45}$$

$$C_{p_{bl}}(\bar{x}|\bar{x}';\omega) = 2\,\bar{C}_{p_{bl}}(\bar{x}|\bar{x}';\omega)\;;\quad 0 \le \omega < \infty\,, \tag{46}$$

$$\bar{C}_{p_{bl}}(\bar{x}|\bar{x}';\omega) = \mathrm{Re}\left[\frac{1}{2\pi}\int_{-\infty}^{\infty} R_{p_{bl}}(\bar{x}|\bar{x}';\tau)\,e^{i\omega\tau}d\tau\right], \tag{47}$$

where $R_{p_{bl}}(\bar{x}|\bar{x}';\tau)$ is the average cross correlation of the pressure over the blocked (immobile) fuselage.

$$R_{p_{bl}}(\bar{x}|\bar{x}';\tau) = \lim_{T\to\infty}\frac{1}{T}\int_{-\frac{T}{2}}^{\frac{T}{2}} \mathrm{Re}\left[p_{bl}(\bar{x},t)\right]\mathrm{Re}\left[p_{bl}(\bar{x}',t+\tau)\right]dt. \tag{48}$$

A major task for Phase III is to develop a suitable representation of $C_{p_{bl}}(\bar{x}|\bar{x}')$ for propeller excitation.

The power inflow to the cabin wall from the interior is as before

$$W_{diss} = \frac{V}{\rho c_o^2}\sum_n \frac{\eta_n \omega_n^2}{\omega_o} \langle p_n^2 \rangle_{S,t}\,. \tag{49}$$

Equating Eqs. (44) and (49) gives the interior space average mean square pressure attributable to the nth acoustic mode.

The interior space-average mean square pressure is given (again) as the sum of the space average mean square modal pressures:

$$\langle p_i^2 \rangle_{s,t} = \sum_n \langle p_n^2 \rangle_{s,t} \, . \tag{50}$$

The average interior pressure ultimately must be related to a significant exterior level, say the maximum occurring nearest the propeller plane.

Note, since

$$\langle p_n^2 \rangle_{s,t} = \frac{\langle p_n^2 \rangle}{V} \int \phi_n^2 \, d\bar{v} \, ,$$

where $\langle p_n^2 \rangle$ is the mean square modal amplitude, the modal amplitude is determinable from

$$\langle p_n^2 \rangle = \epsilon_n \langle p_n^2 \rangle_{s,t} \, ,$$

and theoretically, the mean square pressure at every interior point can be obtained with

$$\langle p_i^2(\bar{\xi}, \omega) \rangle_t = \sum_n \epsilon_n \langle p_n^2 \rangle_{s,t} \, \phi_n^2(\bar{\xi}) \, . \tag{51}$$

It is emphasized here that a good point-by-point prediction may require better input data than can ever be generated, but the point-by-point prediction might be quite informative nevertheless.

3.4 Modal Properties of the Cabin Space (Cylinder with Floor)

In Ref.[1], the acoustic modal characteristics of an ideal cylindrical cavity were presented and various quantities were calculated with the modal data for use in making the interior sound level predictions. The modal data consisted of the mode shapes $\phi_n(\bar{\xi})$, $\bar{\xi}$ being an interior point, resonance frequencies ω_n, and the mode normalization given by the constant ϵ_n. In the present case, consideration must be given to the determination of the same quantities for the case of a cylinder with a floor partition defined by the angle θ_0 as shown in Figure 5.

In the ideal cylinder configuration the modal properties can be determined in closed form by an analytical solution of the wave equation, subject to the appropriate boundary conditions. This is possible because the wave equation is separable in cylindrical coordinates and the boundary conditions can be expressed in these coordinates. When the floor is present, it is no longer possible to derive the mode shapes analytically since the boundary conditions are irregular. Thus it is necessry to resort to numerical methods. There are two possibilities, either finite differences or finite elements. Since in the present case, the modal characteristics in the axial direction are known, a two-dimensional problem remains, and thus the finite difference technique, which is the simpler of the two is chosen. In two dimensions, the finite difference calculations are fairly efficient (fast).

To begin, the two-dimensional problem is solved. Then the axial modal information is factored in. Next the normalization of the data is defined. Finally, use of the data in the calculation of the various quantities required by Eq.(36) is considered.

Finite Difference in Two Dimensions

In the cavity (cabin), the Helmholtz equation applies. In the two-dimensional problem, this is

$$\nabla^2\phi + k^2\phi = 0,$$

where

$$\nabla^2 = \frac{\partial^2}{\partial X^2} + \frac{\partial^2}{\partial Y^2} .$$

The central differences for the grid shown in Figure 6 are:

$$\frac{\partial \phi_{mn}}{\partial X} = \frac{P_{m+1,n} - P_{m-1,n}}{2\Delta X}$$

$$\frac{\partial \phi_{mn}}{\partial Y} = \frac{P_{m,n+1} - P_{m,n-1}}{2\Delta Y}$$

$$\frac{\partial^2 \phi_{mn}}{\partial X^2} = \frac{P_{m+1,n} - 2P_{m,n} + P_{m-1,n}}{(\Delta X)^2}$$

$$\frac{\partial^2 \phi_{mn}}{\partial Y^2} = \frac{P_{m,n+1} - 2P_{m,n} + P_{m,n-1}}{(\Delta Y)^2} ,$$

where P and ϕ are taken to be synonymous. Let

$$\Delta X = \Delta Y = h.$$

Then the Helmholtz equation becomes

$$4P_{m,n} - P_{m+1,n} - P_{m-1,n} - P_{m,n+1} - P_{m,n-1} = k^2h^2P_{m,n} \qquad (52)$$

Eq.(52) applies for all points defined as interior (I) or boundary (B).

For boundary point B, exterior points E are required to write the finite difference equation. The total number of unknowns is the sum of all I + B + E points (Figure 6b). The number of boundary conditions that must be used is equal to the number necessary to eliminate all E's. The resulting matrix for determining the eigenvalues and vectors is

$$[A]\left\{\frac{I}{B}\right\} = \bar{k}^2\left\{\frac{I}{B}\right\} = \lambda\left\{\frac{I}{B}\right\} ,$$

where

$$\bar{k}^2 = k^2 h^2 .$$

Given the eigenvalue λ, the associated resonance frequency is obtained with

$$\frac{\omega^2 h^2}{c_0^2} = \lambda ,$$

or

$$\frac{2\pi f}{c_0} h = \sqrt{\lambda} ,$$

and thus

$$f_i = \frac{c_0\sqrt{\lambda_i}}{2\pi h} .$$

(λ_i is ordered such that $\lambda_{i-1} < \lambda_i < \lambda_{i+1}$).

This is the resonance frequency for $q = 0$, q = axial index, i.e.,

$$k_q = q\pi/L .$$

The resonance frequencies for the cavity are obtained with

$$k_{qi}^2 = k_q^2 + \frac{\lambda_i}{h^2} ,$$

leading to

$$f_{qi} = \frac{c_0}{2\pi}\left[k_q^2 + \frac{\lambda_i}{h^2}\right]^{\frac{1}{2}} .$$

<u>Boundary Conditions</u>

The boundary condition is that the outward normal gradient is zero (the wall admittance β is assumed to be sufficiently small to allow this assumption). Thus, referring to Figure 7

$$\left.\frac{\partial\phi}{\partial r}\right)_{\theta_0 < \theta < 2\pi - \theta_0} = 0,$$

where

$$\frac{\partial\phi}{\partial r} = \left(\frac{\partial\phi}{\partial x}\right)\left(\frac{\partial x}{\partial r}\right) + \left(\frac{\partial\phi}{\partial y}\right)\left(\frac{\partial y}{\partial r}\right) .$$

This gives

$$\frac{\partial\phi}{\partial x}\cdot\frac{\partial x}{\partial r} = -\frac{\partial\phi}{\partial y}\cdot\frac{\partial y}{\partial r} ,$$

or

$$\frac{\partial\phi}{\partial x}\cos\theta = -\frac{\partial\phi}{\partial y}\sin\theta .$$

Now m,n are the X,Y indices: increasing m implies increasing X; increasing n implies increasing Y. From Figure 7

$$\frac{\partial \phi}{\partial x} = -\frac{\partial \phi}{\partial Y} \quad ; \quad \frac{\partial \phi}{\partial y} = \frac{\partial \phi}{\partial X} \quad .$$

This gives the boundary condition as

$$\frac{\partial \phi}{\partial Y} \cos\theta = \frac{\partial \phi}{\partial X} \sin\theta \ ,$$

where

$$\frac{\partial \phi}{\partial Y} = \frac{P_{m,n+1} - P_{m,n-1}}{2h}$$

$$\frac{\partial \phi}{\partial X} = \frac{P_{m+1,n} - P_{m-1,n}}{2h} \ .$$

Therefore, the boundary condition in the region $\theta_0 < \theta < 2\pi - \theta_0$ is

$$(P_{m,n+1} - P_{m,n-1}) \cos\theta_{mn} = (P_{m+1,n} - P_{m-1,n}) \sin\theta_{mn} \cdot \quad (53)$$

In the region $-\theta_0 < \theta < \theta_0$, the boundary condition above can be applied by simply setting $\theta_{mn} = 0$ whenever $\theta_{mn} < \theta_0$.

Details of Calculation

The origin of the rectangular coordinate system is at the floor centerline (capital X and Y in Figure 7) and the cavity is symmetric about X = 0, so only half of the cylinder is considered. The approximate grid spacing chosen is a/7. The exact grid spacing is

$$h = Ga = a \frac{(1+\cos\theta_0)}{\text{Integral Part}\left[7(1+\cos\theta_0)\right]} .$$

This gives an integral number of grid points between the floor and top of the cylinder. The location of the grid points is (NX, NY) at spacing h for

$$NX = -NJ \text{ to } +NJ ,$$

and

$$NY = 0 \text{ to } NK ,$$

where

$$NK = \text{Integral Part}\left[7(1+\cos\theta_0)\right] ,$$

and

$$NJ = \text{Integral Part}\left[\frac{1}{G}+1\right] .$$

The centerline of the fuselage has the coordinates $(0, a\cos\theta_0)$.

To select the grid points representing the curved surface of the cylinder, for a given value of $Y = NY \cdot Ga$, the 2 grid points are identified which lie just inside the cylinder and just outside the cylinder in the following way:

The intersection of the circle with the line $Y = NY \cdot Ga$ is given by

$$X_b = a\left[1 - (\cos\theta_0 - NY \cdot G)^2\right]^{1/2}.$$

The last point inside the cylinder is (NXI, NY), where

$$NXI = \text{Integral part}\left[\frac{1}{G}\left\{1 - (\cos\theta_0 - NY \cdot G)^2\right\}^{1/2}\right].$$

The first point outside the cylinder is $(NXI+1, NY)$. The distance of point (NX, NY) from the boundary of the cylinder is

$$a\left|1 - \left\{(\cos\theta_0 - NY \cdot G)^2 + (NX \cdot G)^2\right\}^{1/2}\right|.$$

A test is performed on the 2 points (NXI, NY) and $(NXI+1, NY)$ to see which point is closest to the cylinder boundary. If the outside point is closest, then it must be included as part of the cylinder.

This procedure is repeated for successive values of NY for $NY=0$ to $NY=NK$.

This will not identify all the boundary points and adjacent exterior points, and a similar procedure is performed for successive values of NX.

The line $X = NX \cdot Ga$ can intersect the cylinder boundary in 2 places, depending upon whether

$$NY \cdot G < \cos\theta_0 \quad \text{or} \quad NY \cdot G > \cos\theta_0.$$

If

$$NY \cdot G < \cos\theta_0,$$

at the floor for

$$NX \cdot G < \sin \theta_0 ,$$

the boundary points are given by $NY = 0$. If

$$NY \cdot G < \cos \theta_0 ,$$

and

$$NX \cdot G > \sin \theta_0 ,$$

the intersection of the circle with $X = NX \cdot Ga$ is given by

$$Y_b = a\left\{ \cos \theta_0 - \left[1 - (NX \cdot G)^2 \right]^{1/2} \right\} .$$

The first point outside the cylinder is $(NX, NYI-1)$, where

$$NYI-1 = \text{Integral Part} \left\{ \frac{1}{G} \left[\cos \theta_0 - \left(1 - (NX \cdot G)^2 \right)^{1/2} \right] \right\} .$$

The first point inside the cylinder is (NX, NYI).

Again the distance from these 2 points to the cylinder boundary is compared, and the point closest to the boundary is included as part of the cylinder.

Now in the case

$$NY \cdot G > \cos \theta_0 ,$$

the intersection of the circle with $X = NX \cdot Ga$ is

$$Y_b = a\left\{ \cos \theta_0 + \left[1 - (NX \cdot G)^2 \right]^{1/2} \right\} .$$

The last point inside the cylinder is (NX, NYI) where

$$NYI = \text{Integral Part} \left\{ \frac{1}{G} \left[\cos \theta_0 + \left(1 - (NX \cdot G)^2 \right)^{1/2} \right] \right\} .$$

The first point outside the cylinder is $(NX, NYI+1)$.

Again the distance to the cylinder boundary is used to select the closest point..

In this manner, the following grid points are therefore identified:-

1) Cylinder interior and boundary points (total = n_i)

2) Cylinder boundary points (total = n_b)

3) External points adjacent to boundary points (total = $n_e = n_b + 2$).

These represent only half the cylinder, since the cavity is symmetric about X = 0. Therefore the total number of cylinder points is

$$2n_i - (NK+1) ,$$

where

$$NK = \text{Integral part}\left[7(1+\cos\theta_0)\right].$$

The total number of boundary points is

$$2n_b - 2 .$$

Let

$\left\{P_I\right\}_{n_i \times 1}$ = pressure at cylinder points (interior + boundary)

$\left\{P_E\right\}_{n_e \times 1}$ = pressure at exterior points, adjacent to cylinder points only.

Using the recurrence relationship for all points I, i.e., Eq.(52), gives

$$\underset{(n_i \times n_i)}{\left[RI\right]}\underset{(n_i \times 1)}{\left\{P_I\right\}} + \underset{(n_i \times n_e)}{\left[RE\right]}\underset{(n_e \times 1)}{\left\{P_E\right\}} = \lambda \underset{(n_i \times 1)}{\left\{P_I\right\}} .$$

For symmetric modes, symmetric about X = 0, when m = 0,

$$P_{-1,n} = P_{1,n} .$$

For antisymmetric modes, antisymmetric about X = 0

$$P_{-1,n} = -P_{1,n} .$$

The matrices $\left[RI\right]$ and $\left[RE\right]$ will be different for symmetric and antisymmetric modes.

The number of points forming the boundary of the cylinder is equal to the number of exterior points adjacent to the cylinder minus 2, i.e.,

$$n_e = n_b + 2 .$$

For each point (m,n) on the boundary of the cylinder the boundary condition for $\theta_{mn} > \theta_o$ is

$$\left[P_{m,n+1} - P_{m,n-1}\right]\cos\theta_{mn} = \left[P_{m+1,n} - P_{m-1,n}\right]\sin\theta_{mn} ,$$

and for $\theta_{mn} < \theta_o$, the above with $\theta_{mn} = 0$.

These boundary conditions give n_b equations, and 2 more equations are required to solve for the n_e exterior pressures $\{P_e\}$.

Two boundary points are selected, close to $\theta = \pi/4$ and $\theta = 3\pi/4$, such that each of these boundary points is adjacent to exterior points in both the X - direction and the Y - direction.

At both of these boundary points, (m,n), it is assumed that

$$P_{m+1,n} - P_{m-1,n} = 0,$$

i.e., the gradient in the X - direction is zero (the gradient normal to the surface has already been equated to zero).

This gives a total of $n_e = n_b + 2$ equations, giving

$$\underset{(n_e \times n_i)}{[BI]}\underset{(n_i \times 1)}{\{P_I\}} + \underset{(n_e \times n_e)}{[BE]}\underset{(n_e \times 1)}{\{P_E\}} = 0. \tag{55}$$

The matrix $[BE]$ is non-singular and

$$\{P_E\} = -[BE]^{-1}[BI]\{P_I\}. \tag{56}$$

Substituting this gives

$$\left[\underset{(n_i \times n_i)}{[RI]} - \underset{(n_i \times n_e)}{[RE]}\underset{(n_e \times n_e)}{[BE]^{-1}}\underset{(n_e \times n_i)}{[BI]}\right]\underset{(n_i \times 1)}{\{P_I\}} = \lambda \underset{(n_i \times 1)}{\{P_I\}}. \tag{57}$$

The eigenvalues and eigenvectors are calculated for symmetric and antisymmetric modes, separately.

The nodes, n_i , represent only half the cylinder (i.e., X > 0) and the generalized mass must be calculated for the whole cylinder. The generalized mass for mode i is

$$\Phi_G(i) = \sum_{j=1}^{n_i} \phi_i^2(j)\, h^2 \times C(j) \;,$$

where $h = Ga$ is the distance between grid points.

$C(j)$ is a factor, either 1 or 2:

$$C(j) = \begin{cases} 1 \text{ for all locations on the centerline, i.e., } X = 0 \\ 1 \text{ for all locations on the cylinder boundary} \\ 2 \text{ for all other locations.} \end{cases}$$

The boundary values of the eigenvectors are extracted from the i eigenvectors, and are defined for X ≥ 0 only. The boundary points must be consecutive along the circumference of the cylinder from the floor centerline (0,0) to the top centerline (0,NK).

The boundary eigenvectors will differ for symmetric and antisymmetric modes for X < 0. For symmetric modes

$$\phi(X,Y) = \phi(-X,Y).$$

For antisymmetric modes

$$\phi(X,Y) = -\,\phi(-X,Y).$$

Each mode must therefore be identified as symmetric or antisymmetric when the boundary eigenvectors are used.

Apart from the boundary eigenvectors, there is no need to distinguish between symmetric and antisymmetric modes in the cylinder response program. The modes are therefore combined, and ranked in ascending order of frequency and the first 20 modes only are used.

The first symmetric mode is a translation mode, with zero frequency and corresponds to the cylinder $(0,0,1)$ mode.

The eigenvalues, λ_i, are used to calculate the resonance frequencies for the (three dimensional) cabin with

$$f_n = f_{qi} = \frac{c_0}{2\pi}\left[\left(\frac{q\pi}{L}\right)^2 + \frac{\lambda_i}{h^2}\right]^{1/2}, \tag{58}$$

where h is the grid spacing = Ga, L and a are the cylinder length and radius, respectively.
The frequencies output by the program are

$$f_i = \frac{c_0}{2\pi G}\sqrt{\lambda_i}\ ,$$

i.e., the frequency for $q=0$ modes and $a=1m$, i.e., for unit radius. The generalized mass is also output for a cylinder of unit radius, i.e.,

$$h^2 = G^2 a^2\ ,$$

where $a = 1m$.

Normalization

The acoustic modes ϕ_n for the three dimensional cabin are

$$\phi_n(\bar{\xi}) = \phi_n(X,Y,z) = \phi_{qi}(X,Y,z) = \cos\frac{q\pi z}{L}\,\phi_i(X,Y),$$

where $\phi_i(X,Y)$ is the eigenvector for the two-dimensional mode ranked i $(i=1,20)$ as calculated with the finite difference technique; i.e., $\phi_i(X,Y)$ is a finite dimension column vector, which contains the values of ϕ_i at all coordinate positions (NX, NY) within and on the boundary of the cabin space.

The normalization of these modes is arbitrary. The maximum value achieved at any coordinate position has been chosen to be unity and the other values adjusted to retain the computed ratios from point-to-point. The normalization is carried into the transmission prediction with the parameter

$$\epsilon_n = \epsilon_{qi} = \frac{V}{\iiint \phi_n^2\, d\bar{v}}.$$

In the case where the floor is present the integral is

$$\iiint \phi_{qi}^2(\bar{\xi})\, d\bar{v} = \left[\int_0^L \cos^2\frac{q\pi z}{L}\, dz\right] \sum_{Area} \phi_i^2\, dArea$$

$$= \frac{L}{2}\,\epsilon_q \sum_{j=1}^{n_i} \phi_i^2(j)\, h^2\, C(j),$$

where j counts over all interior locations, and

$$\epsilon_q = \begin{cases} 2 \; ; & q=0 \\ 1 \; ; & q>0 \end{cases} .$$

The program outputs the generalized mass for unit radius, i.e.,

$$\Phi_G(i) = \sum_{j=1}^{n_i} \phi_i^2(j)\, G^2 C(j) .$$

So

$$\iiint \phi_{qi}^2(\bar{\xi})\, d\bar{v} = \frac{L}{2} \epsilon_q a^2 \Phi_G(i) .$$

The volume enclosed is

$$V = a^2 L \left[\pi - \theta_0 + \cos\theta_0 \sin\theta_0 \right],$$

giving

$$\epsilon_n = \epsilon_{qi} = \frac{2\left[\pi - \theta_0 + \cos\theta_0 \sin\theta_0\right]}{\Phi_G(i)\, \epsilon_q} . \tag{59}$$

3.5 Fuselage Structural Model

In the previous work [1], the basic structural model was for an ideal cylindrical shell, i.e., one without stiffeners or floor. In the present work, the inclusion of the orthotropic properties of the cylindrical shell and the effects caused by the presence of the floor are of concern.

Altnougn the level of sophistication achieved in the present modeling effort is considerable, it is nevertheless to be considered incomplete and further work will be done on the structural representation in Phase III.

The basic analytical technique used to predict the resonance frequencies of the ring-stringer stiffened shell is that of Mikulas and McElman [7]. In this calculation, the effect of the stiffeners are considered in terms of a "smeared out" model. This model is chosen because it is felt that it gives reasonably good predictions when applied to a stiffened cylinder of typical aircraft construction, i.e., one in which the "density" of rings and stringers is sufficient to warrant the "smearing out" or averaging of the added stiffness and mass contributions to the shell. The Mikulas equation definitely breaks down when the subpanels between rings and stringers assume their own modal characteristics.

The test articles used in the present work are not ideally suited to use of the Mikulas formulation because of the sparsity of stiffeners. Nevertheless, the formulation is used and consideration given to its inaccuracies when applied to the test hardware.

The second effect of concern is that of the floor. In Ref.[8], it is shown that the primary influence of a floor partition in a cylindrical shell is to force nodes at the floor line, because of the high in-plane stiffness of the floor. Whether the floor is attached rigidly or with a pinned connection to the cylinder wall is of secondary importance, although some shift in the predicted resonance frequencies will occur. Therefore the chosen structural model of the fuselage (for Phase II) is a curved, orthotropic panel running from floor line-to-floor line (Figure 8a). The calculation is made with the Mikulas equation.

It is emphasized here that this model is of a preliminary nature. A better representation (planned for Phase III) will include the restraint offered by the floor itself and the remaining portion of the fuselage beneath the floor (see Fig.8b). Assuming that there are two modes which for the configurations of Figs.(8a) and (8b)

have the same shape above the floor line, it can be assumed that the lower resonance frequency would be that calculated for (8a), i.e., without the restraint offered by the floor and fuselage below the floor. However, even if the difference in the calculated frequencies is disregarded, there are other factors involved, namely that in the case where the floor and lower fuselage participate in the response, the upper fuselage (cabin wall) will not respond as well to the acoustic field exciting it because the excitation not only has to move the sidewall, in the latter case, it also has to move, simultaneously, the floor and fuselage beneath the floor. This "restraint" can be built into the model. The modes of the more complex configuration are required to do this. For this reason, it seems necessary to have a modal analysis of a configuration at least as complicated as (8b) and this is planned for Phase III. One can go another step and add, say, a wing. In that case, to shake the cabin wall, the floor, lower fuselage and the wing would have to be moved also. A modal analysis of a model including the wing would be required. In the latter case, a finite element modal analysis would be necessary.

Model for a Curved Orthotropic Panel

The resonance frequencies are calculated from the equation

$$\frac{\omega^2 m L^4}{\pi^4 D} = M^4(1+\beta^2)^2 + M^4\left[\frac{E_s I_s}{D\ell_y} + \beta^2\left(\frac{G_s J_s}{D\ell_y} + \frac{G_r J_r}{D\ell_x}\right) + \beta^4 \frac{E_r I_r}{D\ell_x}\right] + \frac{12 L^4(1-\mu^2)}{\pi^4 h^2 a^2}\left[\frac{1+\bar{S}\Lambda_s + \bar{R}\Lambda_r + \bar{S}\bar{R}\Lambda_{rs}}{\Lambda}\right] + \Delta p \frac{a}{2}\frac{M^2 L^2}{\pi^2 D}(1+2\beta^2) \quad , \tag{60}$$

where m = total mass/unit area (skin, stringer, and rings smeared out).

$\frac{E_r I_r}{D \ell_x} =$ ring bending parameter $\qquad \frac{E_s I_s}{D \ell_y} =$ stringer bending parameter

$\bar{R} = \frac{E_r A_r}{E h \ell_x} =$ ring membrane parameter $\qquad \bar{S} = \frac{E_s A_s}{E h \ell_y} =$ stringer membrane parameter

$$\Lambda_s = 1 + 2\alpha^2(\bar{z}_s/a)(\beta^2 - \mu) + \alpha^4(\bar{z}_s/a)^2(1+\beta^2)^2$$

$$\Lambda_r = 1 + 8N^2(\bar{z}_r/a)(1-\mu\beta^2) + 16N^4(\bar{z}_r/a)^2(1+\beta^2)^2$$

$$\Lambda = (1+\beta^2)^2 + 2\beta^2(1+\mu)(\bar{R}+\bar{S}) + (1-\mu^2)\left[\bar{S} + \beta^4\bar{R} + 2\beta^2\bar{R}\bar{S}(1+\mu)\right]$$

$$\Lambda_{rs} = 4N^2\alpha^2\left[\beta^2(1-\mu^2) + 2(1+\mu)\right](\bar{z}_s/a)^2 + 16N^4\left[1-\mu^2 + 2\beta^2(1+\mu)\right](\bar{z}_r/a)^2 + 8N^2(1-\mu^2)(\bar{z}_s/a) + 8N^2(1-\mu^2)(\bar{z}_r/a) + 32N^4(1-\mu)^2(\bar{z}_r/a)(\bar{z}_s/a) + 1-\mu^2.$$

$\Delta p =$ cabin pressure - exterior pressure

$\bar{z}_r$ and $\bar{z}_s$ are the distance to the centroid from the skin middle surface for ring and stringer, respectively, ℓ_x and ℓ_y are the ring and stringer spacings, E_r, E_s; I_r, I_s; A_r, A_s are the elastic modulii, moments of inertia, and areas of the stiffeners, and h is the skin thickness

$$\alpha = M\pi a/L,$$

where M is the number of axial halfwaves.

$$D = Eh^3/12(1-\mu^2),$$

is the skin bending rigidity.

$$\beta = 2NL/M\pi a,$$

where N is the number of circumferential half wavelengths.

It is again emphasized here that the above equation is strictly applicable to a full cylinder. It is also approximately applicable to an open cylindrical shell having all shear diaphragm supports. This boundary condition is obviously not satisfied at the cylinder floor junction. Because of this fact, the theory developed by Peterson and Boyd [8] which includes the full cylinder with floor, is far superior for present needs and will be integrated into the model in the future.

3.6 Calculation of the Structure/Acoustic Coupling Term f'(n,r) (Cylinder with Floor)

The circumferential structural mode shape for the curved panel (floor-to-floor) is given by

$$\psi^N(\theta) = \sin\frac{N\pi(\theta-\theta_0)}{2(\pi-\theta_0)} = \sin\frac{N\pi y}{L_y},$$

where N is the number of circumferential half waves and L_y is the length of the panel from floor-to-floor, i.e.,

$$L_y = 2a(\pi-\theta_0).$$

The acoustic mode eigenvector takes on discrete values on the boundary (as calculated with the finite difference technique). Consider the cylinder boundary point $j=(NX,NY)$. The angle is given by

$$\tan\theta_j = \frac{NX\cdot G}{\cos\theta_0 - NY\cdot G}.$$

The acoustic volume mode eigenvector on the boundary line θ_j is

$$\phi_{qi}(\theta,z) = \phi_i(\theta_j)\cos\frac{q\pi z}{L},$$

where $\phi_i(\theta_j)$ is the ith eigenvector from the finite difference calculation in 2 dimensions at boundary point $j = (NX, NY)$ and angle θ_j.

Let θ_{1j} and θ_{2j} define the points on the circumference half-way between boundary point (NX, NY) and the adjacent boundary points. Assume that the eigenvector $\phi_i(\theta_j)$ applies over the range θ_{1j} to θ_{2j}. Then

$$f'(n,r) = f'(qns, MN) \equiv f'(qi, MN)$$

$$= \frac{1}{LL_y}\int_0^L \cos\frac{q\pi z}{L}\sin\frac{M\pi z}{L}\,dz\int_0^{L_y}\sin\frac{N\pi y}{L_y}\,\phi_i(y)\,dy.$$

Now

$$\int_0^{L_y}\sin\frac{N\pi y}{L_y}\,\phi_i(y)\,dy = \sum_{j=1}^{n_b} a\int_{\theta_{1j}}^{\theta_{2j}}\sin\frac{N\pi(\theta-\theta_0)}{2(\pi-\theta_0)}\,\phi_i(\theta_j)\,d\theta$$

$$= \sum_{j=1}^{n_b} a\,\phi_i(\theta_j)\left[\cos\frac{N\pi(\theta_{1j}-\theta_0)}{2(\pi-\theta_0)} - \cos\frac{N\pi(\theta_{2j}-\theta_0)}{2(\pi-\theta_0)}\right]\frac{2(\pi-\theta_0)}{N\pi},$$

where n_b is the number of cylinder boundary points.

Thus,

$$f'(qi, MN) = f_{qM} \frac{2a(\pi-\theta_o)}{L_y(N\pi)} \sum_{j=1}^{n_b} \phi_i(\theta_j) \left[\cos \frac{N\pi(\theta_{1j}-\theta_o)}{2(\pi-\theta_o)} - \cos \frac{N\pi(\theta_{2j}-\theta_o)}{2(\pi-\theta_o)} \right],$$

where, for the case considered (shell length L = cavity length L_c,

$$f_{qM} = \begin{cases} \frac{1}{2\pi} \left[\frac{1-\cos(M+q)\pi}{M+q} + \frac{1-\cos(M-q)\pi}{M-q} \right] & ; M \neq q \\ 0 & ; M = q \end{cases}$$

If $L \neq L_c$, f_{qM} is given by Eq.(25) of Reference [1]. Finally, noting $L_y = 2b_a(\pi-\theta_o)$, the above reduces to

$$f'(qi, MN) = \frac{f_{qM}}{N\pi} \sum_{j=1}^{n_b} \phi_i(j) \left[\cos \frac{N\pi(\theta_{1j}-\theta_o)}{2(\pi-\theta_o)} - \cos \frac{N\pi(\theta_{2j}-\theta_o)}{2(\pi-\theta_o)} \right], \tag{61}$$

where i is the index assigned to the ordered 2D-acoustic mode (s is always equal to unity if the floor is present), and M, N are the number of axial and circumferential halfwaves of the structural mode.

3.7 Calculation of the Acoustic Loss Factor

The calculation of the acoustic loss factor at frequency ω has been discussed in Section 3.1 (resulting in Eq.28). This has to be formatted properly for the case where the floor is present. Also, when the test articles are considered the absorption capability of the end caps has to be considered. In both test cases where the floor is present, the end caps are covered with fiberglass that is exposed to the interior. The end cap admittance calculation is as follows (where the subscript e indicates their consideration):

$$\beta_e = \rho c_o \left[\frac{i\omega a_{21}}{a_{11}} \right],$$

$$\xi_e = Re\left[\beta_e\right] ,$$

$$a_{11} = C ,$$

$$a_{21} = \frac{-iS}{\omega W} .$$

In this simple model, the end caps themselves have been considered to have a high impedance. The loss factor for the interior is

$$\eta_n = \frac{\omega c_o}{\omega_n^2} \frac{\epsilon_n}{V} \left[\xi \int_{\substack{\text{curved}\\\text{surface}}} \phi_n^2 \, d\bar{x} + 2\xi_e \int_{\substack{\text{end}\\\text{cap}}} \phi_n^2 \, d\bar{x} \right] .$$

Here

$$\int_{\substack{\text{curved}\\\text{surface}}} \phi_n^2 \, d\bar{x} = \frac{L}{2} \epsilon_q a \sum_{j=1}^{n_b} \phi_i^2(j) \left[\theta_{2j} - \theta_{1j} \right] ,$$

where n_b is the number of boundary points, and

$$\int_{\substack{\text{end}\\\text{cap}}} \phi_n^2 \, d\bar{x} = \sum_{\text{Area}} \phi_n^2 \, d\text{Area} = \sum_{j=1}^{n_i} \phi_i^2(j) \, h^2 C(j) ,$$

where n_i is the number of interior points.

Therefore at low frequencies

$$\eta_n = \frac{\omega c_0}{\omega_n^2} \frac{\epsilon_n}{V} \left\{ \xi \frac{L}{2} \epsilon_q a \sum_{j=1}^{n_b} \phi_i^2(j) \left[\Theta_{2j} - \Theta_{1j} \right] \right.$$

$$\left. + 2 \xi_e a^2 \Phi_q(i) \right\} , \qquad (62)$$

where the volume mode is $n = (q, n, s) \equiv (q, i)$.

At high frequencies

$$\bar{\eta}_n = \frac{8 c_0}{4 \omega V} \left[\xi S + 2 \xi_e S_e \right] \quad , \qquad (63)$$

S and S_e being the curved surface and end cap areas.

3.8 Noise Reduction in the Volume Stiffness Controlled Region

The frequencies of concern here are those confined below the first (lowest) resonance frequency of the acoustic modes. Since the lengths of the cylinders used in this study exceed their diameters, the frequencies lie below that where the wavelength in the air equals twice the length of the cylinder. For the present models, $L_c = 1.219$m (48 inches) and the frequencies lie below about 140 Hz. In this frequency range, the noise reduction depends on the net volume displacement of the shell structure, and on the compliance of the cavity (as an airspring). If C_c is the compliance of the cavity (confined air volume) i.e.,

$$C_c = \frac{V}{\rho_0 c_0^2} , \qquad (64)$$

and C_p is the compliance of the shell, i.e.,

$$C_p = \frac{\Delta V}{p^o - p_i}, \tag{65}$$

where ΔV is the total volume displaced by the shell structures [including end-caps] when exterior pressure p^o is applied and interior pressure p_i is realized, then the noise reduction is found to be

$$NR = 20 \log \left[1 + \frac{C_c}{C_p} \right]. \tag{66}$$

Section 3.8.2 of Ref.[1] may be consulted for the development of this result.

There have been numerous studies [9, 10, 11] of the low frequency noise reduction of cylinders (both stiffened and unstiffened) where it has been found that the measured noise reductions and theoretical predictions do not agree in the extreme low frequency range. In fact, in the Phase I study [1] significant over-prediction at low frequencies was found to occur. Without exception, the (measured) low frequency noise reduction is less than the predicted noise reduction. End cap transmission and leaks have been postulated as the culprits, but while end caps can be significant transmitters, they do not tell the whole story. Neither do leaks, which can be prevented.

The basic question which remains unanswered is why a cylinder's noise reduction, typically, turns out to be only 25 or 30 dB when theoretically it should be 50 or 60 dB, or more.

Now for purposes of the present study, there are two types of shells to be considered (i.e., stiffened and unstiffened). For either, the fundamental modal characteristics lead to the occurrence of the first mode (in flexure) above the lowest acoustic mode. That being the case, the compliance of the cylinders is dominated by their stiffness. Since the noise reduction is still significant, the cylinder compliance is approximately

$$C_p = \frac{\Delta V}{p}, \tag{67}$$

where $p = p^0$ is the exterior pressure. Thus to calculate C_p, a static analysis might simply be considered. The displacement $w_1 = w$ over the cylinder surface is computed due to an applied pressure p, and integrated over the surface to obtain ΔV.

To begin this study, consider some results for an ideal cylinder. The basic partial differential equations for an isotropic cylindrical shell element are given by Kraus [12]. His axial coordinate is x (this report has previously used z for the axial coordinate). The equations of interest are

$$\frac{\partial^2 u}{\partial x^2} + \frac{1-\mu}{2r^2}\frac{\partial^2 u}{\partial \theta^2} + \frac{1+\mu}{2r}\frac{\partial^2 v}{\partial x \partial \theta} + \frac{\mu}{r}\frac{\partial w}{\partial x} - \frac{1-\mu^2}{E}\rho\frac{\partial^2 u}{\partial t^2} = 0 \tag{68}$$

$$\frac{1+\mu}{2r}\frac{\partial^2 u}{\partial x \partial \theta} + \frac{1-\mu}{2}\frac{\partial^2 v}{\partial x^2} + \frac{1}{r^2}\frac{\partial^2 v}{\partial \theta^2} + \frac{1}{r^2}\frac{\partial w}{\partial \theta} - \frac{1-\mu^2}{E}\rho\frac{\partial^2 v}{\partial t^2} = 0 \tag{69}$$

$$\frac{h^2}{12}\nabla^4 w + \frac{1}{r}\left[\frac{w}{r} + \frac{1}{r}\frac{\partial v}{\partial \theta} + \mu\frac{\partial u}{\partial x}\right] + \frac{1-\mu^2}{E}\rho\frac{\partial^2 w}{\partial t^2} = \frac{-(1-\mu^2)}{Eh}p \ . \tag{70}$$

The shell is assumed to extend from $x=0$ to $x=L$. u, v, and w are the displacements in the x, θ, and z directions, z pointing outward from the middle surface of the skin, with

$$\nabla^4 = \nabla^2(\nabla^2) = \nabla^2\left(\frac{\partial^2}{\partial x^2} + \frac{\partial^2}{\partial s^2}\right),$$

where

$$s = r\theta.$$

p is taken to be uniform circumferentially and axially, positive inward.

The above can be simplified by neglecting the longitudinal and circumferential inertia terms, i.e., by setting

$$\rho\frac{\partial^2 u}{\partial t^2} = \rho\frac{\partial^2 v}{\partial t^2} = 0.$$

In the case of a perfectly circular shell $(r=a)$, closed on the ends, with uniform external pressure, it can be shown [12, p.94], that

$$u = -\frac{pa}{Eh}\left(x - \frac{L}{2}\right)\left(\frac{1}{2} - \mu\right).$$

This result also holds true for the case where the radius varies slightly. It follows that an approximation can be used

$$\frac{\partial u}{\partial x} = -\frac{pr}{Eh}\left(\frac{1}{2} - \mu\right),$$

and Eq. (70) then reduces to

$$\frac{h^2}{12}\nabla^4 w + \frac{1}{r}\left(\frac{w}{r} + \frac{1}{r}\frac{\partial v}{\partial \theta}\right) + \frac{1-\mu^2}{E}\rho\frac{\partial^2 w}{\partial t^2} = -\frac{1-\mu/2}{Eh}p. \tag{71}$$

This differs only slightly from the result one would get if $\partial u/\partial x$ had simply been set to zero in Eq.(70); Eq.(71) is a slightly better approximation. The axial strain has little influence on the result.

It also follows that Eq.(69) reduces to

$$\frac{1-\mu}{2}\frac{\partial^2 v}{\partial x^2}+\frac{1}{r^2}\frac{\partial^2 v}{\partial \theta^2}+\frac{1}{r^2}\frac{\partial w}{\partial \theta}=0. \tag{72}$$

Eqs.(71) and (72) are independent of u and thus Eq.(68) is no longer of concern.

The membrane theory solution is obtained by setting $v=0$, and letting the bending resistance of the shell go to zero (i.e., setting the first term in Eq.(71) = 0), yielding

$$\frac{w}{r^2}+\frac{1-\mu^2}{E}\rho\frac{\partial^2 w}{\partial t^2}=-\frac{1-\mu/2}{Eh}p.$$

At sufficiently low frequencies, this reduces to the simple form

$$\left.\frac{w}{r^2}\right)_{r=a}=-\frac{1-\mu/2}{Eh}p,$$

or

$$w=-\frac{1-\mu/2}{Eh}pa^2. \tag{73}$$

The membrane stiffness controlled compliance of the cylinder is approximately (neglecting local bending near the ends of the cylinder)

$$C_p = \int_0^L \int_0^{2\pi} \frac{a^2}{Eh}(1-\mu/2)\, a\, d\theta\, dx$$

$$= \frac{2\pi a^3 L}{Eh}(1-\mu/2). \tag{74}$$

For the 0.020" thick stiffened cylinder

$$C_p = 1.26 \text{ in}^3/\text{psi}.$$

The compliance of the acoustic cavity is

$$C_c = \frac{V}{\rho c_0^2} = 742 \text{ in}^3/\text{psi}.$$

This gives a noise reduction due to the cylinder wall displacement of

$$NR = 20 \log\left[1 + \frac{742}{1.26}\right] = 55.4 \text{ dB}$$

As will be seen in Section 4, the actual measurements indicate about 30 dB. The noise reduction due to the stiffness compliance of the end caps (which will be considered later) varies between 47 and 49 dB. Adding up the end caps and cylinder membrane compliances gives C_p in the range = 3.9 to 4.6 in^3/psi or a noise reduction of 45.6 - 44.2 dB., which is still well above 30 dB.

It follows that bending deflections of the cylinder wall have to be considered. However, if the radius r is constant, w must of

necessity be independent of θ and the only bending effects must be associated with the axial direction and related to the supporting end conditions. The θ independency of w does not apply when the concern is with an orthotropic shell (stiffened with rings and stringers). For such a shell, Eq.(71) can be generalized somewhat to

$$D_x \frac{\partial^4 w}{\partial x^4} + 2D_{xs} \frac{\partial^4 w}{\partial x^2 \partial s^2} + D_s \frac{\partial^4 w}{\partial s^4}$$

$$+ \frac{Eh}{1-\mu^2}\left[\frac{w}{r^2} + \frac{1}{r^2}\frac{\partial v}{\partial \theta}\right] + m\frac{\partial^2 w}{\partial t^2} = -\frac{(1-\mu/2)}{1-\mu^2} p \,, \tag{75}$$

where m is the average surface mass. Eq.(72) remains unchanged.

Eq.(75) applies for an orthotropic shell in which the rings and stringers have been smeared into the shell. The bending rigidities D_x and D_s are for the sections perpendicular to the x and θ (i.e., s) axes respectively and D_{xs} is the cross rigidity.

One solution of Eqs.(72) and (75) is for the case of a free-ended cylinder where v is independent of x and

$$w = -\frac{\partial v}{\partial \theta} \,,$$

at every point in the shell. Then

$$D_x \frac{\partial^4 w}{\partial x^4} + 2D_{xs} \frac{\partial^4 w}{\partial x^2 \partial s^2} + D_s \frac{\partial^4 w}{\partial s^4}$$

$$+ m\frac{\partial^2 w}{\partial t^2} = -\frac{(1-\mu/2)}{1-\mu^2} p \,. \tag{76}$$

In this case, the shell deforms in bending only. The condition

$$w = -\frac{\partial v}{\partial \theta}, \tag{77}$$

is the Rayleigh criterion for inextensible vibrations of a ring. If Eq.(77) holds, the middle surface of the shell (i.e., ring) does not stretch. One might hypothesize that a shell's end conditions could be such as to allow Eq.(77) to hold approximately (not perfect supports) but if that is the case, the subpanel transmission (i.e., between rings and stringers) would turn out to be so great that the predicted noise reduction would be less than that measured.

For instance for a subpanel of the stiffened cylinder used in this study, as shown in Figure 9, Eq.(76) would reduce to

$$D\nabla^4 w + m\frac{\partial^2 w}{\partial t^2} = -\frac{(1-\mu/2)}{1-\mu^2}p, \tag{78}$$

which is independent of the curvature effects. The displacement in the first mode which satisfies (78) is

$$w \simeq \frac{4}{A}\frac{p}{m}\frac{\psi^{1,1}(x,s)}{\omega_{11}^2}\int_0^{\ell_x}\int_0^{\ell_y}\psi^{1,1}(x',s')\,dx'ds',$$

where

$$\omega_{11}^2 = \frac{D}{m}\left[\left(\frac{\pi}{\ell_x}\right)^2+\left(\frac{\pi}{\ell_y}\right)^2\right]^2.$$

Letting

$$\psi^{1,1}(x,s) = \sin\frac{\pi x}{\ell_x}\sin\frac{\pi s}{\ell_y},$$

gives

$$w = \frac{16}{\pi^2}\frac{p}{m}\frac{1}{\omega_{11}^2}\psi^{1,1}(x,s). \tag{79}$$

The displaced volume is then

$$\Delta V = \frac{64}{\pi^4} \frac{p}{m} \frac{l_x l_y}{\omega_{11}^2} , \tag{80}$$

yielding (with the data from Fig. 9)

$$C_p \simeq 77 \text{ in}^3/\text{psi}.$$

This leads to a noise reduction

$$NR = 20 \log \left[1 + \frac{742}{77} \right] = 20.5 \text{dB}$$

if only one sub-panel is considered. However, there are 30 sub-panels, so the total compliance is

$$C_p = 30(77) = 2310 \text{ in}^3/\text{psi}$$

giving a noise reduction of only

$$NR = 20 \log \left[1 + \frac{742}{2310} \right] = 2.4 \text{dB}.$$

If one considers the subpanels clamped along their edges, the compliance is 13.64 in^3/psi per subpanel leading to an overall

$$C_p = 30 \times 13.6 = 409 \text{ in}^3/\text{psi}$$

and $$NR = 9 \text{ dB}.$$

Thus throwing out curvature effects leads to an underprediction of the noise reduction. Since the inextensibility assumption is almost impossible to justify, there are good reasons, as seen above, not to invoke it.

It follows from all the discussion preceding, that it appears membrane stresses are in fact working, but that the deflection of the cylinder wall is not obeying the simple result given by Eq.(73). In fact, if the noise reduction is as low as has been calculated (less than 10 dB), and the measured is 30 dB, one might conclude that membrane stresses have to be present. That being the case, it should follow that solutions of the simple equation

$$\frac{w}{r^2} = -\frac{1-\mu/2}{Eh} p , \tag{81}$$

should be examined. It also seems crucial to study the effects of out-of-roundness (i.e., non-circularity).

Suppose non-circularity of the cylinder is considered, say by letting the radius of the shell be given by

$$r = a\left(1-\epsilon f(\theta)\right) \; ; \; \epsilon \ll 1 .$$

Then at first, the solution appears to be

$$w = -\frac{1-\mu/2}{Eh} p a^2 \left(1-2\epsilon f(\theta)\right).$$

However, this result is not correct because the parameter r in Eq.(81) is the <u>radius of curvature</u>!

To distinguish between the radius of curvature and the radius of the shell, let the radius of curvature be given by cap R. Then Eq.(81) becomes

$$\frac{w}{R^2} = -\frac{1-\mu/2}{Eh} p \; . \tag{82}$$

Also

$$C_p = \int_0^L \int_0^{2\pi a} -\frac{1-\mu/2}{Eh} R^2 \, dx \, ds \, , \tag{83}$$

$$\simeq \frac{L(1-\mu/2)}{Eh} \int_0^{2\pi} R^2 a \, d\theta \, . \tag{84}$$

[Incidentally, $ds \neq R\,d\theta$, since θ is measured from the center of the cylinder instead of from the center of curvature (which moves about)].

Since the radius of curvature of a shell with a slight variation in radius can differ greatly from the radius itself, it can be seen from Eq.(83), that if $R \to \infty$, C_p can become very large relative to that of the perfect cylinder (thereby reducing the noise reduction).

In cylindrical coordinates, the radius of curvature is given by

$$R = \frac{\left[r^2 + \left(\frac{dr}{d\theta}\right)^2\right]^{3/2}}{r^2 + 2\left(\frac{dr}{d\theta}\right)^2 - r\frac{d^2r}{d\theta^2}} \, . \tag{85}$$

Now if

$$r = a\left(1 - \epsilon f(\theta)\right), \tag{86}$$

where $f(\theta)$ is a smooth positive function normalized such that $f(\theta)_{max} = 1$, then

$$\frac{dr}{d\theta} = -a\epsilon f'(\theta)$$

$$\left(\frac{dr}{d\theta}\right)^2 = a^2\epsilon^2 f'^2(\theta)$$

$$\frac{d^2r}{d\theta^2} = -a\epsilon f''(\theta) ,$$

and

$$R = \frac{a\left[1 - \epsilon f(\theta) + \epsilon^2\left(f^2(\theta) + f'^2(\theta)\right)\right]^{3/2}}{\left\{1 + \epsilon\left[f''(\theta) - 2f(\theta)\right] + \epsilon^2\left[f^2(\theta) + 2f'^2(\theta) - f(\theta)f''(\theta)\right]\right\}} ,$$

or

$$R \cong \frac{a}{1+\epsilon f''(\theta)} , \tag{87}$$

since $f'(\theta)$ is considered small.

Suppose now, the out-of-roundness occurs over an arc length of shell $\Delta s = a\Delta\theta = a\theta_1$, as shown in the Figure 10. Then if a length ℓ (axially) is considered, the compliance, C_p' for that length is according to Eqs.(84) and (87)

$$C_p' = \frac{\ell(1-\mu/2)a^3}{Eh}\left[\int_0^{\theta_1} \frac{d\theta}{\left(1+\epsilon f''(\theta)\right)^2} + \int_{\theta_1}^{2\pi} d\theta\right] . \tag{88}$$

This reduces to

$$C_p' = \frac{\ell(1-\mu/2)a^3}{Eh}\left[(2\pi-\theta_1)+\Theta_1\right]$$

$$= \frac{\ell(1-\mu/2)a^3}{Eh}\left[2\pi+(\Theta_1-\theta_1)\right], \qquad (89)$$

where

$$\Theta_1 = \int_0^{\theta_1} \frac{d\theta}{(1+\epsilon f''(\theta))^2} \quad . \qquad (90)$$

It is obvious from Eq.(89) that whenever the integral Θ_1 exceeds the interval θ_1, that portion (shell length ℓ) transmits better than the classical membrane theory predicts. The compliance for the whole cylinder becomes.

$$C_p = \frac{2\pi(L-\ell)(1-\mu/2)a^3}{Eh} + \frac{\ell(1-\mu/2)a^3}{Eh}\left[2\pi+(\Theta_1-\theta_1)\right]$$

$$= \frac{2\pi(1-\mu/2)a^3L}{Eh}\left[1+\frac{\ell}{L}\frac{(\Theta_1-\theta_1)}{2\pi}\right] . \qquad (91)$$

If the length of out-of-roundness extends over the entire length of the shell, $\ell = L$, and

$$C_p = \frac{(1-\mu/2)\, a^3 L}{Eh}\left[2\pi + (\Theta_1 - \theta_1)\right], \tag{92}$$

which is consistent with Eq.(89).

Before considering evaluation of the integral Θ_1, it is also useful to consider a solution in which the transverse displacement v is not assumed to be zero. From Eq.(71), the membrane result is obtained by setting $h=0$ (also $\omega=0$).

$$\frac{1}{R^2}\left[w + \frac{\partial v}{\partial \theta}\right] = -\frac{1-\mu/2}{Eh}\, p, \tag{93}$$

and from Eq.(72), by writing (since R is a function of θ)

$$\frac{1-\mu}{2}\frac{\partial^2 v}{\partial x^2} + \frac{1}{R}\frac{\partial}{\partial \theta}\left[\frac{1}{R}\left(\frac{\partial v}{\partial \theta} + w\right)\right] = 0. \tag{94}$$

Then substituting Eq.(93) into Eq.(94) gives

$$\frac{1-\mu}{2}\frac{\partial^2 v}{\partial x^2} + \frac{1}{R}\frac{\partial}{\partial \theta}\left[\frac{1}{R}\left(\frac{-(1-\mu/2)}{Eh}\, p R^2\right)\right] = 0,$$

or

$$\frac{1-\mu}{2}\frac{\partial^2 v}{\partial x^2} = \frac{1}{R}\frac{\partial}{\partial \theta}\left[\frac{1-\mu/2}{Eh}\, pR\right]$$

$$= \frac{1-\mu/2}{Eh}\,\frac{p}{R}\,\frac{\partial R}{\partial \theta}$$

$$= \frac{1-\mu/2}{Eh} \frac{p}{R} \frac{\partial}{\partial\theta}\left[\frac{a}{1+\epsilon f''(\theta)}\right]$$

$$= \frac{1-\mu/2}{Eh} \frac{p}{R} \left[\frac{-a\epsilon f'''(\theta)}{(1+\epsilon f''(\theta))^2}\right].$$

Using Eq.(87), this becomes

$$\frac{1-\mu}{2} \frac{\partial^2 v}{\partial x^2} = -\frac{(1-\mu/2)\epsilon f'''(\theta)}{1+\epsilon f''(\theta)} \frac{p}{Eh},$$

or

$$\frac{\partial^2 v}{\partial x^2} = -\frac{2-\mu}{1-\mu} \frac{p}{Eh} \frac{\epsilon f'''(\theta)}{1+\epsilon f''(\theta)}. \tag{95}$$

This can be integrated to yield

$$v(x,\theta) = \frac{V_1 x^2}{2} + V_2 x + V_3,$$

where

$$V_1(\theta) = -\frac{2-\mu}{1-\mu} \frac{p}{Eh} \frac{\epsilon f'''(\theta)}{1+\epsilon f''(\theta)}, \tag{96}$$

and V_2, V_3 are constants of integration, (which may be functions of θ).

If at some locations (say at the rings) $v(x,\theta)=0$, then V_2 and V_3 can be determined. Take

$$v(0,\theta) = 0$$
$$v(\ell,\theta) = 0 .$$

Then

$$V_3 = 0$$
$$V_2 = -\frac{V_1 \ell}{2},$$

and one can write

$$v(x,\theta) = V_1(\theta)\cdot V(x) \tag{97}$$

where

$$V(x) = \frac{x^2}{2} - \frac{\ell x}{2} .$$

This can be substituted back into Eq.(93) to obtain w, i.e.,

$$w = -\frac{1-\mu/2}{Eh} p R^2 - \frac{\partial v}{\partial \theta}$$
$$= -\frac{1-\mu/2}{Eh} p R^2 - V(x)\frac{\partial V_1}{\partial \theta} .$$

But

$$\frac{\partial V_1}{\partial \theta} = -\frac{2-\mu}{1-\mu}\frac{p}{Eh}\frac{(1+\epsilon f''(\theta))\epsilon f^{IV}(\theta) - \epsilon^2 f'''^2(\theta)}{(1+\epsilon f''(\theta))^2},$$

so an approximate solution (neglecting any flexure) is

$$w = -\frac{(2-\mu)p}{Eh(1+\epsilon f''(\theta))^2}\left[\frac{a^2}{2} - \epsilon\frac{V(x)}{1-\mu}\left(f^{IV} + \epsilon f'' f^{IV} - \epsilon f'''^2\right)\right]. \tag{98}$$

This gives over the length ℓ

$$C_p = \int_0^{2\pi}\int_0^{\ell} \frac{w}{p}\, a\, d\theta\, dx \,.$$

This integral contains in its denominator the same term $(1+\epsilon f''(\theta))^2$ as Eq.(90). If $\epsilon f''(\theta) \to -1$, i.e., if $R \to \infty$ over any interval, the membrane stress (hoop tension) is broken over length ℓ. Only the bending resistance remains in the shell in this region. This leads to a conclusion that over certain axial regions, the cylinder transmission may be totally controlled by flexure and over others totally controlled by the hoop tension.

Now examine the integral Θ_1 for some selected functional forms, $f(\theta)$ [refer to Fig.10]. Suppose

$$f(\theta) = \sin\frac{\pi s}{\Delta s} = \sin\frac{\pi}{\theta_1}\theta \,.$$

Then

$$\Theta_1 = \int_0^{\theta_1} \frac{d\theta}{(1 - e\sin \pi\theta/\theta_1)^2}$$

$$= \frac{\theta_1}{\pi}\int_0^{\pi} \frac{d\alpha}{(1 - e\sin\alpha)^2}$$

where $e = \epsilon\pi^2/\theta_1^2$.

This can be evaluated to yield [13]

$$\Theta_1 = \frac{\theta_1}{\pi(1-e^2)}\left\{\frac{2}{(1-e^2)^{1/2}}\left[\frac{\pi}{2} - \tan^{-1}\left(\frac{-e}{(1-e^2)^{1/2}}\right)\right] + 2e\right\}. \tag{99}$$

Since $(1-e^2)^{1/2}$ is imaginary for $e>1$, Θ_1 does not exist in this region. This is interpreted as total relief of the membrane stress.

Suppose one chooses

$$f(\theta) = \sin^2 \frac{\pi}{\theta_1}\theta .$$

This function has zero slope at $\theta = 0$ and θ_1, which is probably a more realistic representation. Then

$$\Theta_1 = \int_0^{\theta_1} \frac{d\theta}{(1+\bar{e}\cos 2\pi\theta/\theta_1)^2} ,$$

where $\bar{e} = 2\epsilon\pi^2/\theta_1^2$, giving

$$\Theta_1 = \frac{\theta_1}{2\pi}\int_0^{2\pi} \frac{d\alpha}{(1+\bar{e}\cos\alpha)^2} .$$

For $\bar{e} < 1$, the solution is [13]

$$\Theta_1 = \frac{\theta_1}{(1-\bar{e}^2)^{3/2}} . \tag{100}$$

A plot of this function is shown in Figure 11.

This integral also does not exist (is divergent) for $\bar{e} > 1$, thus the membrane stress is relieved.

From the form of these solutions, it is seen that the likelihood of Θ_1 growing large relative to θ_1 may be small since combinations of ϵ (or Δ) and θ_1 may not exist which will yield $\bar{e} \simeq 1$. But the possibility of $\bar{e} > 1$ may be real (i.e., $R \to \infty$ over the range $\Delta\theta = 0$ to θ_1).

Let's choose $\bar{e}$ (rather than e) as a criterion for relief of the membrane stress. It can be considered an approximate (as opposed to an exact) criterion for $R \to \infty$ over an interval $\Delta\theta = \theta_1$. $\bar{e}$ is plotted versus θ_1 and ϵ in Figure 12. When $\bar{e} > 1$ the membrane stress is relieved.

Now consider some example calculations. Suppose a very slight indentation of the skin of the 0.020" thick cylinder existed, say $\Delta = 0.001$ in. Then according to Figure 12, if $\theta_1 < 0.045$ rad (2.6°), $\bar{e} > 1$ and the membrane stress is relieved. While 0.001 in. may seem small, the amplitude of the membrane displacement w for the ideal cylinder is from Eq.(73)

$$w = \frac{1-\mu/2}{Eh} p a^2 ,$$

which for the 0.508 m (20 in) diameter cylinder gives

$$w = 4.2 \times 10^{-4} p .$$

At 100 dB, p is only 2.9×10^{-4}psi, giving $w = 12 \mu in$. In comparison Δ is huge. Unless the pressure is high enough to increase w to the same order of magnitude as Δ , the shell would not stretch enough to displace its out-of-roundness. This would

apparently require a pressure of about 2 psi or more for the .001 in. selected. The interpretation is that very slight variations in radius over small angular regions (wrinkles) can be highly detrimental at acoustic pressures.

Now experience tells us that putting dents in a cylinder will not change its low frequency noise reduction very much. However in our experience, we have never worked with a perfect cylinder. Suppose for example that there existed a perfect cylinder with wall thickness $h =$ 0.020 in., a radius $a =$ 10 in., and length $L =$ 48 in. The noise reduction is as has been calculated before, i.e., 55.4 dB. Suppose that over some axial expanse of length ℓ, there exists around the circumference a region for which $\bar{e} > 1$. For instance, on the stiffened cylinder of this study there is about a 2 in. diameter inward depression that is about 0.030 in. deep. Setting $\ell = 2$ inches and $\Delta =$ 0.030 in., it is found that

$$\theta_1 = \frac{\ell}{a} = 0.2$$

$$\epsilon = \frac{\Delta}{a} = 0.003 \cdot$$

From Fig.12, $\bar{e} = 1.48 > 1$ and thus the membrane stress is relieved. The cylinder model is now one where a length $L - \ell$ is membrane controlled, the rest (length ℓ) is flexure controlled. Consider now a strip running between stiffeners 2 in. wide, and from Figure 9 of 11.59 in. length. The compliance for the membrane controlled section is

$$C_p^m = \frac{2\pi a^3 (L-\ell)}{Eh} (1-\mu/2)$$

$$= 1.21 \text{ in}^3/\text{psi} \cdot$$

The compliance for the strip in flexure between stringers is

$$C_p^f = \frac{64}{\pi^4} \frac{12A(1-\mu^2)}{Eh^3\left[\left(\frac{\pi}{\ell_y}\right)^2+\left(\frac{\pi}{\ell}\right)^2\right]^2}$$

$$= 0.315 \text{ in}^3/\text{psi}.$$

Since there are 5 stringers (i.e., 5 strips)

$$C_p^f = 5(0.315) = 1.57 \text{ in}^3/\text{psi}$$

Also, for the whole cylinder

$$C_p = C_p^m + C_p^f = 2.78 \text{ in}^3/\text{psi},$$

and the noise reduction would be

$$NR = 20\log\left[1 + \frac{742}{2.78}\right] = 48.6 \text{ dB}.$$

Thus, this single depression would reduce the noise reduction from 55.4 dB to 48.6 dB, or about 7 dB, which is a sizable reduction.

But if the cylinder is not perfect, say without the depression its noise reduction is only 35 dB, then its C_p would be (overall)

$$C_p = \frac{C_c}{10^{NR/20}-1} = \frac{742}{10^{35/20}-1} = 13.43 \text{ in}^3/\text{psi}.$$

If length ℓ was perfectly circular, the portion of the compliance above due to it would be

$$C_p^m = \frac{2\pi a^3 \ell (1-\mu/2)}{Eh} = 0.053 \text{ in}^3/\text{psi}.$$

With the depression $\Delta = 0.03$ in. and $\theta_1 = .2$, over length ℓ, the same length's compliance would become

$$C_p^f = 1.57 \text{ in}^3/\text{psi}.$$

Thus with the depression

$$C_p = 13.43 - 0.053 + 1.57 = 14.97 \text{ in}^3/\text{psi}.$$

This gives a noise reduction of 34.1 dB. For the non-ideal cylinder, the same depression thus gives only a 0.9 dB reduction in the NR. Thus in the non-ideal cylinder case adding a wrinkle or depression will not profoundly effect the (already low) noise reduction.

To generalize all of this, a stiffened cylinder with n_s stringers will have a compliance given

$$C_p = \frac{2\pi a^3 (L-\ell)(1-\mu/2)}{Eh} + \frac{128\, a\, \ell}{\pi^3 D \left[\left(\frac{n_s}{2a}\right)^2 + \left(\frac{\pi}{\ell}\right)^2\right]^2},$$

where ℓ is length for which $\bar{e} > 1$.

Since in general, there may be N regions of length ℓ_i with $\bar{e}_i > 1$, the final expression becomes

$$C_p = \frac{2\pi a^3 \left(L - \sum_i^N \ell_i\right)(1-\mu/2)}{Eh} + \frac{128 a}{\pi^3 D} \sum_{i=1}^{N} \frac{\ell_i}{\left[\left(\frac{n_s}{2a}\right)^2 + \left(\frac{\pi}{\ell_i}\right)^2\right]^2}, \qquad (101)$$

where $\ell_i = 0$ if $\bar{e}_i < 1$ and inward depressions only are considered.

It should be noted in Eq.(101) that larger ℓ_i's have more significant impact. Thus a four inch length in which $\bar{e} > 1$ would be far more detrimental to the noise reduction than 4 one-inch segments.

3.9 End Cap Transmission

The end caps of the test articles are stiffness controlled well beyond the fundamental acoustic resonance at 140 Hz. The internal pressure due to each end cap's deformation is computed with

$$p_i(\bar{\xi}) = -\rho_0 \omega^2 \int G_p(\bar{x}|\bar{\xi})\, w_1(\bar{x})\, d\bar{x},$$

where $\bar{\xi}$ is an interior point and $\bar{x}$ lies on the end cap. $G_p(\bar{x}|\bar{\xi})$ is the interior space Green's function as previously defined. The displacement of the end cap under uniform pressure p^0 is [14]

$$w_1(\bar{x}) = w_1(r, \theta, z=0) = w(r) = \frac{p^0}{64D}\left[-a^4 \frac{5+\mu}{1+\mu} + 2a^2 r^2 \frac{3+\mu}{1+\mu} - r^4\right],$$

where D is the bending rigidity.

Consider the response of the first acoustic mode only. Then

$$G_p(\bar{x}|\bar{\xi}) = \frac{2c_0^2}{V} \frac{\cos \pi z / L_c}{\omega_n^2 - \omega^2 - i\eta_n \omega_n^2}.$$

Substituting, this gives, for both end caps

$$p_i(\bar{\xi}) = -p^o \frac{4\rho_o c_o^2}{V}\left[\frac{\pi a^6}{64D}\left(\frac{-(7+\mu)}{3(1+\mu)}\right)\right]$$

$$\times \frac{\omega^2}{\omega_n^2-\omega^2-i\eta_n\omega_n^2}\cos\pi z/L_c \,.$$

The space average mean square pressure is obtained with

$$\langle p_i^2\rangle_{s,t} = \frac{1}{2V}\int p_i(\bar{\xi})\, p_i^*(\bar{\xi})\, d\bar{v} \,,$$

$$= \langle p^{o2}\rangle_t \left\{\frac{2\rho_o c_o^2}{V}\left[\frac{\pi a^6}{64D}\left(\frac{7+\mu}{3(1+\mu)}\right)\right]\right\}^2 \frac{2\omega^4}{(\omega_n^2-\omega^2)^2+\eta_n^2\omega_n^4} \,.$$

This is averaged over each frequency band of concern, where $\langle p^{o2}\rangle_t$ is assumed to be the mean square exterior pressure in the band with an approximately uniform frequency content. Then

$$\frac{\langle p_i^2\rangle_{s,t}}{\langle p^{o2}\rangle_t} = \frac{2}{\Delta\omega}\left\{\frac{2\rho_o c_o^2}{V}\left[\frac{\pi a^6}{64D}\left(\frac{7+\mu}{3+3\mu}\right)\right]\right\}^2 \int_{\omega-\frac{\Delta\omega}{2}}^{\omega+\frac{\Delta\omega}{2}} \frac{\bar{\omega}^4\, d\bar{\omega}}{(\omega_n^2-\bar{\omega}^2)^2+\eta_n^2\omega_n^4} \,, \tag{102}$$

where ω is the band center frequency and $\Delta\omega = c_\omega \omega$ is the bandwidth.

Integration gives

$$\int_{\omega-\frac{\Delta\omega}{2}}^{\omega+\frac{\Delta\omega}{2}} \frac{\bar{\omega}^4 d\bar{\omega}}{(\omega_n^2-\omega^2)^2+\eta_n^2\omega_n^4} = \bar{\omega} + \ln \frac{\bar{\omega}^2 - 2k\bar{\omega}\cos\frac{\alpha}{2} + k^2}{\bar{\omega}^2 + 2k\bar{\omega}\cos\frac{\alpha}{2} + k^2}$$

$$\times \frac{\omega_n}{8\cos\frac{\alpha}{2}} \left[\frac{2}{(1+\eta_n^2)^{1/4}} - (1+\eta_n^2)^{1/4} \right]$$

$$+ \tan^{-1} \frac{2k\bar{\omega}\sin\frac{\alpha}{2}}{k^2-\bar{\omega}^2} \cdot \frac{\omega_n}{4\sin\frac{\alpha}{2}} \left[\frac{2}{(1+\eta_n^2)^{1/4}} + (1+\eta_n^2)^{1/4} \right] \Bigg|_{\omega-\frac{\Delta\omega}{2}}^{\omega+\frac{\Delta\omega}{2}} ,$$

where

$$k = \omega_n (1+\eta_n^2)^{1/4} ,$$

$$\tan\alpha = \eta_n ,$$

and

$$\omega_n = 2\pi \times 140 \text{ Hz} .$$

η_n is the measured value of the loss factor for the acoustic mode (at its resonance (140 Hz)). The noise reduction is obtained using

$$NR = -10 \log \frac{\langle p_i^2 \rangle_{s,t}}{\langle p_o^{02} \rangle_t} . \qquad (103)$$

3.10 Status of the Interior Noise Program (Phase II)

A brief status report concerning the computer programs that exist for the present (Phase II) calculations is warranted. An overview of the software is provided in Figure 13.

The main program is called FCYLNR and calculates the noise reduction of the cylinder with or without floor. If the floor is present, it utilizes the output (on tape) from the program CYL2D that computes the acoustic modes of the cross section of the cylinder with floor. If the floor is not present, subroutines CINDEX and OMEGAN are used as they were for the empty cylinder in Phase I. CINDEX indexes the cavity (cabin) modes. The structural modes are computed using the Mikulas and McElman scheme as outlined in Section 3.5. There are two programs - MSTRUC which prepares input data in proper form to describe the skin, stringer, and frame (ring) properties for the stiffened (orthotropic) cylinder, and MINCYL which calculates the modes (resonance frequencies). Output is again to a tape read by FCYLNR.

Various subroutines in FCYLNR compute the structure/acoustic coupling factors, joint acceptances, radiation loss factors, and all other quantities needed in Eqs.(36) and (41). These subroutines are structured to handle the modal data for the cylinder with or without floor. Finally, subroutine TRIM computes the trim panel transfer matrix data and the required transmission coefficients, loss factor, η_r', and the surface admittance β of the trim.

4.0 EXPERIMENTS

The Phase II study has a two-fold objective: development and validation of the analytical models. Section 3 considered the development; Section 5 will consider the validation. This section considers the experimental program that was undertaken to obtain a data base to allow comparisons against predictions for a number of different parameters needed in the noise reduction calculation. Also the noise reductions of three test articles were measured.

Most of the experimental work was done at NASA Langley Research Center. One simple test was performed at BBN/LA to obtain data for checking out the quality of the finite-difference calculations of cabin modes when the floor is present. The two main tests were:

1) Measurements of the structural and acoustic loss factors of the test cylinders and cavities

2) Measurement of the noise reduction of the cylinders, i.e., the difference between the exterior and interior sound pressure levels given a random, diffuse (reverberant) exterior acoustic field.

Other tests done at Langley involved the acquisition of acceleration response data on the cylinder walls to provide some experimental insight into the modal characteristics of the shell structures.

4.1 NASA Tests

The cylinders were tested in a 221m^3 (7800 ft^3) reverberation room having dimensions of about 6x9x4m (20x28x14 ft) with a reflection coefficient of about 0.95. The principal room mode was near 16 Hz.

The testing consisted of the measurement of the noise reductions of the test articles (cylinders) and the rate of decay of acoustic vibrations in the cylinder cavity and structural vibrations of the cylinder wall.

Description of Models

The cylinders tested were the unstiffened cylinder with floor and the stiffened cylinder with and without floor, with the various trims outlined in Section 1. The external dimensions were 0.508 m (20 in.) diameter by 1.219 m (48 in) long (see Figs. 14 and 15). The cylinders were equal in weight with one having an unstiffened 0.0016 m (0.064 in) thick skin of 2024-T3 aluminum. The other had the shell weight equally divided between the skin, stringers and ring frames.

The skin was attached to 0.0127 m (0.50 in.) thick annular end rings and the 0.41 m (16 in.) diameter opening in the end rings was closed with a 0.46 m (18 in.) dia. 0.0127 m (0.5 in.) thick cover plate (end cap). The cylinder was airtight except for the 0.00018 m (0.007 in.) radial clearance between the mike support tube and bushings. The bushings and the end caps were attached by bolts, the remainder of the attachments and seams were epoxy bonds. Both cylinder seams had a 0.00457 m (0.18 in) wide double skin thickness; the unstiffened cylinder had a butt-joint with outside strap, the stiffened cylinder had a lap joint.

The stiffened cylinder had 5 stringers, 0.0254 x 0.0254 x 0.00318 m (1 x 1 x 0.125 in) angles at 72° spacing and 5 ring frames, made from 0.00229 m (.09 in) thick sheet, at 0.203 m (8 in) spacing. The frames were made in two pieces, a 0.034 m (1.34 in) wide ring with a butt joint, and an annulus with a 0.555 m (21.87 in) outside diameter that slipped over the ring to form a 0.024 x 0.034 x 0.0023 m (0.937 x 1.34 x .09 in) frame cross section.

In the tests conducted with a floor and trim added to the basic cylinder configuration, as shown for the stiffened cylinder in Fig. 16, the floor was made from 0.0008 m (0.032 in) thick aluminum sheet. The floor was 1.1938 m (47 in) long with flaps on the ends to close off the compartment below the floor. A bead of silicon rubber (RTV) was used to attach the floor to the skin and seal the lower compartment. The floor was stiffened by two 0.0158 x 0.0158 x 0.00158 m (0.625 x 0.625 x 0.062 in) angles underside of the floor. The ends of the stiffeners were bolted to two 0.0254 x 0.0254 x 0.0032 m (1 x 1 x .125 in) angles on the upper side of the floor that provided lateral stiffness and were bolted to the end rings to locate the floor about 0.163 m (6.46 in) below the cylinder centerline ($\theta_0 = 49°$).

The trim insulation was Owens-Corning PF-105 Fiberglas supplied 0.013 m (0.50 in.) thickness. The supplier, Flight Insulation Marietta, Georgia, added a 2 mil vinyl facing on one side. A vinyl sound barrier weighting 2.44 kg/m^2 (0.5 lb/ft^2) was used. The lead-vinyl had a fiberglas cloth facing on one side with a total thickness to about 0.00119 m (0.047 in.).

Instrumentation & Apparatus

In the noise reduction tests, six microphones were located inside the cylinder as shown in Fig. 14. The microphones were mounted on a bar attached to a 0.0254 m (1 in) tube on the cylinder centerline. The tube could be rotated and translated to position the microphone array at the desired measurement location. Exterior levels were measured by 2 microphones on floor stands. The noise load was supplied by one or two 100 watt speakers (Fig.17).

The exterior spectrum was produced by a GenRad noise generator and passed through a power amplifier to two Altec "studio monitor" speakers. The level was controlled by the volume knob on the

noise generator. The amplified microphone output was fed, one channel at a time, by a selector switch to an analyzer and digital volt meter. Overall levels of all microphones were hand recorded from the DVM, one-third octave spectra for selected microphones were taped and some NR spectra were plotted. Post test analysis and listings of spectra were obtained by recalling the taped spectra into the analyzer memory and reading the analyzer memory through an IEEE computer interface.

In the reverberation time measurements, structural and acoustic modes were excited by a 5 in diameter speaker mounted on the microphone bar. A time history of the signal decay of an interior microphone or an accelerometer on the skin was captured by the "Hold" function of the analyzer. The time history was then recorded by the digital plotter.

In the mode identification tests, a tone was played through the small speaker. One axis of the analyzer scope was connected to the speaker and the other to a hand held microphone. The frequency was swept until the microphone response peaked. The microphone was then moved over the skin surface and the number of slope changes in the display per longitudinal and circumferential circuit were counted.

Test Procedure

The floor and trim were installed in the cylinders. A microphone mount short enough to allow the desired rotation was selected, and the mikes were installed in the cylinder. The cover plates were bolted on the cylinder and the cable access hole sealed with modeling clay. The cylinder was suspended from a wood 2 x 4 "sawhorse" fixture by aircraft bungee cord as shown in Fig. 18. The fixture was located off center in the room because the spatial gradients in the sound pressure level for the low frequency bands were highest near the room center. The exterior microphones were

placed about 0.254 m (10 in) from the skin to avoid the increase in SPL that occurred for $d < 0.178$m (7 in). Spectra for the exterior microphones at the 4 "corners" of the cylinder were monitored and minor adjustments to the location and orientation of the cylinder and speakers was made to obtain approximately equal SPL in the 20 and 25 Hz bands. Above these bands the sound field was fairly uniform throughout the room. Below these bands the interior levels were sometimes lost in the background noise.

A speaker output level high enough to produce measurable levels on the interior microphone nearest the centerline was selected and used for all data for the given test configuration. The speaker was turned on, OASPL from the DVM was read for all microphones, an external spectra was acquired, stored on tape, and transferred to analyzer memory "B". An internal spectra was acquired, taped, and the difference in current and stored spectra was plotted. After comparing the desired microphones the speaker was turned off and the microphone array rotated to the next location.

For reverberation time measurements a 1/3 octave filter, B&K 1614, was added between the noise generator and amplifier (Fig.17) and between the microphone selector switch and analyzer. The speaker output was down 10 dB for the adjacent 1/3 octave bands on either side of the selected one, and down about 50 dB for the second band on either side. Time histories of vibration decay were captured by simultaneously hitting a switch to disconnect the signal to the power amplifier and tripping the "Hold" switch on the analyzer. If the decay was too irregular to analyze, a tone was substituted for the pink noise and the frequency was swept manually until a resonance was located. If the decay was smooth the record length (time scale factor) and transducer gain was adjusted until the decay record filled the CRT screen. The display was checked to see that the low-pass filter associated with the time scale knob was higher than the frequency of the band being studied, and that the decay extended over more time than the 4-cycle time-constant

of the filter. The record was then plotted, an arbitrary zero time marked on the plot 2 or 3 cycles after the surge due to the speaker power switching transient, a curve was hand faired for the "average" envelope of the response, and the double amplitude of the voltage scaled off at about 4 selected times, converted to dB and plotted on semilog paper. A straight line was faired through the data points. The reverberation time, T_{60}, i.e. the 60 dB down time was calculated from the slope of the faired line.

Application of trim

In the stiffened model there was bare metal exposed. The areas were the top of the floor, the top of the leg of the stringers, and the face of the end rings. The inner side of the cover plate had a 0.406 m (16 in.) disk of fiberglass with the facing film next to the metal and attached by a few small strips of double-back tape. The remainder of the interior surface was covered with a double blanket 0.0127 m (0.5 in.) thick made by placing the facing of the fiberglass layer against the facing of the lead-vinyl layer. The fiberglass side of the blanket was placed next to the skin and the lead-vinyl side was placed next to the underside of the floor. The lead-vinyl was cemented to the floor and the fiberglass attached by double back tape. For the skin insulation, the two layers of the blanket were not attached. In the lower compartment the blanket was held against the skin by gravity. In the upper compartment, small bowed retainer strips, covered wagon hoop style, held the blanket against the skin by the buckling pressure of the retainer ends against the stringers. The retainers compressed the blanket to about 35 to 70 percent its nominal thickness of about 0.014 m (0.55 in.). This left about 0.01524 m (0.6 in.) of one leg of the stringers bare. Photographs showing the exposed stringers are included as Appendix B.

4.2 BBN Test

The sole BBN test consisted of the measurement of the mode shape and resonance frequency of an acoustic mode of the cylinder with floor. A 0.457 m (18 in.) diameter ceramic cylinder approximately 0.304 m (12 in) high was used. A 0.019 m (0.75 in.) thick fiberboard cover was fitted to the cylinder. Holes were drilled for insertion of a 0.0064 m (0.25 in.) microphone. A 0.0064 m (0.25 in.) thick plywood partition simulating the floor was taped to the side of the cylinder. Excitation of the acoustic mode was with a tone, the input being from a small speaker located at the top center of the lid of the cylinder. Partitions simulating θ_G = 0°, 15°, and 30° were tested, for purposes of determining the influence of the floor and for comparison to the predictions with the finite difference technique. The test considered the effect of the floor on the empty cylinder (0,0,2) mode. Results and comparisons are presented in the next section.

4.3 Noise Reduction Data Analysis

Noise reductions, NR_i, defined as the difference between the mean exterior sound pressure level and the interior level, at measurement position, i, were calculated and averaged in accordance with the relation

$$NR = -10 \log_{10} \left[\frac{1}{N} \sum_{i=1}^{N} 10^{-NR_i/10} \right] ,$$

where N is the number of sampled (equal volume) interior points. The results is the cylinder noise reduction, NR. The associated standard deviation for the noise reduction measurements was also calculated with

$$s = \left[\frac{1}{N-1} \sum_{i=1}^{N} \left(10^{-NR_i/10} - 10^{-NR/10} \right)^2 \right]^{1/2} .$$

To quantify the accuracy of the estimates, 99% confidence intervals for the noise reduction estimates were also calculated using the relationship

$$NR_{99} = -10 \log_{10}\left[10^{-NR/10} \pm \frac{s}{\sqrt{N}} t_{m;0.005}\right],$$

where $t_{m;0.005}$ is the 0.005 percentage point of the Student "t" variable with m = N - 1 degrees-of-freedom. It was assumed that the individual noise reduction estimates were statistically independent, which is believed to be an acceptable assumption.

5.0 RESULTS AND COMPARISONS

In this section, results from various tests are considered in a sequence which allows for a gradual confirmation of some of the basic analytical models used in the noise reduction predictions prior to the comparisons of the predictions with the measured noise reductions themselves. Each test article is considered in turn.

5.1 Cavity Modes (Cabin with Floor)

To begin this study, it is first interesting to examine some basic experimental results that were obtained from the test discussed in Section 4.2. A very strongly responding acoustic mode in the empty ceramic cylinder was identified as the $(q,n,s) = (0,0,2)$ mode. The mode shape is [1, p.22]

$$\phi_{0,0,2}(\bar{\xi}) = J_0(m_{02}r),$$

where the root of $J_0'(m_{02}a) = 0$ is $m_{02} = 3.83/a$, where a is the radius. The theoretical resonance frequency is [1, p. 22]

$$f_{0,0,2} = \frac{c_0}{2\pi} m_{02} = \frac{3.83\, c_0}{2\pi a},$$

which for the 0.457 m (18 in) diameter cylinder gives

$$f_{0,0,2} = 915 \text{ Hz}.$$

The measured mode is shown in Figure 19. The resonance frequency is almost exactly the theoretical value and the mode shape closely matches the theory.

In Fig. 20 a small perturbation has been introduced by a 15° floor and the same mode has been identified. The resonance frequency has shifted upward to 922 Hz and the mode shape shows slight bulges appearing at about the 0°, 100° and 260° positions.

The change in modal pattern is even more pronounced in Fig. 21 where the results for a 30° floor are shown. The resonance frequency has shifted to 930 Hz and the mode shape bears little resemblance to that of the no-floor case.

It was after the results of these experiments were available that a decision was made to abandon a perturbation approach to the acoustics problem in favor of the finite different technique. After the theory of Section 3.4 was developed, predictions were compared against these data to assure the proper working of the computer program and the sufficiency of the chosen grid spacing.

Fig. 22 shows the data of Fig. 21 in a more detailed form. The measured resonance frequency is (as previously stated) at 930 Hz. However this measurement is for a 0.2286 m (9 in) radius cylinder. The test articles are 0.254 m (10 in.) radius. Thus this mode would have appeared at (9/10) x 930 Hz or 837 Hz if the test had been performed in a 0.254 m (10 in) radius cylinder.

Fig. 23 shows the third symmetric mode for a 0.254 m (10 in) radius cylinder calculated with the finite difference technique. The computed resonance frequency is 836 Hz. The calculation is for a 40° floor. It should have been made for a 30° floor for a direct comparison but there was a slight communications problem in house. Nevertheless the first twenty symmetric and anti-symmetric modes were calculated with the finite difference technique, then a search for a symmetric mode closest to the measured frequency (837 Hz) was undertaken, and the mode of Fig. 23 was found. Comparisons of Figs. 22 and 23 show that the finite difference technique is quite accurate, certainly accurate enough

for the present purposes. In fact, the acoustic mode shapes and frequencies can be considered as perhaps some of the best data that is input to the noise prediction scheme.

Appendix C contains the first 11 modes computed for a cabin with a $\theta_0 = 49°$ floor per the test articles. The modes are ranked in terms of the λ_i. Mode 5 (symmetric) is the same mode considered in Figs. 19 through 23. The computed value of the resonance frequency for this mode (for $a = 1$ m) is 213 Hz. This gives, for a 0.254 m (10 in) radius cylinder, a resonance frequency of 838 Hz.

5.2 Noise Reduction Measurements, Predictions, and Comparisons

As stated previously, the primary purpose of the present work is to demonstrate the feasibility of the calculation of sound transmission into the interiors of certain complex test articles. The noise reduction (in one-third octaves) has been chosen as the measure for comparison. The three test articles are:

1) a bare ring-stringer stiffened cylinder without floor or trim; wall thickness of 0.000508 m (0.020 inches).

2) a 0.0016 m (0.063 in.) thick unstiffened cylinder (the Phase I test article) modified with a floor partition, lined with a 0.0127 m (0.50 in.) thick layer of PF-105 fiberglass that is covered with a 0.0000508 m (0.002 in.) vinyl film, with a 0.0127 m (0.50 in.) layer of PF-105 fiberglass on the inside of each end cap exposed directly to the interior.

3) a 0.000508 m (0.020 in.) ring-stringer stiffened cylinder (same as (1) above) with a floor partition lined with a simulated trim consisting of a 0.0127 m (0.50 in.) thick

layer of PF-105 fiberglass covered with a 0.00119 m (0.047 in.) thick layer of lead vinyl weighing 2.44 kg/m^2 (0.50 lb/ft^2), with a 0.0127 m (0.50 in.) layer of PF-105 fiberglass on the inside of each end cap exposed directly to the interior.

In Cases (2) and (3) above the exposed floor surface in the cavity (cabin) is bare metal. In Case (3) the (internal) stringers protrude somewhat above the trim exposing a height of about 0.1524 m (0.6 in.) of bare metal on each of five stringers.

Noise Reduction Measurements

Fig. 24 shows the equal volume sampling scheme used when the floor was present. The sampling was done at 18 positions on three measurement planes representing one-fourth of the cylinder volume. Because of the nature of the exterior field and the symmetry present, the 54 measurement positions are sufficient to compute the space average mean square interior level and the ratio of exterior level to average interior level, i.e., the noise reduction. In reality, this was accomplished by measuring the individual noise reductions NR_i at the 54 positions and averaging according to the relations given in Section 4.3. The standard deviation and the 99% confidence intervals were also based on these 54 measurements. In the case of the stiffened cylinder without floor, a slightly different measurement procedure was followed, with larger sampling volumes, resulting in only 38 measurement locations. Figs. 25, 26, and 27 show the measured noise reductions.

5.2.1 Predictions for the Bare 0.020 in. Ring-Stringer Stiffened Cylinder

If insulation (or insulation and lining, i.e.,trim) is present, the wall conductance can be estimated using Eq.(33) and then the

acoustic loss factor can be computed with Eq.(28). Also the added structural damping induced by the trim can be determined (η_r'). The structural loss factor (without trim present) must always be measured for input to the computer program. In the case of a bare cylinder, the program requires the input of both acoustic and structural loss factors. Figs. 28 and 29 show the measured values used for the bare ring-stringer stiffened cylinder.

The acoustic and structural resonance frequencies are also required in addition to the loss factors. The acoustic resonance frequencies for the cylinder without floor are computed with the relation

$$\omega_{qns} = c_0 \lambda_{qns} ,$$

where λ_{qns} is given on page 22 of Ref.[1]. The structural resonance frequencies come from Eq.(60) of this report. Once the ω_n's and ω_r's are known, the constants b_n, b_r, c_n, c_r, D_{nr} $\arctan_n$, $\arctan_r$, $\ln_n$, and $\ln_r$, i.e., everything in the braces $\{\ \}$ in Eq.(36), can be computed. The acoustic mode normalization ϵ_n comes from Eqs.(19) and (20) of Ref.[1]; the modal mass M_r from Eq.(23) of Ref.[1]. Since trim is not present $T_t = |C^w|^2 = 1$. The acoustic/structure coupling term $f'(n,r)$ is given by Eq.(24) or (25) of Ref.[1], the joint acceptance j_r^2, by Eqs. (26), (27) and (28) of that same reference.

Structural Model

The stiffened cylinder is made up of a thin skin with 5 external rings and 5 internal stringers. It is freely supported at its ends, and the mode shapes are assumed to be of the form

$$\psi^{MN}(\theta,z) = \sin\frac{M\pi z}{L}\begin{Bmatrix}\cos N\theta \\ \sin N\theta\end{Bmatrix} .$$

Given below is a tabulation of the data used to specify the properties of the stiffened cylinder as required by Eq.(60).

Stiffened Cylinder Properties
(Dimensions in Meters)

Cylinder Data

Length = 1.2192
Radius = .25375
Skin Thickness = .508000E-3
Youngs Modulus = .72400E+11 N/m^2
Poissons ratio = 0.33
Density = 2700 kg/m^3
Total mass/unit area = 4.27217 kg/m^2

Stringer Data

Stringer Spacing = .318867
Cross-Sectional Area = .151209E-03
Mass per Unit Length = .408265E+00
Moment of Inertia About Centroid = .904240E-08
Distance of Centroid to Skin Middle Surface = -.007768
Torsional Constant for Stiffener = .465416E-09
Stringer Element Input Data

Width	Height	z to Skin Inner surface
.0254000	.0031750	-.0015875
.0031750	.0222250	-.0142875

Frame Data

Frame Spacing = .203200
Cross-Sectional Area = .121935E-03
Mass per Unit Length = .329225E+00
Moment of Inertia About Centroid = .453716E-08
Distance of Centroid to Skin Middle Surface = -.005207
Torsional Constant for Stiffener = .200933E-09
Frame Element Input Data (Frame Elements)

Width	Height	z to Skin Inner Surface
.0342900	.0022860	+.0016510
.0022860	.0190500	+.0123190

Resonance frequencies calculated for the "smeared-out" stiffened cylinder and an unstiffened 0.02 in. cylinder are shown in Figure 30. For the stiffened cylinder the membrane stiffness term dominates until $N \geqslant 5$. By the time the bending stiffness term dominates, the modes have at least one-half wavelength circumferentially between the stringers. As the axial mode number increases to $M \geq 6$, the effects of the rings are reduced and the subpanel motion begins to dominate.

Hu, Gormley, and Lindholm [15] analyzed a ring stiffened cylinder using discrete elements for the rings and shell. Their more exact analysis suggests that the Mikulas formulation over-predicts the resonance frequencies slightly until the sub-panels break-up, at which time the Mikulas theory is not applicable.

Since the cylinder being analyzed is a thin cylinder (.02 in. thick) with relatively heavy stiffeners, the effects of the rings dominate for low orders of M and N. The resonance frequencies calculated using the 'smeared-out' rings and stringers are therefore used when calculating the cylinder noise reduction, since the cavity modes at these frequencies couple to the lower order values of M and N.

Referring to Fig. 30, it is seen that the lowest predicted frequency is for the (M,N) = (1,2) mode. Examination of the response curve of Fig. 31, made with a shaker attached to the skin, shows a resonance frequency at 205 Hz. Another resonance occurs at 292 Hz. The first resonance is a structural mode, the second is apparently the (2,0,1) acoustic mode (see Table 1, p. 84, Ref.[1]). The next significant response is at 407 Hz which could be structural or acoustic. On the basis of this measurement, the (M,N) = (1,2) mode is shifted downward to 205 Hz. The (2,2) mode predicted at 660 Hz is shifted to 645 Hz. The (1,3) mode is not shifted since it is a more questionable action.

Noise Reduction Prediction

Figure 32 gives the calculated noise reduction curve. Also plotted are the measured values. Table 1 gives a breakdown of the five (5) highest contributing acoustic and structural modal pairs in a fashion similar to the manner presented for the unstiffened .063 in. cylinder of Phase I.

TABLE 1

Modal Pairs Having Highest Contributions to Interior Level
Stiffened Cylinder

Band Center Freq. (Hz)	Acoustic Mode q,n,s	Freq.	Structural Mode M,N	Freq.	Contribution $\frac{\langle p_i^2 \rangle}{\langle p_e^2 \rangle}$	Overall $\frac{\langle p_i^2 \rangle}{\langle p_e^2 \rangle}$	Noise Reduction NR
50	END CAPS				.1122E-04	.1122E-04	49.5
63	END CAPS				.1348E-04	.1348E-04	48.7
80	END CAPS				.1949E-04	.1949E-04	47.1
100	END CAPS				.4168E-04	.4168E-04	43.8
125	END CAPS				.5248E-02	.5248E-02	22.8
160	1,0,1	141.7	4,0	3440.6	.1207E-05		
	0,1,1	396.1	1,1	627.4	.5798E-05		
	2,2,1	715.6	1,2	205.0	.8295E-05		
	0,2,1	657.1	1,2	205.0	.5379E-04		
	1,0,1	141.7	2,0	3440.6	.5640E-04		
	END CAPS				.1219E-01	.1231E-01	19.10
200	2,1,1	487.1	1,1	627.4	.2127E-05		
	4,2,1	867.9	1,2	205.0	.9443E-05		
	0,1,1	396.1	1,1	627.4	.2576E-04		
	2,2,1	715.6	1,2	205.0	.5512E-03		
	0,2,1	657.1	1,2	205.0	.3363E-02		
	END CAPS				.2512E-05	.3954E-02	24.03

TABLE 1 (continued)

Modal Pairs Having Highest Contributions to Interior Level
Stiffened Cylinder

Band Center Freq. (Hz)	Acoustic Mode q,n,s	Freq.	Structural Mode* M,N	Freq.	Contribution $\frac{\langle p_i^2 \rangle}{\langle p_e^2 \rangle}$	Overall $\frac{\langle p_i^2 \rangle}{\langle p_e^2 \rangle}$	Noise Reduction NR
250	1,1,1	420.7	2,1	1305.4	.1571E-05		
	2,1,1	487.1	1,1	627.4	.8492E-05		
	2,2,1	715.6	1,2	205.0	.3074E-04		
	0,1,1	396.1	1,1	627.4	.1271E-03		
	0,2,1	657.1	1,2	205.0	.1902E-03	.3619E-03	34.41
315	2,0,1	283.5	3,0	3440.6	.2268E-04		
	2,0,1	283.5	1,0	3440.6	.3606E-04		
	2,1,1	487.1	1,1	627.4	.4132E-04		
	0,2,1	657.1	1,2	205.0	.9055E-04		
	0,1,1	396.1	1,1	627.4	.1265E-02	.1490E-02	28.27
400	0,1,1	396.1	3,1	1784.3	.2021E-03		
	0,2,1	657.1	1,2	205.0	.2079E-03		
	2,1,1	487.1	1,1	627.4	.5979E-03		
	1,1,1	420.7	2,1	1305.4	.1158E-01		
	0,1,1	396.1	1,1	627.4	.6021E+00	.6148E+00	2.11

* N = number of circumferential waves.

TABLE 1 (continued)

Modal Pairs Having Highest Contributions to Interior Level
Stiffened Cylinder

Band Center Freq. (Hz)	Acoustic Mode q,n,s	Freq.	Structural Mode M,N	Freq.	Contribution $\frac{\langle p_i^2 \rangle}{\langle p_e^2 \rangle}$	Overall $\frac{\langle p_i^2 \rangle}{\langle p_e^2 \rangle}$	Noise Reduction NR
500	0,3,1	903.6	1,3	506.5	.7287E-03		
	1,2,1	672.2	2,2	645.0	.9537E-03		
	2,1,1	487.1	3,1	1784.3	.1981E-02		
	0,1,1	396.1	1,1	627.4	.4823E-02		
	2,1,1	487.1	1,1	627.4	.2987E+00	.3083E+00	5.11
630	3,2,1	782.7	2,2	645.0	.1727E-01		
	0,1,1	396.1	1,1	627.4	.2748E-01		
	4,1,1	691.6	1,1	627.4	.3063E-01		
	0,2,1	657.1	1,2	205.0	.1787E+00		
	1,2,1	672.2	2,2	645.0	.1629E+02	.1658E+02	-12.20
800	2,2,1	715.6	1,2	205.0	.1051E-01		
	2,3,1	947.2	3,3	813.9	.1986E-01		
	2,2,1	715.6	3,2	1038.9	.2099E-01		
	4,2,1	867.9	3,2	1038.9	.3837E-01		
	3,2,1	782.7	2,2	645.0	.9341E-01	.2140E+00	6.70

TABLE 1 (continued)

Modal Pairs Having Highest Contributions to Interior Level

Stiffened Cylinder

Band Center Freq. (Hz)	Acoustic Mode q,n,s	Freq.	Structural Mode M,N	Freq.	Contribution $\frac{\langle p_i^2 \rangle}{\langle p_e^2 \rangle}$	Overall $\frac{\langle p_i^2 \rangle}{\langle p_e^2 \rangle}$	Noise Reduction NR
1000	5,3,1	1148.5	4,3	1085.3	.3201E-01		
	6,2,1	1074.7	3,2	1038.9	.3448E-01		
	0,3,1	903.8	3,3	813.9	.3601E-01		
	2,3,1	947.2	3,3	813.9	.1004E+00		
	3,3,1	998.8	4,3	1085.3	.1738E+00	.5193E+00	2.85
1250	4,4,1	1276.8	5,4	1370.8	.6198E-01		
	5,3,1	1148.5	4,3	1085.3	.1198E+00		
	3,4,1	1220.5	4,4	1143.2	.1254E+00		
	1,4,1	1152.7	4,4	1143.2	.2947E+00		
	0,4,1	1380.2	1,5	1395.3	.4214E+00	.1352E+01	-1.31

At 1600 Hz and above the calculations are made with the high frequency result, Eq.(41).

Discussion of Results

Referring to Fig. 32, it is noted that below 125 Hz, in the volume stiffness controlled region, a good prediction cannot be made because the compliance of the cylinder is determined by the relief of the membrane stresses as discussed in Section 3.8. The predicted values shown in Fig. 32 (below 125 Hz) are based on the flexure of the end caps (Section 3.9).

Now suppose there exists a region for which $\bar{\epsilon} > 1$ and the membrane stresses are relieved. Then if the length involved is ℓ = 0.05 m (2 in), the noise reduction at 50 Hz is predicted to be 46 dB, i.e., based on the compliance of the shell, C_p, given by Eq.(101). If the length is 0.076 m (3 in) the noise reduction is predicted to be only 35 dB. For ℓ = 0.10 m (4 in), the value is only 24 dB. However data do not exist that can be used to determine the extent of the regions for which $\bar{\epsilon} > 1$ for the present shell. Thus a prediction is really not possible below 125 Hz.

Above 125 Hz, a fairly good prediction has been made based on the NASA measurements of the acoustic and structural loss factors and the modal characteristics of the shell. The 630 Hz band is anomalous due to the predicted presence of a highly resonant (2,2) structural mode closely coupled in both wavenumber and frequency to a resonant acoustic mode, i.e., the (1,2,1) mode. The (2,2) mode has a very high joint acceptance because it has acoustically fast wavespeeds in both the axial and circumferential directions. From the data in Table 1, the contribution of the (2,2) and (1,2,1) modes can be seen to significantly dominate the prediction. The noise reduction can easily be computed without their participation. The result is the dashed curve in Figure 32 which falls much closer to the measurement. If the prediction is viewed with the (2,2) mode contribution suppressed, it is seen that the prediction follows the measurement with reasonable accuracy from 125 Hz out. The noise reduction climbs to a maximum in the 250 Hz band where there are no resonant acoustic nor structural modes, then nose-dives to a value of only 2 dB at 400 Hz. This is followed by a plateau where the noise reduction remains below 10 dB before increasing slightly in the last few bands.

5.2.2 Predictions for the 0.063 in. Unstiffened Cylinder with Floor and Insulation

As in the previous case, the acoustic and structural loss factors are required; also the resonance frequencies, acoustic and

structural mode normalizations, coupling factors $f'(n,r)$, and joint acceptances. Since the floor is present, the finite difference acoustic modal data are used and since insulation is included, the trim transfer coefficient τ_t is needed.

Figure 33 shows the calculated structural loss factor for two different values of the polyester film loss factor η_t that appears in the calculation of η_r' through the parameter C_w, given by the trim transfer matrix coefficients on p. 34. Also shown is the measured value of η_r that was used in Phase I. The Phase I data were available and were used as the bare cylinder input. However, since the insulation was present, and the cylinder was so lightly damped without it, the value of η_r could have been set to zero without affecting the calculated value of η_r' significantly. Generally there is an overprediction in η_r', however, the fact that the predicted and measured values generally lie in the range between 0.01 and 0.10 is encouraging, that is, basically the right order of magnitude is being predicted.

The acoustic loss factor measurements and predictions are shown in Fig.34. As can be seen the amount of damping afforded by the flexure of the 0.00005 m (0.002 in) vinyl film is quite dramatic. The calculation for various values of η_t are shown. The equations used to calculate η_n were those of Section 3.7, specifically Eqs.(62) and (63) where the conductance came from Eq.(33). A good comparison was never achieved and as a result, the envelope of the measured acoustic loss factor indicated by the horizontal line at η_n = 0.05 and sloping off above 2000 Hz was used as computer input. As can be seen, the measured acoustic loss factors bounce around and identifying the few data points with any specific acoustic modes was impossible.

Figure 35 shows the computed value of the trim transfer coefficient (i.e., $-10 \log \tau_t$). Again the influence of the value of η_t is apparent. For the present work, a value of $\eta_t = 0.5$ was selected to prevent a large negative excursion in the range between 1000 and 2000 Hz.

The acoustic modes were computed with Eq.(58) and the structural modes with Eq.(60), where the model was a curved isotropic panel running from floor line to floor line. The acoustic mode normalization was determined with Eq.(59) and the coupling factors with Eq.(61). The joint acceptances came from Eq.(26) of Ref.[1] where j_M^2 is computed with Eq.(26) as is, and j_N^2 with Eq.(26) changed such that N replaces M and L_y replaces L_x. As before

$$j_r^2 = j_{MN}^2 = j_M^2 \cdot j_N^2 .$$

Figure 36 shows the predicted noise reduction and Table 2 presents the computations in detail.

TABLE 2

Modal Pairs Having Highest Contributions to Interior Level

Unstiffened Cylinder with Floor and Insulation

Band Center Freq.	Acoustic Mode q,i (or n)	Freq.	Structural Mode* M,N	Freq.	Contribution $\frac{\langle p_i^2 \rangle}{\langle p_e^2 \rangle}$	Overall $\frac{\langle p_i^2 \rangle}{\langle p_e^2 \rangle}$	Noise Reduction NR
50	END CAPS				.1072E-04	.1072E-04	49.7
63	END CAPS				.1288E-04	.1288E-04	48.9
80	END CAPS				.1905E-04	.1905E-04	47.2
100	END CAPS				.4074E-04	.4074E-04	43.9
125	END CAPS				.2630E-01	.2630E-01	15.8
160	0,5	837.5	1,5	140.9	.5008E-04		
	0,3	657.5	1,4	187.3	.6510E-04		
	2,0	283.5	1,5	140.9	.7123E-04		
	0,2	444.9	1,5	140.9	.8867E-04		
	0,1	379.6	1,4	187.7	.9732E-04		
	END CAPS				.1049E-02	.1761E-02	27.5
200	2,1	473.8	1,4	187.7	.9104E-04		
	2,3	716.0	1,4	187.7	.1166E-03		
	0,6	937.1	1,4	187.7	.2262E-03		
	0,3	657.5	1,4	187.7	.7076E-03		
	0,1	379.6	1,4	187.7	.1163E-02		
	END CAPS				.2511E-04	.2553E-02	25.9

* N = number of circumferential half-waves.

TABLE 2 (continued)

Modal Pairs Having Highest Contributions to Interior Level

Unstiffened Cylinder with Floor and Insulation

Band Center Freq.	Acoustic Mode q,i (or n)	Freq.	Structural Mode M,N	Freq.	Contribution $\frac{\langle p_i^2 \rangle}{\langle p_e^2 \rangle}$	Overall $\frac{\langle p_i^2 \rangle}{\langle p_e^2 \rangle}$	Noise Reduction NR
250	0,1	379.6	1,2	620.1	.5523E-04		
	0,1	379.6	1,4	187.7	.8284E-04		
	2,0	283.5	1,9	245.1	.1133E-03		
	0,2	444.9	1,3	309.6	.1549E-03		
	2,0	283.5	1,3	309.6	.1709E-02	.2466E-02	26.08
315	2,2	527.5	1,3	309.6	.8007E-03		
	0,1	379.6	1,2	620.1	.8769E-03		
	0,4	703.7	1,3	309.6	.2269E-02		
	0,2	444.9	1,3	309.6	.1094E-01		
	2,0	283.5	1,3	309.6	.3384E-01	.5033E-01	12.98
400	0,1	379.6	1,4	187.7	.6424E-03		
	3,0	425.2	2,5	434.4	.3012E-02		
	1,2	466.9	2,5	434.4	.3064E-02		
	0,2	444.9	1,3	309.6	.1165E-01		
	0,1	379.6	1,2	620.1	.1576E-01	.3719E-01	14.30

TABLE 2 (continued)

Modal Pairs Having Highest Contributions to Interior Level

Unstiffened Cylinder with Floor and Insulation

Band Center Freq.	Acoustic Mode q,i (or n)	Freq.	Structural Mode M,N	Freq.	Contribution $\frac{\langle p_i^2 \rangle}{\langle p_e^2 \rangle}$	Overall $\frac{\langle p_i^2 \rangle}{\langle p_e^2 \rangle}$	Noise Reduction NR
500	2,2	527.5	1,3	309.6	.1337E-02		
	0,1	379.6	1,2	620.1	.2001E-02		
	1,2	466.9	2,5	434.4	.3485E-02		
	2,1	473.8	1,2	620.1	.6951E-02		
	0,2	444.9	1,3	309.6	.9709E-02	.2751E-01	15.60
630	3,1	570.0	2,4	622.6	.3651E-02		
	2,1	473.8	1,2	620.1	.3664E-02		
	0,1	379.6	1,2	620.1	.6530E-02		
	1,3	672.6	2,4	622.6	.5600E-01		
	0,3	657.5	1,2	620.1	.7078E-01	.1552E+00	8.09
800	3,3	783.0	2,4	622.6	.1863E-02		
	1,4	717.9	2,3	960.2	.2184E-02		
	3,4	822.2	2,3	960.2	.2477E-02		
	0,5	837.5	3,5	829.4	.4922E-02		
	2,5	884.1	3,5	829.4	.1144E-01	.3643E-01	14.39

TABLE 2 (continued)

Modal Pairs Having Highest Contributions to Interior Level

Unstiffened Cylinder with Floor and Insulation

Band Center Freq.	Acoustic Mode q,i	(or n)Freq.	Structural Mode M,N	Freq.	Contribution $\frac{\langle p_i^2 \rangle}{\langle p_e^2 \rangle}$	Overall $\frac{\langle p_i^2 \rangle}{\langle p_e^2 \rangle}$	Noise Reduction NR
1000	2,7	1001.3	3,5	829.4	.2361E-02		
	3,6	1029.0	4,6	971.3	.2678E-02		
	2,6	979.0	3,4	1128.2	.3087E-02		
	2,5	884.1	3,5	829.4	.3591E-02		
	4,6	1095.2	3,4	1128.2	.6439E-02	.4339E-01	13.83
1250	5,9	1322.7	6,7	1351.8	.2767E-02		
	3,9	1195.0	4,5	1228.3	.3792E-02		
	5,7	1193.5	4,5	1228.3	.5530E-02		
	4,6	1095.2	3,4	1128.2	.5838E-02		
	4,10	1329.8	5,6	1297.4	.6185E-02	.5306E-01	12.75

Discussion of Results

In general the results of the predictions are good, the shapes of the measured and predicted curves being quite similar. Below 125 Hz the predictions are based on the end caps. The plateau appearing in the measurement between 250 and 1000 Hz has been predicted. This is followed by a rise in the noise reduction and then a sharp increase between 3150 and 5000 Hz due to the 2 mil vinyl film covering the fiberglass on the cylinder wall. This conclusion is evident from examination of Fig. 35. In the

160 and 200 Hz bands, the measured noise reduction exceeds the predicted value, however, the sharp drop at 250 Hz is basically predicted once the density of resonant acoustic modes is sufficient. Another interesting observation is that the prediction generally tries to follow the measurement beyond 1000 Hz, that is rising slightly to a value above 20 dB before the effect of the vinyl film is felt. It is emphasized that this calculation is made using the complex modal characteristics of the cabin space created by the floor partition. To our knowledge no sound transmission prediction of comparable complexity has been attempted before.

5.2.3 Predictions for the 0.02 in Ring-Stringer Stiffened Cylinder with Floor and Trim

The calculation of the acoustic modes was made with Eq.(58). The finite difference data were used because of the presence of the floor. The structural modes were computed with Eq.(60), where the model was that of a curved orthotropic panel running from floor line to floor line. The acoustic mode normalization was determined with Eq.(59) and the coupling factors with Eq.(61). The joint acceptances came from Eq.(26) of Ref.[1] and were calculated in the same manner as they were previously for the 0.063 in cylinder with floor (see 5.2.2).

Acoustic Loss Factors and Trim Transfer Coefficient

Predictions were made of the acoustic loss factors for various values of η_t of the lead-vinyl covering the fiberglass on the sidewall. These are compared to measurements in Figure 37. If there is assumed to be no dissipation in the trim ($\eta_t = 0$), the predicted acoustic loss factors do not match well with the measured data. However by assuming the trim panel is dissipative and taking a loss factor of 0.5 or greater, fairly good predictions can be achieved. Not only are the wide excursions in the

predictions of the acoustic loss factor suppressed, but also those present in the trim transfer coefficient as seen in Figure 38. A value of η_t = 0.5 was chosen for the noise reduction computation.

Structural Loss Factors

Figure 39 shows the measured structural loss factors. Also shown are the predicted values of η_r'. Since the trim was present when the structural loss factor was measured, theoretically η_r' was measured. However, the excitation was with a speaker inside the cylinder and ideally, to determine η_r', the exterior should be excited allowing the trim to react to that response to provide the added damping. Although the predicted η_r' is very high at 400 Hz and below, it is seen from Fig.38 that this is precisely the region over which -10 log τ_t is negative, that is, when an increase in the power flow to the interior due to the presence of the trim is predicted (as compared to the no trim case). The terms dominating the η_r' are determined by the value of the parameter C_w which becomes large and acts to reduce the power flow, i.e., in opposition to the effects caused by τ_t being greater than unity. At frequencies where τ_t is less than unity (i.e., - 10 log τ_t >0), η_r' drops by at least an order of magnitude.

Influence of Stringer Exposure

At high frequencies, when the cavity response is resonant and the structure response is also, the exposed stringers (protruding above the trim) can be a significant contributor to the interior sound level. In fact, if the power flow through the trim itself becomes sufficiently low, the stringers can become the primary contributing source. In the present case, the power flow through the trim is predicted to be very low at high frequencies leading to high noise reductions. Since the primary contributing structural modes are all acoustically fast, the radiation off the stringers is simply the ratio of exposed area of the stringers to

the transmitting area (with trim). Thus the acoustic power inflow due to radiation from the stringers is estimated to be (approximately) given by the power flow computed to pass through the cylinder wall had the trim not been present, multiplied by the ratio of the exposed stringer area to the cylinder wall area (floor-to-floor), but allowing for the increased structural damping present (i.e., η_r') being created by the trim. This leads to

$$W_{in}^{\text{stringers exposed}} = \frac{A_{\text{stringers}}}{A_{\text{cyl. wall}}} \times \frac{W_{in}^{\text{trim on wall}}}{|C^w|^2} .$$

The dissipation in the cavity is almost exactly the same in both cases, i.e., with or without stringer exposure. Thus the space average mean square pressure in the interior due to stringer exposure is given by

$$\frac{\langle p^2 \rangle_{s,t}^{\text{stringers exposed}}}{\langle p^2 \rangle_{s,t}^{\text{no exposure}}} = \frac{W_{in}^{\text{stringers exposed}}}{W_{in}^{\text{trim on wall}}} ,$$

or the difference in interior sound pressure levels is

$$SPL^{\text{w/o exposure}} - SPL^{\text{w/ exposure}} = 10 \log \frac{A_{\text{stringers}}}{A_{\text{cyl. wall}}} - 10 \log |C^w|^2 .$$

Thus the interior level with stringers exposed is estimated to be greater than the interior level without exposure by an amount in dB equal to

$$TL_t + 10 \log \frac{A_{\text{stringers}}}{A_{\text{cyl. wall}}} .$$

Figure 40 shows the predicted noise reductions and Tables 3 and 4 present the computations in detail.

TABLE 3

Modal Pairs Having Highest Contributions to Interior Level

Stiffened Cylinder with Floor and Trim

Band Center Freq.	Acoustic Mode q,i (or n)	Freq.	Structural Mode* M,N	Freq.	Contribution $\frac{\langle p_i^2 \rangle}{\langle p_e^2 \rangle}$	Overall $\frac{\langle p_i^2 \rangle}{\langle p_e^2 \rangle}$	Noise Reduction NR
50	END CAPS				.1445E-04	.1445E-04	48.4
63	END CAPS				.1737E-04	.1737E-04	47.6
80	END CAPS				.2512E-04	.2512E-04	46.0
100	END CAPS				.5370E-04	.5370E-04	42.7
125	END CAPS				.1698E-02	.1698E-02	27.7
160	2,0	283.5	1,1	961.7	.1854E-05		
	1,0	141.7	2,5	676.7	.3578E-05		
	0,1	380.0	1,2	416.5	.1236E-04		
	1,0	141.7	2,3	636.6	.3208E-04		
	1,0	141.7	2,1	1727.7	.7993E-04		
	END CAPS				.1698E-02	.1828E-02	27.3
200	0,2	445.3	1,3	298.8	.4178E-05		
	1,0	141.7	2,1	1727.7	.5409E-05		
	2,1	474.1	1,2	416.5	.6116E-05		
	2,0	283.5	1,1	961.7	.1117E-04		
	0,1	380.0	1,2	416.5	.8178E-04	.1276E-03	38.94

* N = number of circumferential half-waves.

TABLE 3 (continued)

Modal Pairs Having Highest Contributions to Interior Level

Stiffened Cylinder with Floor and Trim

Band Center Freq.	Acoustic Mode q,i (or n)	Freq.	Structural Mode M,N	Freq.	Contribution $\frac{\langle p_i^2 \rangle}{\langle p_e^2 \rangle}$	Overall $\frac{\langle p_i^2 \rangle}{\langle p_e^2 \rangle}$	Noise Reduction NR
250	0,2	445.3	1,3	298.8	.2687E-04		
	2,1	474.1	1,2	416.5	.4111E-04		
	2,0	283.5	1,3	298.8	.3309E-03		
	2,0	283.5	1,1	961.7	.7044E-03		
	0,1	380.0	1,2	416.5	.7146E-03	.1914E-02	27.18
315	0,2	445.3	1,3	298.8	.2222E-03		
	2,1	474.1	1,2	416.5	.2415E-03		
	2,0	283.5	1,1	961.7	.1357E-02		
	2,0	283.5	1,3	298.8	.1400E-02		
	0,1	380.0	1,2	416.5	.1161E-01	.1536E-01	18.14
400	1,2	467.3	2,3	636.6	.1862E-03		
	1,1	405.5	2,2	967.0	.2452E-03		
	2,1	474.1	1,2	416.5	.7846E-03		
	0,2	445.3	1,3	298.8	.1253E-02		
	0,1	380.0	1,2	416.5	.7657E-02	.1081E-01	19.66

TABLE 3 (continued)

Modal Pairs Having Highest Contributions to Interior Level

Stiffened Cylinder with Floor and Trim

Band Center Freq.	Acoustic Mode q,i (or n)	Freq.	Structural Mode M,N	Freq.	Contribution $\frac{\langle p_i^2 \rangle}{\langle p_e^2 \rangle}$	Overall $\frac{\langle p_i^2 \rangle}{\langle p_e^2 \rangle}$	Noise Reduction NR
500	2,2	527.9	1,3	298.0	.2160E-03		
	0,1	380.0	1,2	416.5	.4274E-03		
	0,2	445.3	1,3	298.8	.7272E-03		
	1,2	467.3	2,3	636.6	.8114E-03		
	2,1	474.1	1,2	416.5	.1321E-02	.4200E-02	23.77
630	0,3	658.1	1,2	416.5	.3011E-03		
	0,3	658.1	1,4	397.4	.3685E-03		
	1,3	673.2	2,4	552.4	.6084E-03		
	1,4	718.5	2,3	636.6	.8336E-03		
	3,2	615.7	2,3	636.6	.1105E-02	.4402E-02	23.56
800	0,5	838.3	3,5	808.5	.1508E-03		
	2,3	716.8	3,4	811.9	.2682E-03		
	2,5	884.9	3,5	808.5	.3294E-03		
	4,3	868.6	3,4	811.9	.4294E-03		
	1,4	718.5	2,3	636.6	.6685E-03	.2874E-02	25.42

TABLE 3 (continued)

Modal Pairs Having Highest Contributions to Interior Level

Stiffened Cylinder with Floor and Trim

Band Center Freq.	Acoustic Mode q,i (or n)	Freq.	Structural Mode M,N	Freq.	Contribution $\frac{\langle p_i^2 \rangle}{\langle p_e^2 \rangle}$	Overall $\frac{\langle p_i^2 \rangle}{\langle p_e^2 \rangle}$	Noise Reduction NR
1000	4,4	904.2	3,3	1004.2	.5173E-04		
	2,6	979.9	3,6	960.1	.6108E-04		
	5,5	1097.7	4,5	1032.0	.6253E-04		
	3,6	1029.9	4,4	1108.5	.8596E-04		
	3,7	1051.1	4,5	1032.0	.2210E-03	.1250E-02	29.03
1250	4,9	1253.4	3,7	1218.7	.1426E-04		
	3,9	1196.0	2,7	1174.3	.1446E-04		
	1,9	1126.8	2,7	1174.3	.2042E-04		
	6,7	1263.4	5,5	1309.0	.2724E-04		
	0,9	1117.9	1,7	1165.1	.3816E-04	.3467E-03	34.60

TABLE 4

Effect of Stringer Exposure+

Frequency (Hz)	Computed NR w/o Stringer Exposure	$-10 \log\|C^w\|^2$	Estimate of NR with Stringer Exposure+
1000	29.0	20.8	17.0
1250	34.6	25.4	18.0
1600	40.8	29.6	20.0
2000	50.9	33.8	25.9
2500	59.9	37.5	31.2
3150	65.3	40.7	33.4
4000	71.6	43.5	36.9
5000	74.7	45.9	37.6

+ Stringers exposed area = 0.145 m^2
Cylinder wall area (trim covered) = 1.09 m^2
$\eta_t = 0.5$

Discussion of Results

As in the previous cases, the prediction below 125 Hz is based on the end caps' transmission. While the prediction below 125 Hz is not particularly of concern, it can be seen that the measured noise reduction is in closer agreement to the prediction than it was for the bare stiffened cylinder. It can be seen from Table 3 that at 125 and 160 Hz the end caps dominate. This is due to their intimate coupling with the (1,0) acoustic mode at 141.7 Hz. Incidentally, recall the (1,0) acoustic mode is q = 1, i = 0 where i is the assigned order of the 2 dimensional modal pattern

in the cylinder cross section when the floor is present (mode 0 of Appendix C). By 200 Hz, the end cap contribution can be ignored. The measured and predicted noise reductions rise sharply due to the absense of any resonant acoustic modes and then fall dramatically as has been observed in the previous two comparisons. However the curves rapidly bend upward because the trim lining is so heavy (see Fig.38). The prediction is that the noise reduction could rise to over 70 dB by 5000 Hz if the stringers were not exposed. Actually, it is a pretty remote possibility that it would ever achieve that level even if the stringers were not exposed because of other shorting paths (vibration of the end caps, exposed metal such as the floor, etc.) In the present case, the stringers are obviously the shorting mechanism (Table 4). The transition between the two curves in Figure 40 (stringers exposed versus not exposed) is not clear, although it could probably have been determined; it did not seem important to do so. It is felt that the present interpretation of the results is reasonably accurate, and that basically all the structure in the curves has been explained with the present model.

5.3 Statistical Analysis of Prediction Error

The remaining question to be answered is whether there is a bias in the predictions, that is, does the analytical model (with the best input data that can be generated) tend to over or under predict the noise reduction on the average.

Table 5 contains the measured and predicted noise reductions for the three test articles. It includes the noise reductions for frequencies at and above 125 Hz, and excludes the transition region data for the stiffened cylinder with floor and trim where the stringers' exposure first begins to contribute significantly.

Of interest is whether there is a statistically significant difference, on the average, between the predictions and the measurements for these data, i.e., are the predictions biased?

TABLE 5

Predicted versus Measured Noise Reductions

Band Center Freq.	.02 Stiffened w/o Floor		.06 Unstiffened w/Floor		.02 Stiffened w/Floor & Trim	
	Predicted	Measured	Predicted	Measured	Predicted	Measured
125	22.8	22.7	29.8	27.9	27.7	30.4
160	19.1	19.2	27.5	34.9	27.7	31.9
200	24.0	18.3	25.9	35.1	38.9	36.7
250	34.4	24.9	26.1	17.6	27.2	30.9
315	28.3	11.5	13.0	16.6	18.1	27.0
400	2.1	2.6	14.3	15.4	19.7	20.0
500	5.1	5.3	15.6	16.4	23.8	16.9
630	-12.2	4.2	8.1	17.8	23.6	21.3
800	6.7	6.3	14.4	16.2	25.4	22.1
1000	2.8	6.1	13.6	15.0	Transition region	
1250	-1.3	3.9	12.8	21.5	data are not	
1600	4.2	4.1	19.3	23.3	included.	
2000	5.7	4.6	20.7	23.5	25.9	30.4
2500	7.3	3.8	24.2	24.1	31.2	32.1
3150	8.2	3.3	24.0	22.1	33.4	31.6
4000	10.6	8.0	31.1	29.2	36.9	36.7
5000	12.3	10.0	34.4	36.3	37.6	39.4

To determine if there is any bias, the differences Δ_i; i = 1,2, ..., n, between the predictions and measurements in each one-third octave band are computed and their mean and standard deviation determined by pooling all data from the three tests, providing a sample size of n = 48. The sample mean and standard deviation are

$$\bar{\Delta} = -0.56 \text{ dB} \quad ; \quad s = 5.46 \text{ dB}.$$

Under the hypothesis that there is no discrepancy on the average, that is,

$$H_0 : \mu_\Delta = 0,$$

the sampling distribution of $\bar{\Delta}$ becomes

$$\bar{\Delta} = \frac{s}{\sqrt{n}} t_{n-1} ,$$

where t_{n-1} is the student "t" variable with n-1 = 47 degrees of freedom. The acceptance region for the hypothesis above is given by

$$-\frac{s}{\sqrt{n}} t_{n-1,\alpha/2} < \bar{\Delta} \leq \frac{s}{\sqrt{n}} t_{n-1;\alpha/2}$$

For a two-sided test at the α = 0.05 level of significance, $t_{47;0.025}$ = 2.01: so $\bar{\Delta}$ must fall between -1.59 and +1.59 dB. Since the sample mean $\bar{\Delta}$ (=-0.56 dB) falls within the acceptance region, there is no reason to question the validity of the hypothesis, i.e., there is not a statistically significant difference between the predictions and measurements on the average (at the α = 0.05 level of significance).

On the other hand, there is a substantial random error in the predictions versus measurements as indicated by the standard deviation of s = 5.5 dB for the Δ_i values. This means that one can expect a discrepancy of more than 5 or 6 dB for about one-third of the predictions.

In the future, output from the interior noise program should include, in addition to the predicted noise level, a measure of the quality of the prediction based upon a statistical analysis of the comparison data accumulated in the various tests. This measure would be the confidence intervals, which might be computed for the various frequency bands by scaling-up the test articles to the fuselage diameter of concern. It is felt that there will continue to be a substantial random error although its existence will almost always be associated with input data deficiencies.

REFERENCES

1. Pope, L. D., Rennison, D. C., and Wilby, E. G., "Analytical Prediction of the Interior Noise for Cylindrical Models of Aircraft Fuselages for Prescribed Exterior Noise Fields, Phase I: Development and Validation of Preliminary Analytical Models", NASA CR 159363 (1980).

2. Pope, L. D., and Wilby, J. F., "Band-limited Power Flow into Enclosures", *J. Acoust. Soc. Am.*, **62**, 4, 906-911 (1977).

3. Pope, L. D., and Wilby, J. F., "Band-limited Power Flow into Enclosures, II", *J. Acoust. Soc. Am.*, **67**, 3, 823-826 (1980).

4. Schultz, T. J., "Wrappings, Enclosures and Duct Linings", Chapter 15 in Noise and Vibration Control, L. L. Beranek, Editor, McGraw-Hill, New York 1971.

5. Beranek, L. L., and Work, G. A., "Sound Transmission through Multiple Structures Containing Flexible Blankets", *J. Acoust. Soc. Am.*, **21**, 4, 419-428 (1949).

6. Zwikker, C., and Kosten, C. W., Sound Absorbing Materials, Elsevier, New York 1949.

7. Mikulas, M. M., and McElman, J. A., "On Free Vibrations of Eccentrically Stiffened Cylindrical Shells and Flat Plates", NASA TN D-3010 (1965).

8. Peterson, M. R., and Boyd, D. E., "Free Vibrations of Circular Cylinders with Longitudinal, Interior Partitions", *J. Sound and Vib.*, **60**(1), 45-62 (1978).

9. Pope, L. D., "On the Transmission of Sound through Finite Closed Shells: Statistical Energy Analysis, Modal Coupling, and Nonresonant Transmission", *J. Acoust. Soc. Am.*, **50**, 3, 1004-1018 (1971).

REFERENCES (continued)

10. Plotkin, K. J., Kasper, P, K., and Glenn, P. K., "Prediction of Low Frequency Sound Transmission through Aerospace Structures, with Application to Space Shuttle", Wyle Research Report WR78-5 (1978).

11. Lyon, R. H., et. al., "Low-Frequency Noise Reduction of Spacecraft Structures", NASA CR-589 (1966).

12. Kraus, H., Thin Elastic Shells, Wiley, New York 1967.

13. Bois, G. P., Tables of Indefinite Integrals, Dover, New York 1961.

14. Roark, R. K., Formulas for Stress and Strain, McGraw-Hill, New York 1975.

15. Hu, W. C. L., Gormley, J. F., and Lindholm, U. S., "An Analytical and Experimental Study of Vibrations of Ring-Stiffened Cylindrical Shells", Southwest Research Institute Technical Report #9 (1967).

APPENDIX A

Transfer Matrix for Trim Insulation

Transfer Matrix for Trim Insulation

Consider a harmonic pressure wave moving from left to right in the insulation of Figure 1 (imagine that the skin and lining are not present). When the wave reaches x = L, it is reflected. If the pressure amplitude in the incident wave at x = L is p_i and the pressure amplitude in the reflected wave is p_r, then the pressure at any point x measured from left to right is (dropping the $e^{-i\omega t}$ dependence)

$$p(x) = p_i e^{i(k+i\alpha)(x-L)} + p_r e^{-i(k+i\alpha)(x-L)}, \qquad \text{(A1)}$$

where k is the acoustic wavenumber in the insulation and α is the decay constant. Note, that when x = L,

$$p(L) = p_i + p_r .$$

Let $\gamma = \alpha - ik$. Then

$$p(x) = p_i e^{\gamma(L-x)} + p_r e^{-\gamma(L-x)}. \qquad \text{(A2)}$$

The particle velocity is

$$v(x) = \frac{p_i}{W} e^{\gamma(L-x)} - \frac{p_r}{W} e^{-\gamma(L-x)}, \qquad \text{(A3)}$$

where W is the wave impedance in the material, that is

$$W = p/v,$$

where p is the pressure and v is the particle velocity for a wave running in the material when the material has unlimited extent (W is independent of x).

Then, when x = L,

$$v(L) = \frac{p_i - p_r}{W}.$$

Now let

$$p(0) = p_1 \qquad v(0) = v_1$$

$$p(L) = p_2 \qquad v(L) = v_2.$$

Also define the impedance Z_2 as

$$Z_2 = p_2/v_2. \tag{A4}$$

Then,

$$p_2 = p_i\left(1 + \frac{Z_2 - W}{Z_2 + W}\right).$$

But

$$p_i = \frac{p_1}{e^{\gamma L} + \frac{Z_2 - W}{Z_2 + W} e^{-\gamma L}}.$$

Therefore

$$p_2 = \frac{Z_2 p_1}{Z_2 \cosh \gamma L + W \sinh \gamma L} . \tag{A5}$$

Also, it is found that

$$v_2 = \frac{W v_1}{Z_2 \sinh \gamma L + W \cosh \gamma L} . \tag{A6}$$

Let

$$\cosh \gamma L = C$$
$$\sinh \gamma L = S .$$

Using Eqs. (A4), (A5), and (A6), after some algebra, it is found that

$$p_2 = \frac{C}{C^2 - S^2} p_1 - \frac{WS}{C^2 - S^2} v_1 ,$$

and

$$v_2 = \frac{C}{C^2 - S^2} v_1 - \frac{S/W}{C^2 - S^2} p_1 .$$

Now

$$C^2 - S^2 = 1 ,$$

so

$$\left.\begin{matrix} p_2 \\ v_2 \end{matrix}\right\} = \begin{bmatrix} C & -WS \\ -S/W & C \end{bmatrix} \left.\begin{matrix} p_1 \\ v_1 \end{matrix}\right\}$$

This is the desired transfer matrix in terms of input and output pressures and velocities.

APPENDIX B

Photographs of Test Articles

NASA
L-81-2440

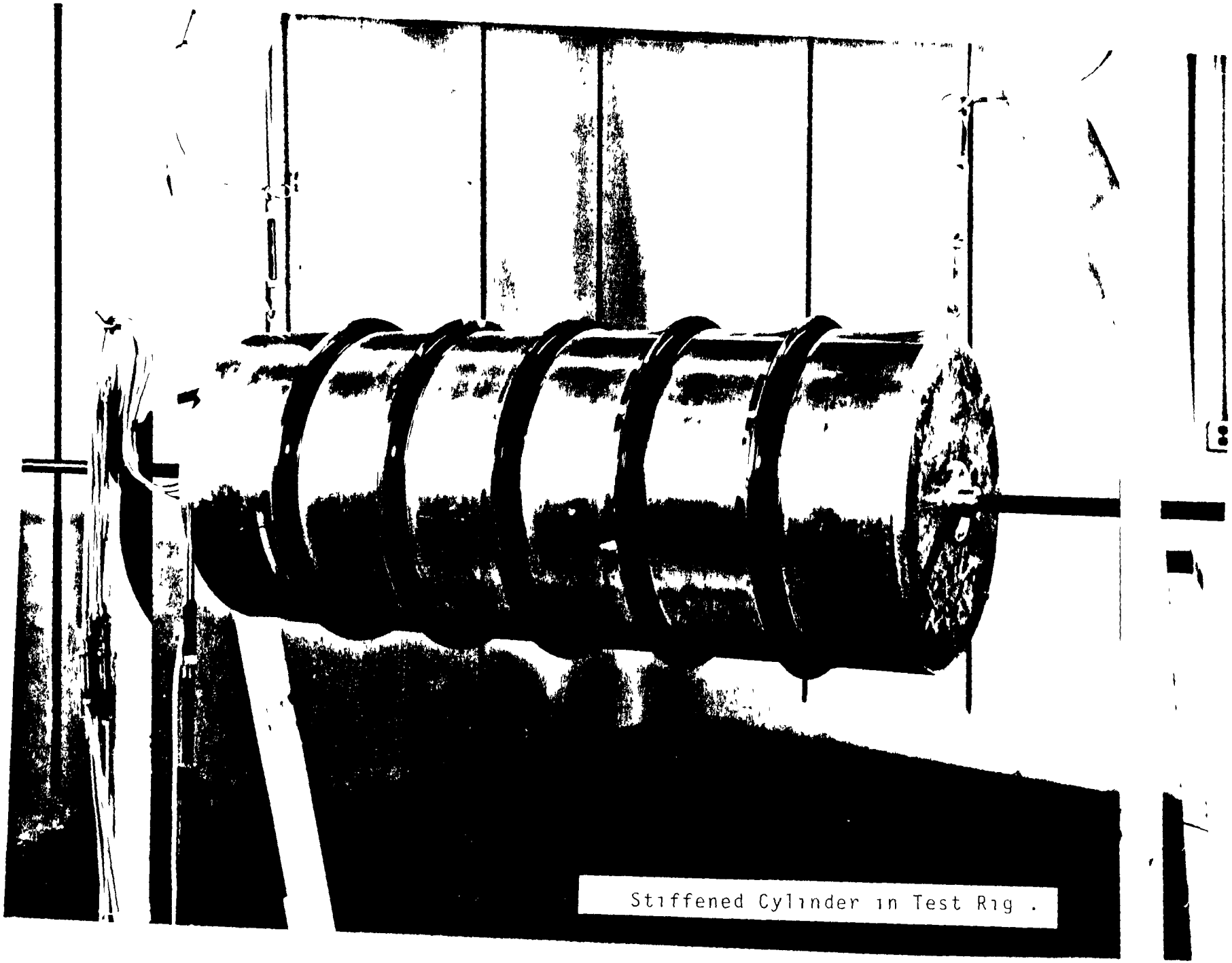

Stiffened Cylinder in Test Rig .

NASA
L-81-10,179

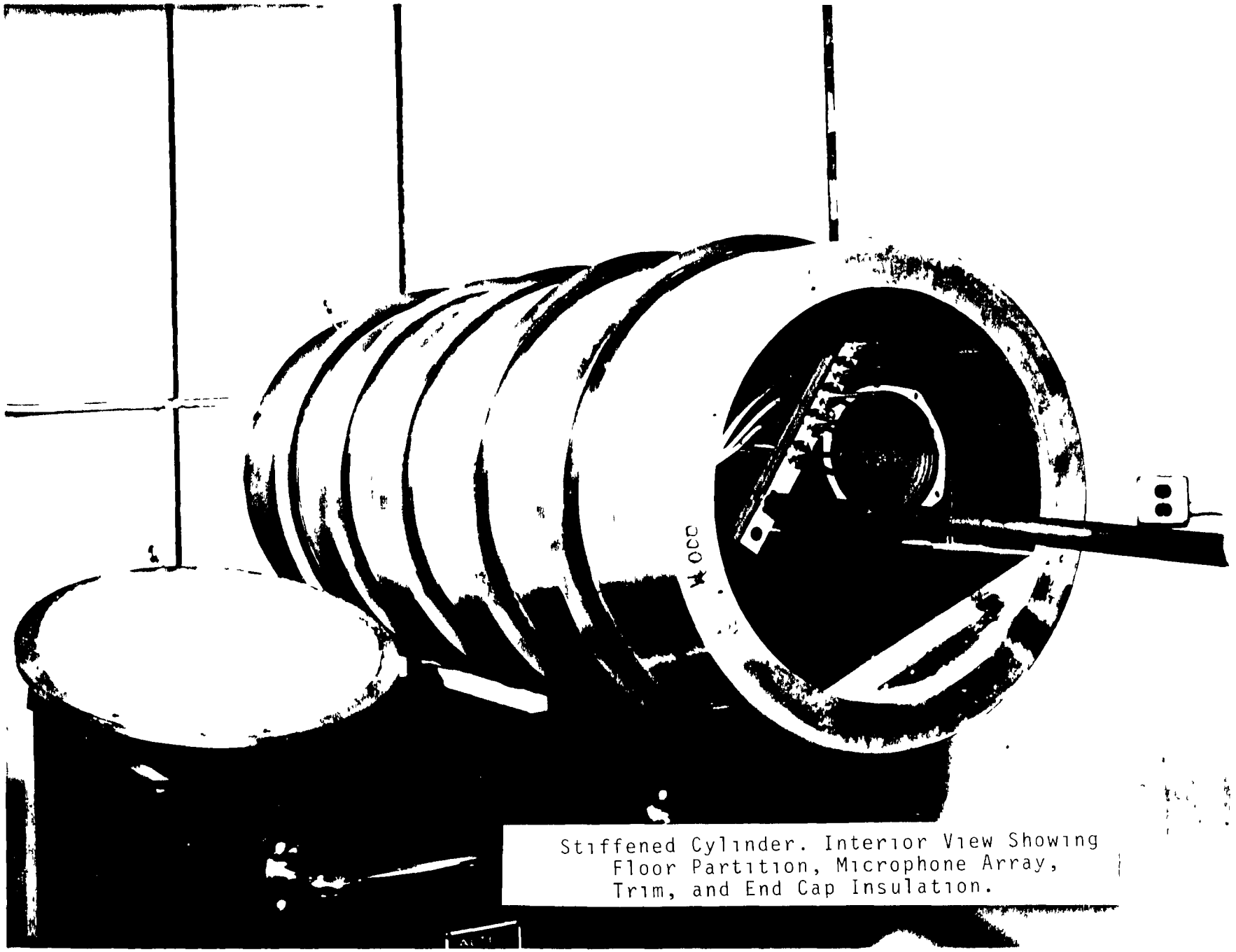

Stiffened Cylinder. Interior View Showing Floor Partition, Microphone Array, Trim, and End Cap Insulation.

NASA
L-81-10,178

Interior of the Stiffened Cylinder Note the Exposed Stringers.

NASA
L-81-10,180

View Showing Exposed Stringers, Bowed Retainer Strips, Floor, and End Cap Insulation.

APPENDIX C

Finite Difference Results
Acoustic Modal Patterns and Resonance Frequencies

$$\theta_0 = 49^\circ$$
$$a = 1\,m$$
$$q = 0$$

MODE 0. SYMMETRIC

FREQ = 0.000

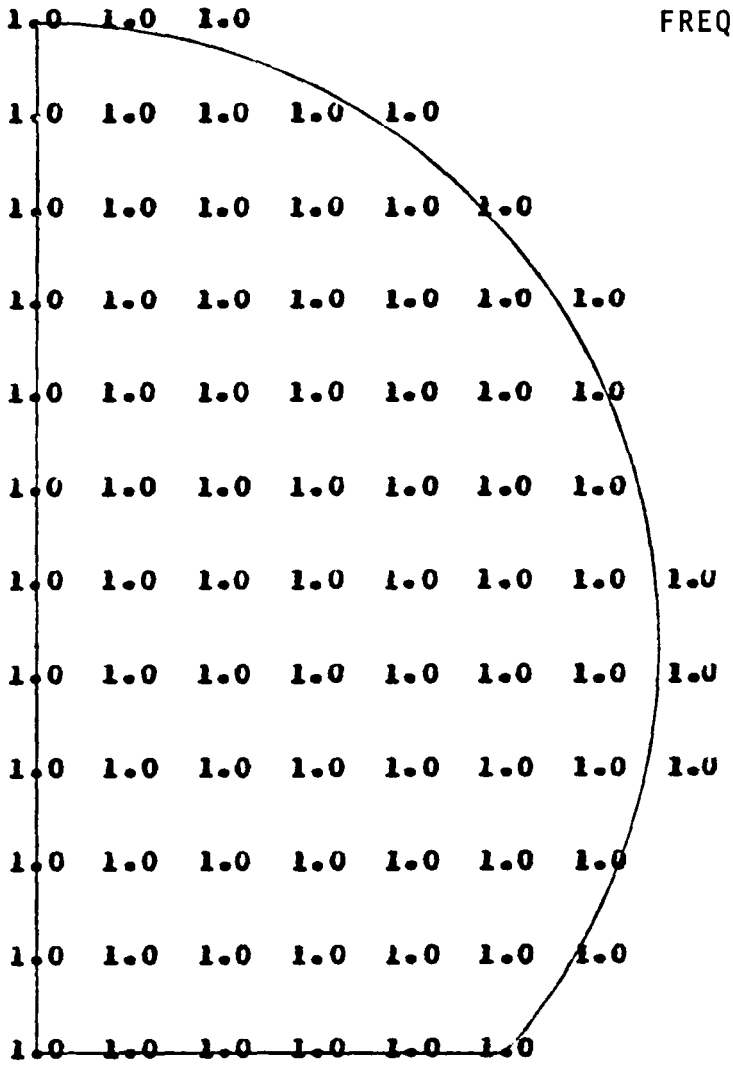

MUDE 1. ANTISYMMETRIC

FREQ = 96.416

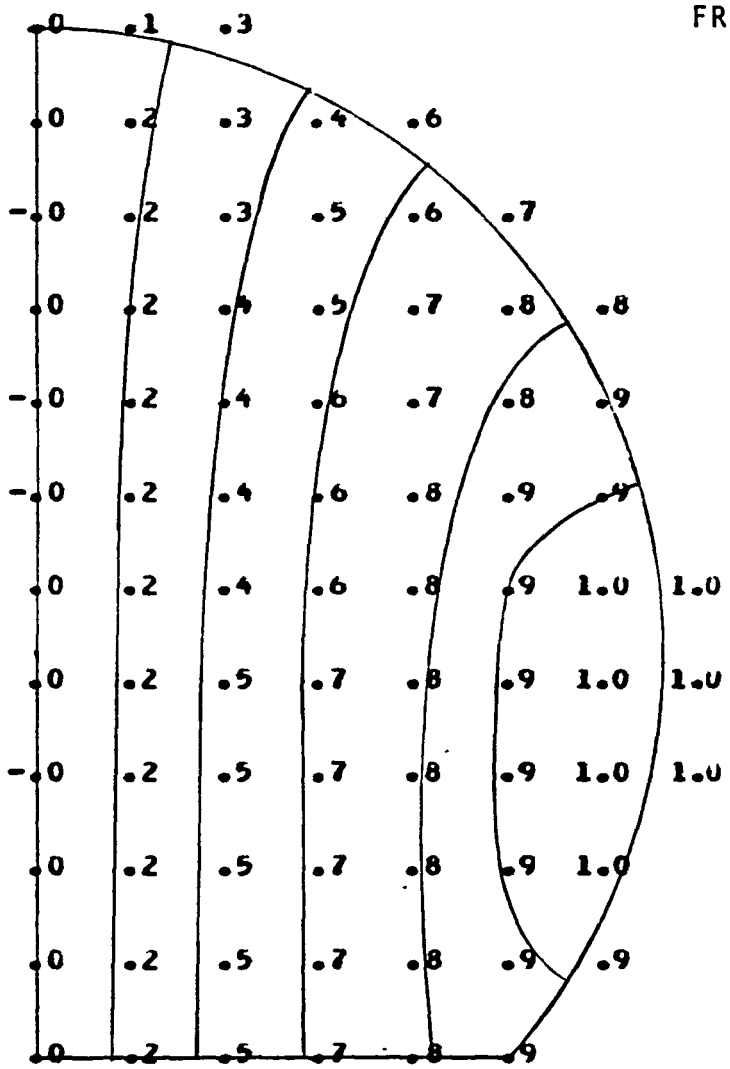

MODE 2. SYMMETRIC

FREQ = 113.002

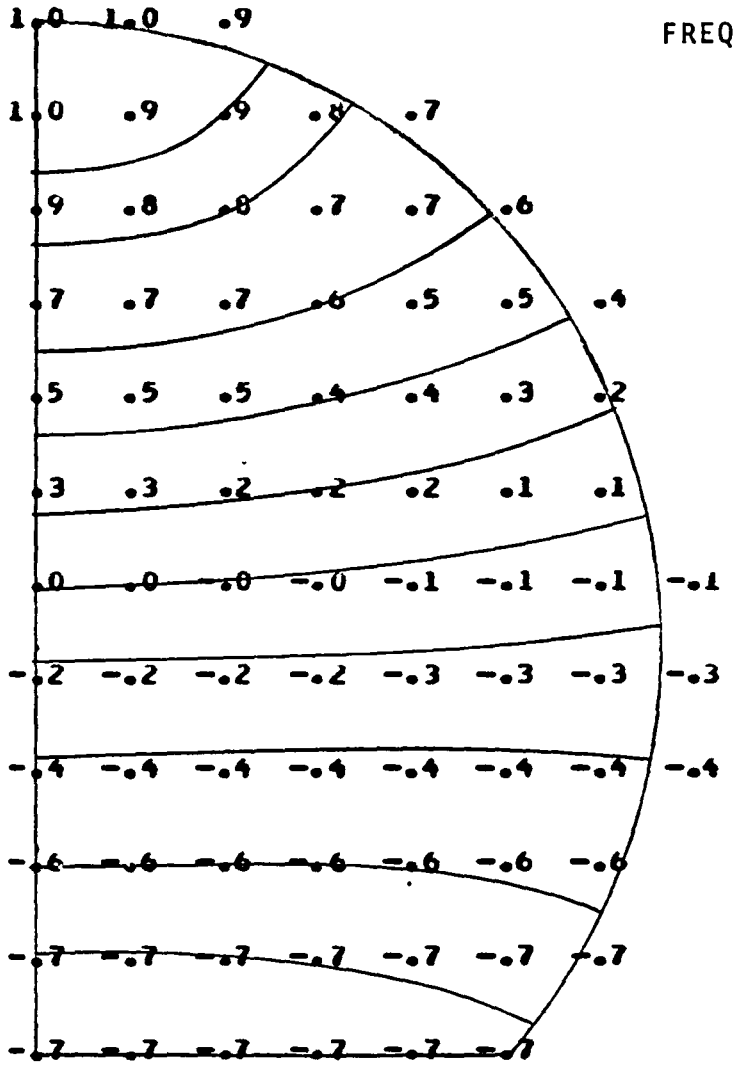

MODE 3. ANTISYMMETRIC

FREQ = 166.997

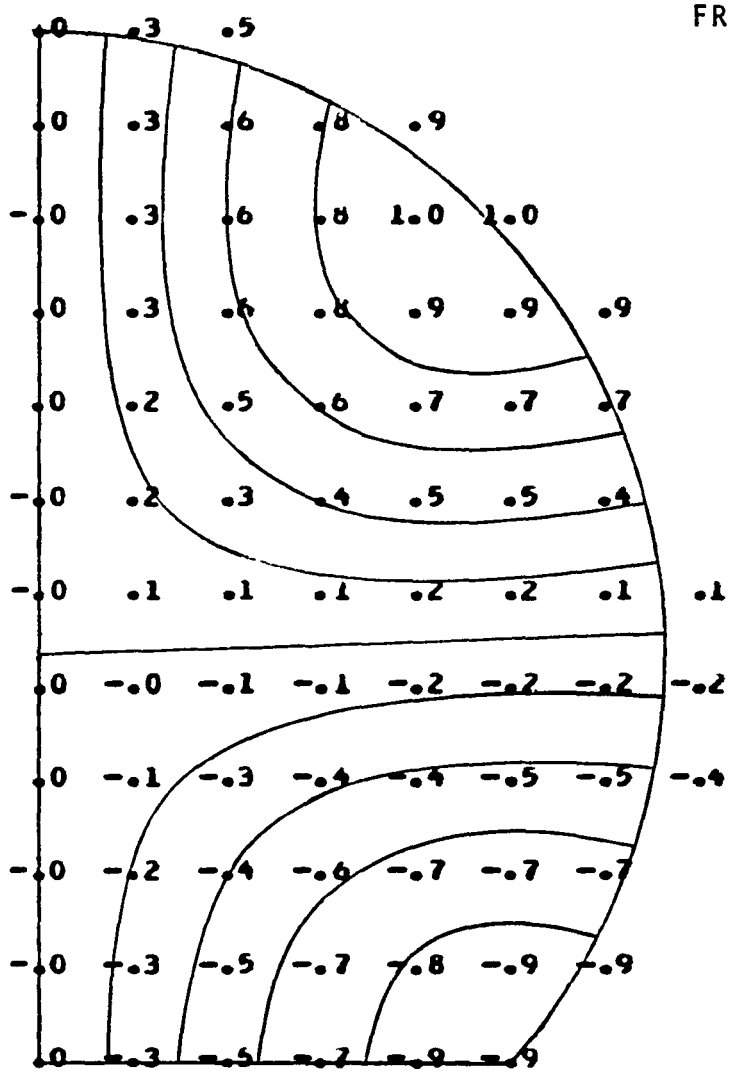

MUDE 4. SYMMETRIC

FREQ = 178.748

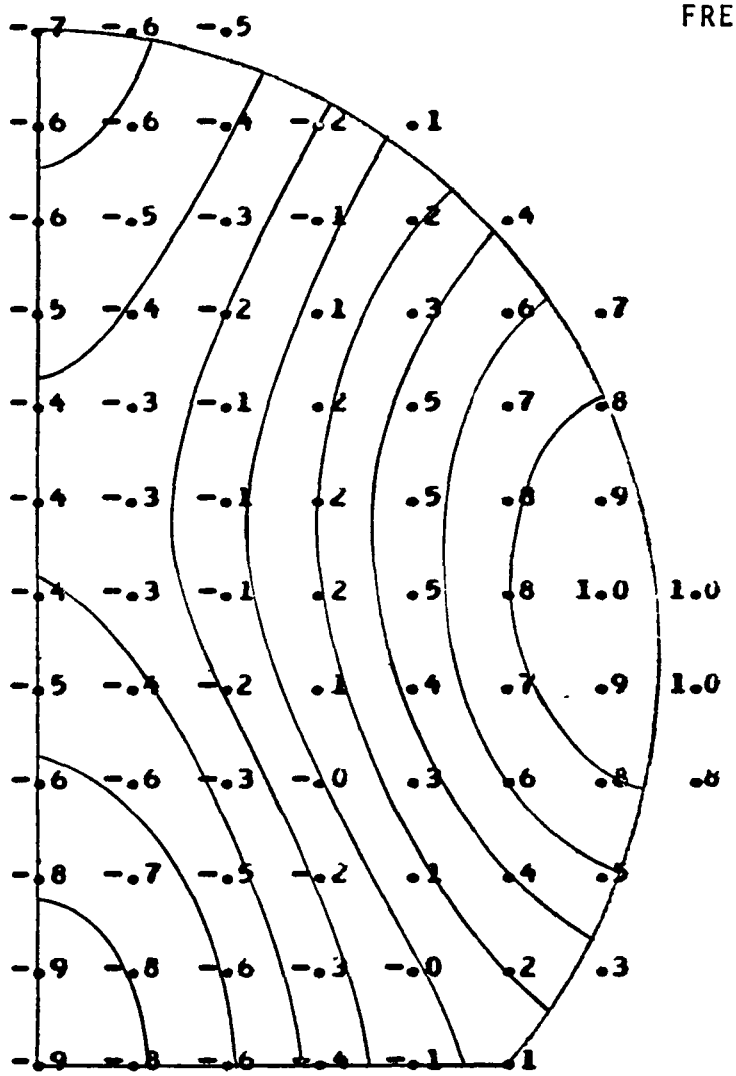

MODE 5. SYMMETRIC

FREQ = 212.718

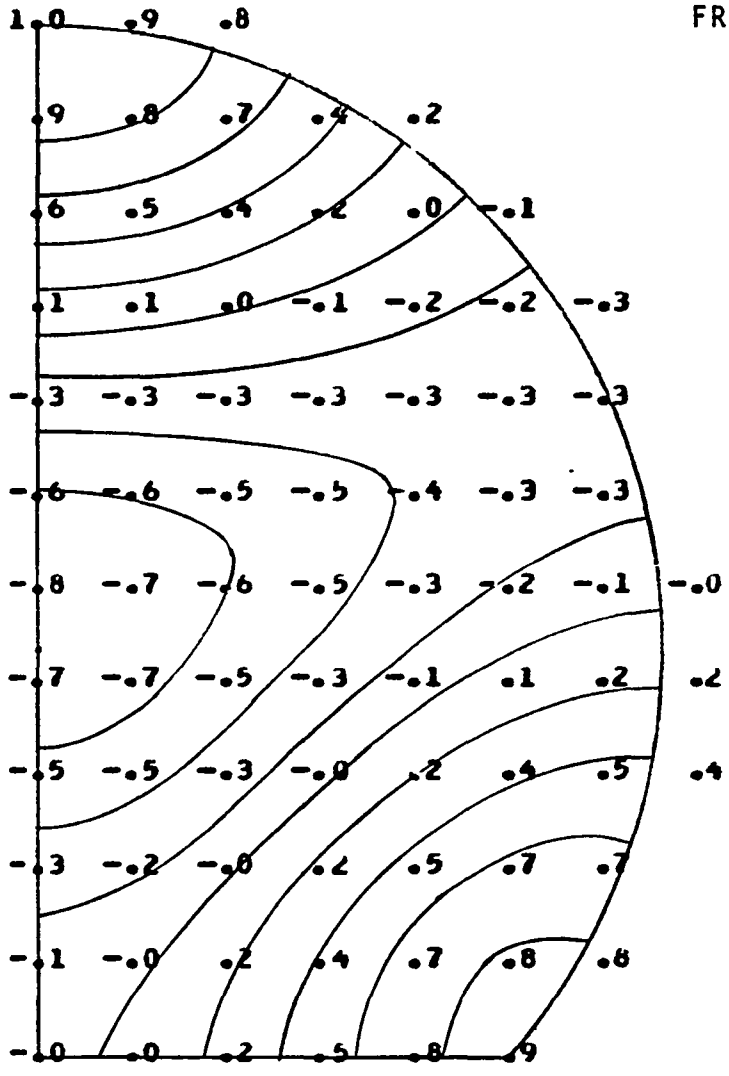

MODE 6. ANTISYMMETRIC

FREQ = 238.019

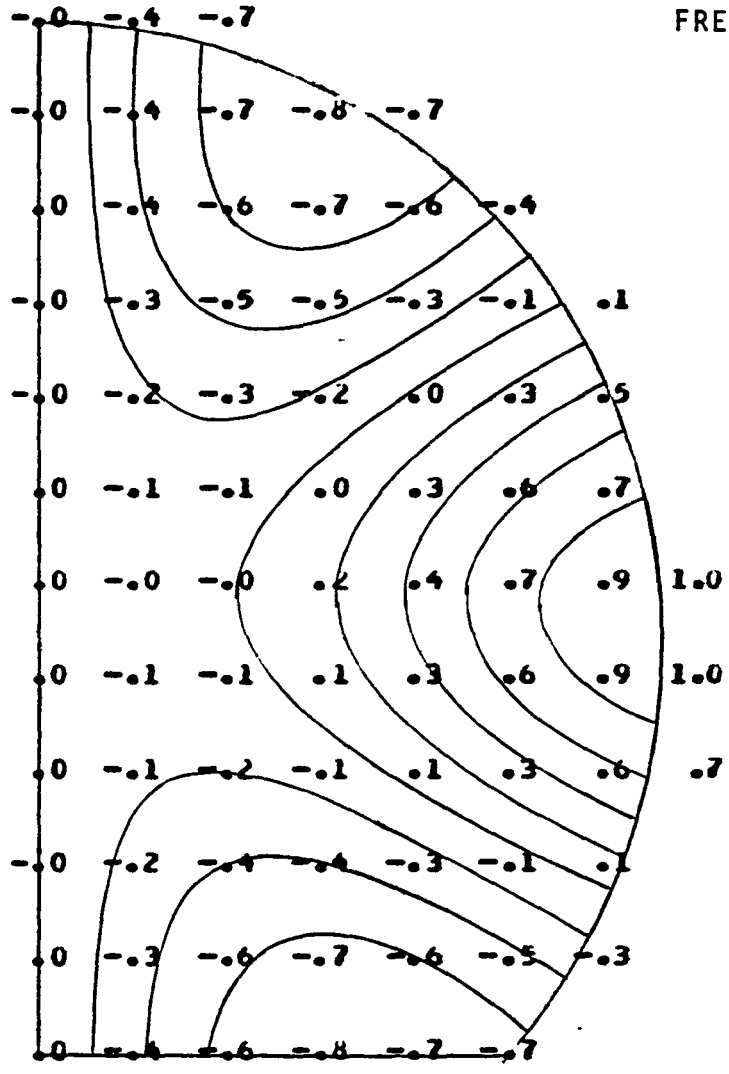

MODE 7. SYMMETRIC

FREQ = 243.915

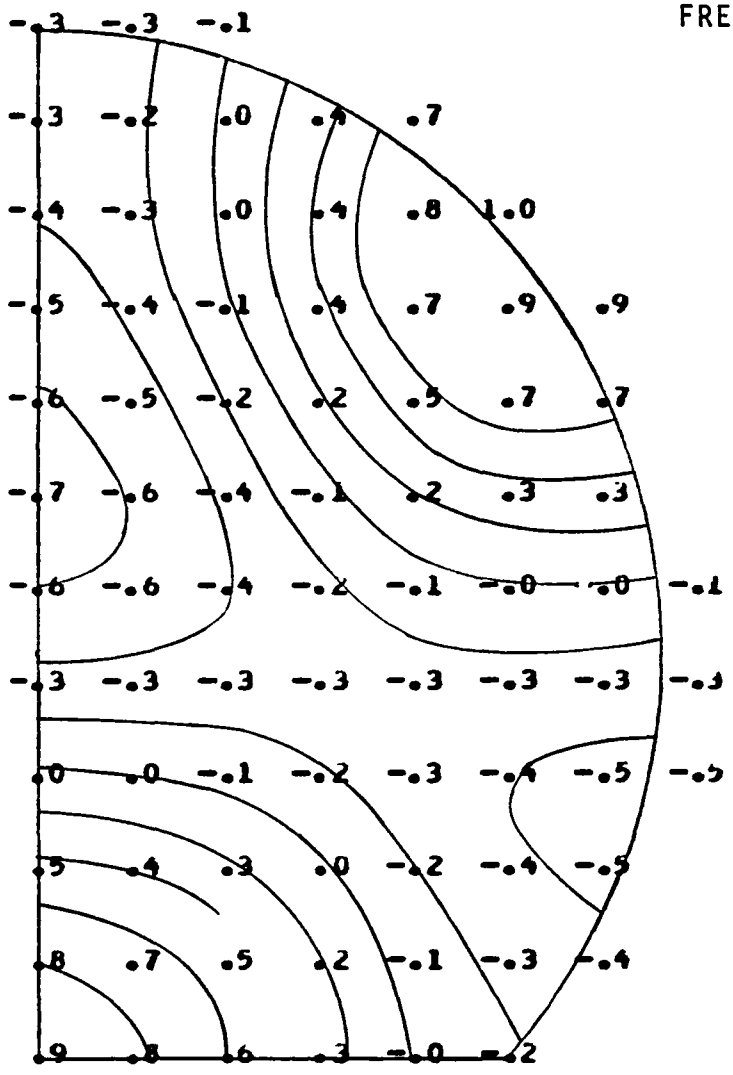

MODE 8. ANTISYMMETRIC

FREQ = 280.915

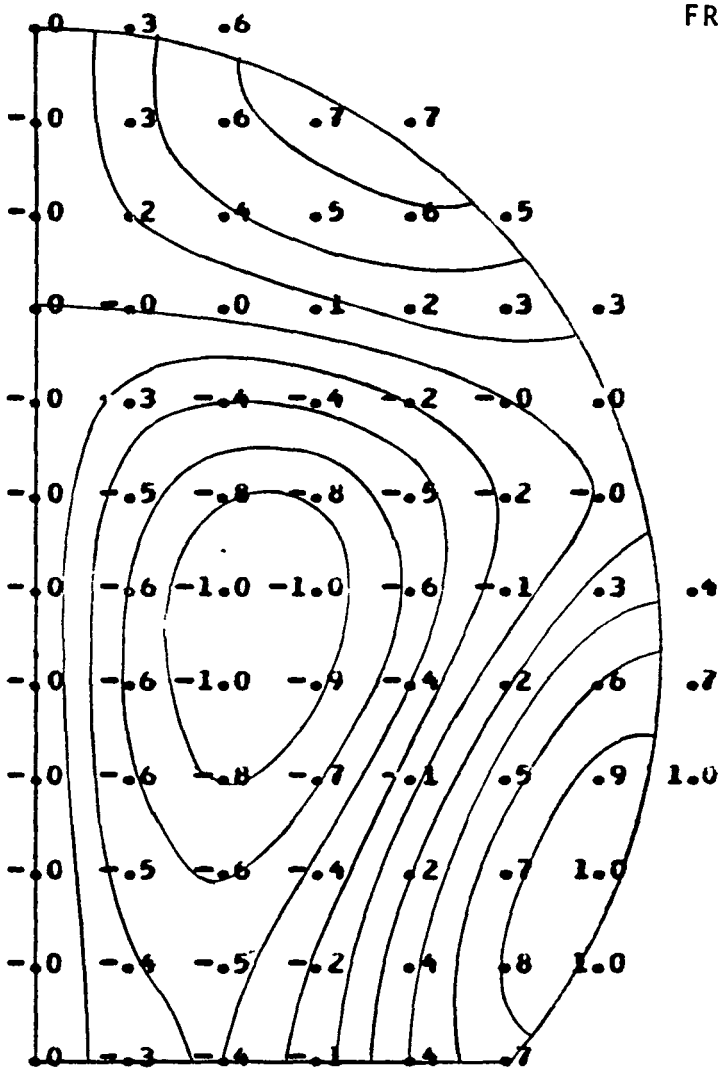

MODE 9. SYMMETRIC

FREQ = 283.663

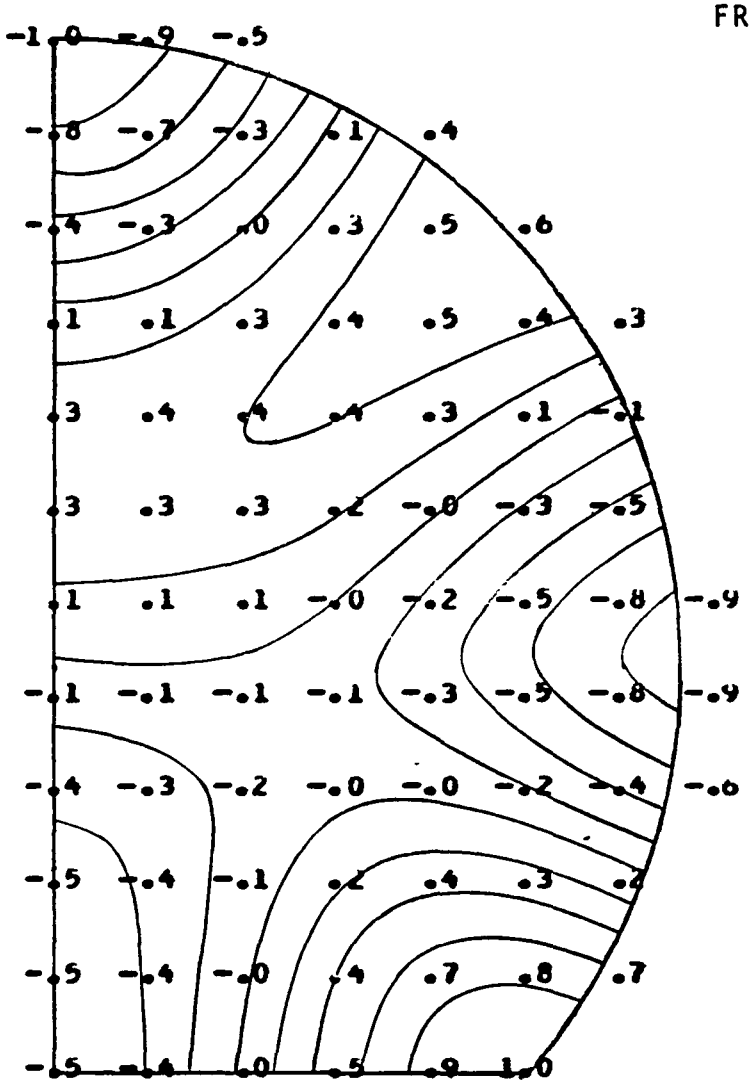

MODE 10. ANTISYMMETRIC

FREQ = 305.542

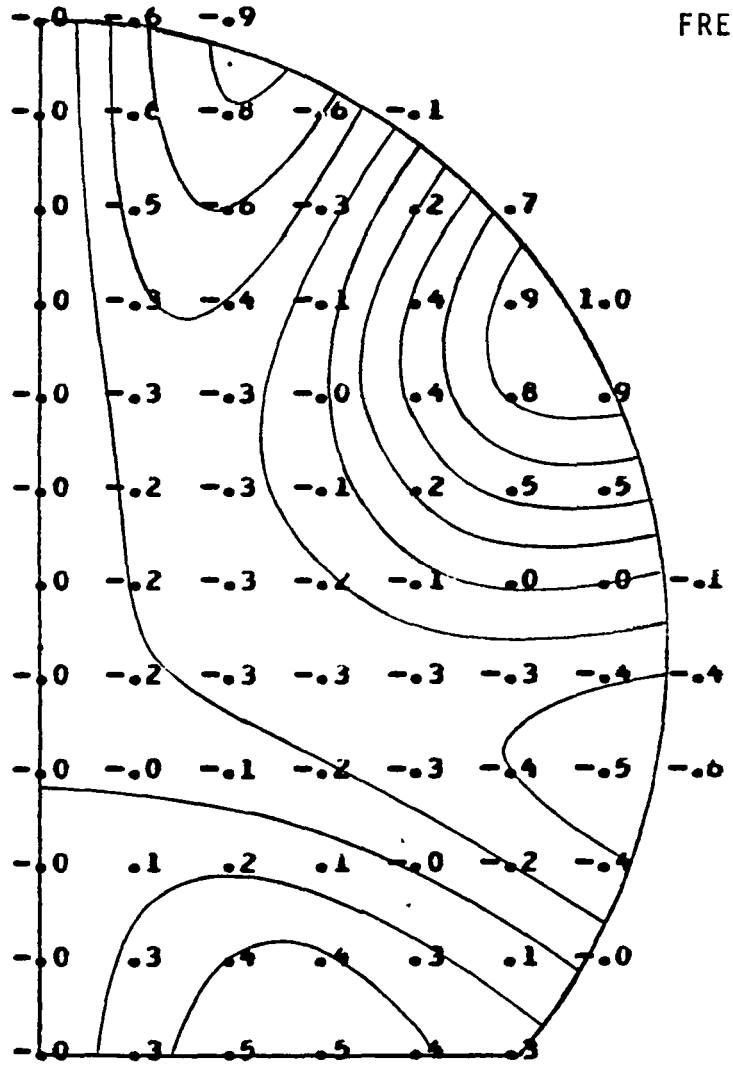

FIGURES

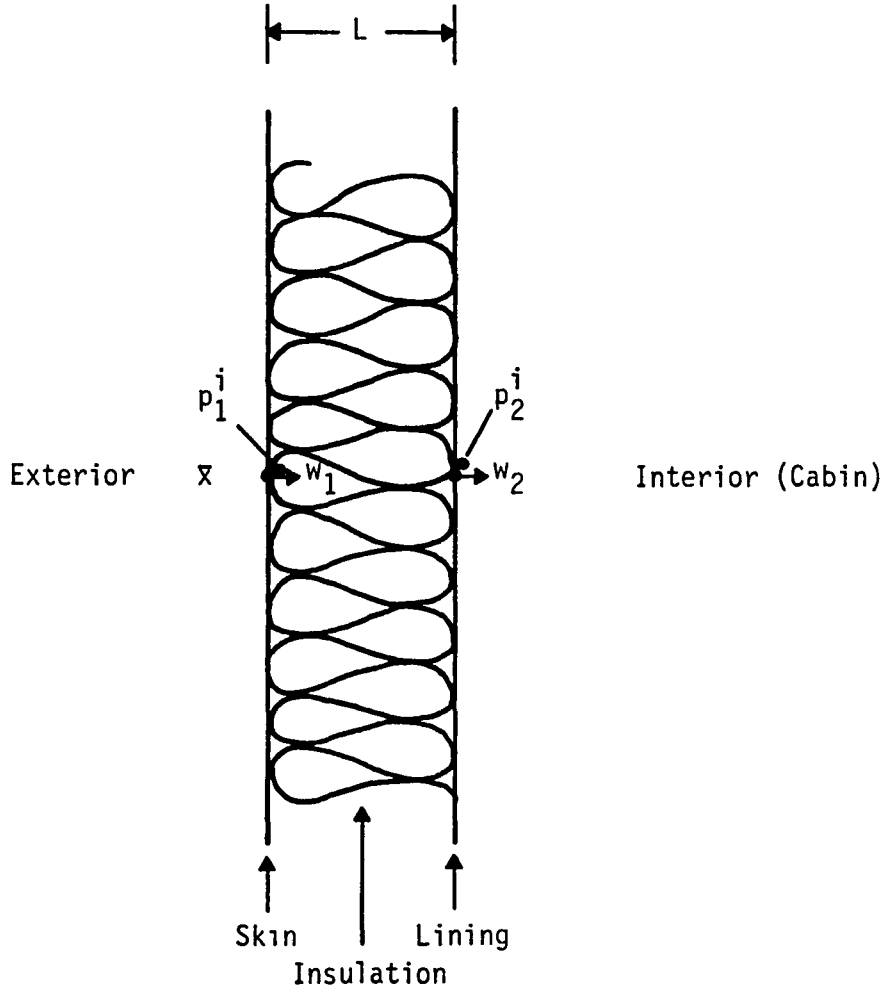

FIGURE 1. TRIM MODEL - INSULATION AND LINING

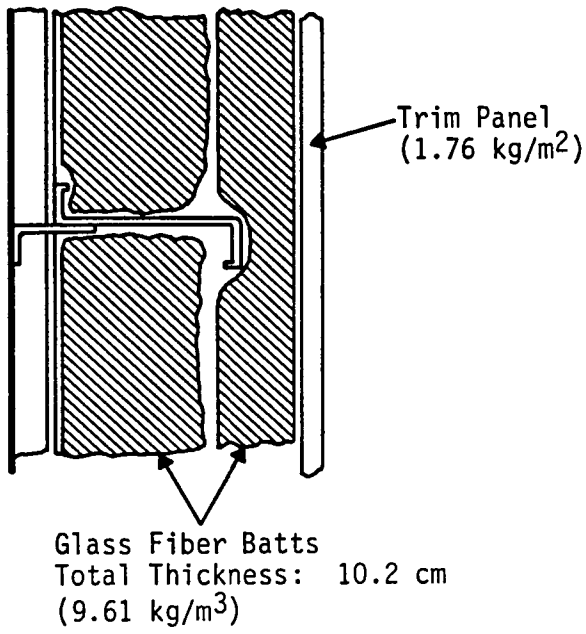

FIGURE 2. TYPICAL WIDE BODY TRIM INSTALLATION

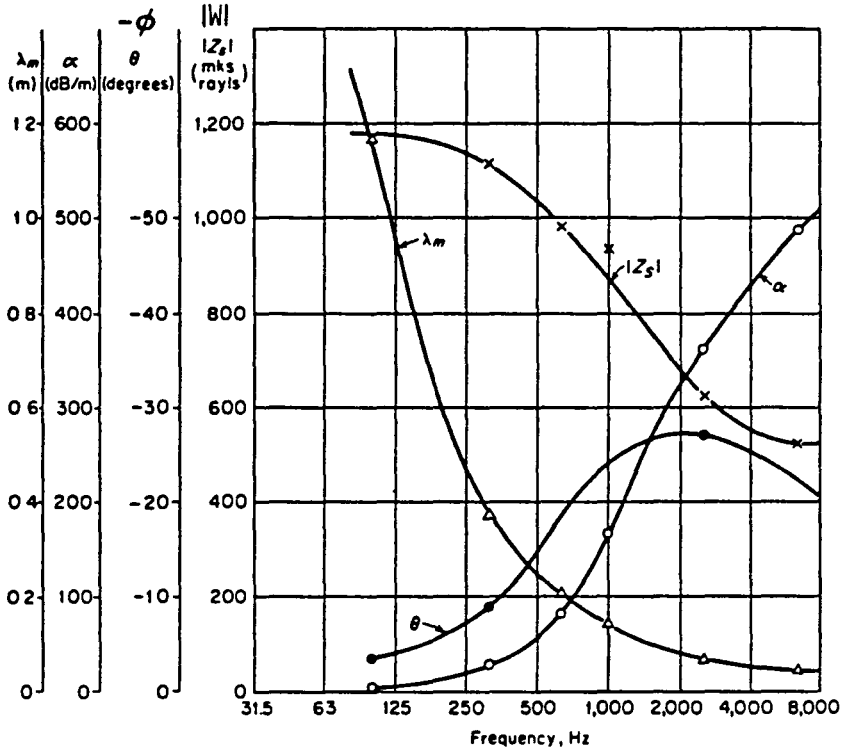

FIGURE 3. ACOUSTICAL PARAMETERS FOR OWENS-CORNING FIBERGLAS TYPE PF 105. FIBER DIAMETER IS 1 MICRON AND BULK DENSITY IS 9.6 kg/m^3 (0.6 lb/ft^3) [4]

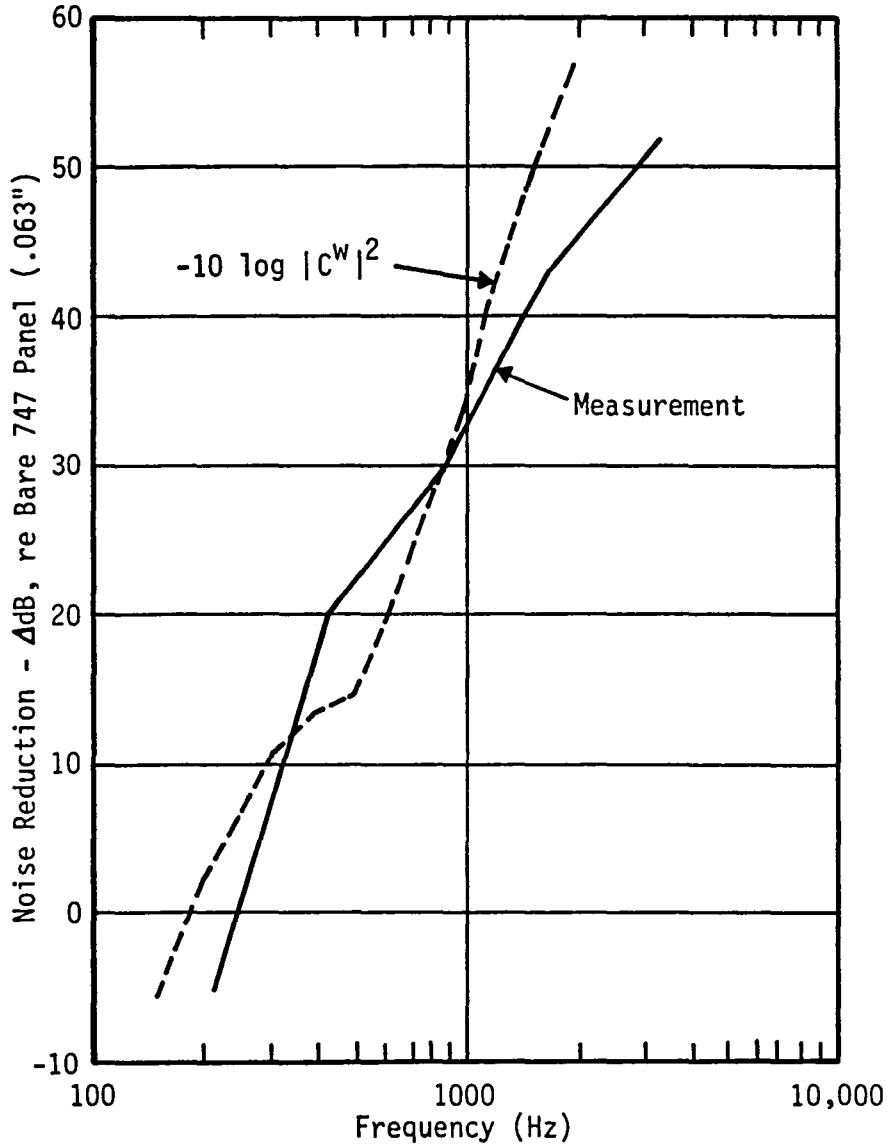

FIGURE 4. COMPARISON OF TRIM TRANSFER COEFFICIENT PREDICTION WITH MEASUREMENT

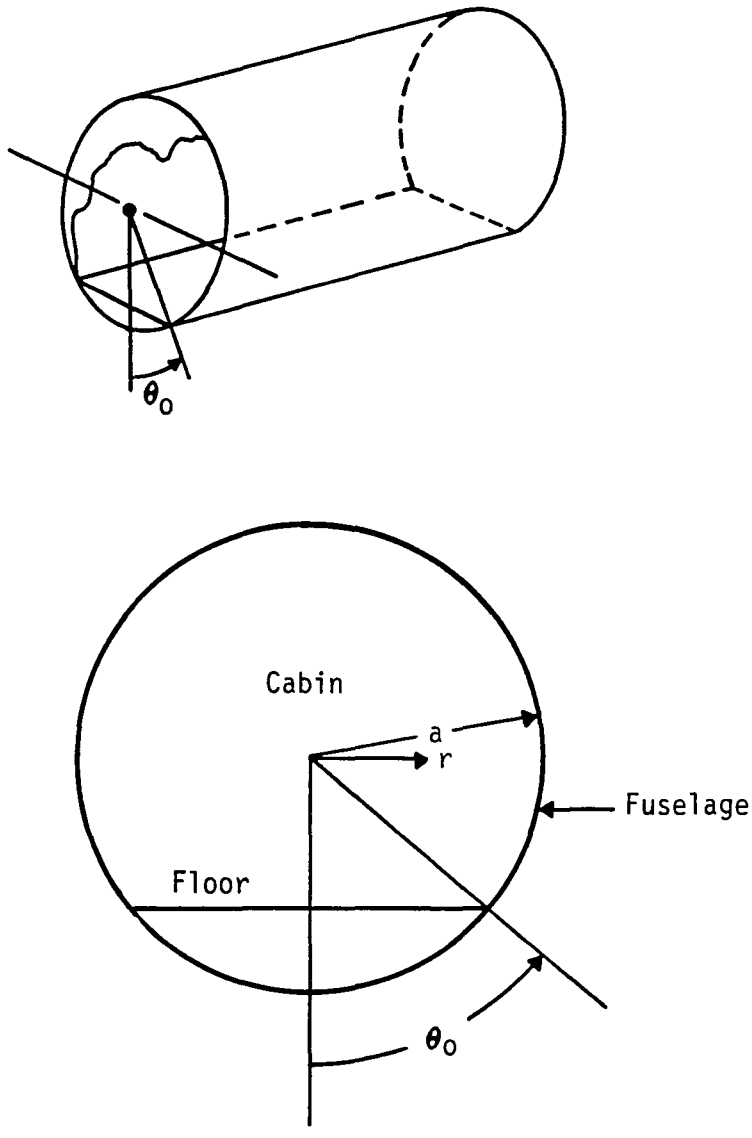

FIGURE 5. FUSELAGE MODEL - CYLINDER WITH FLOOR PARTITION

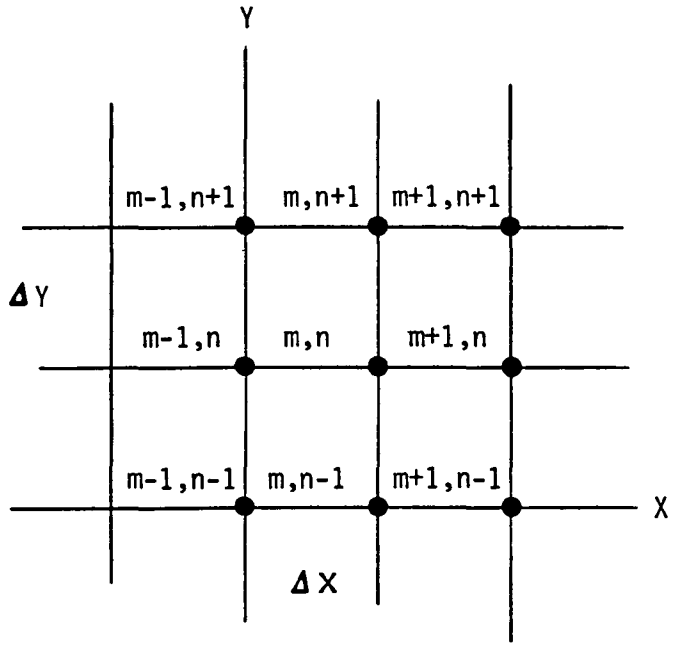

(a)

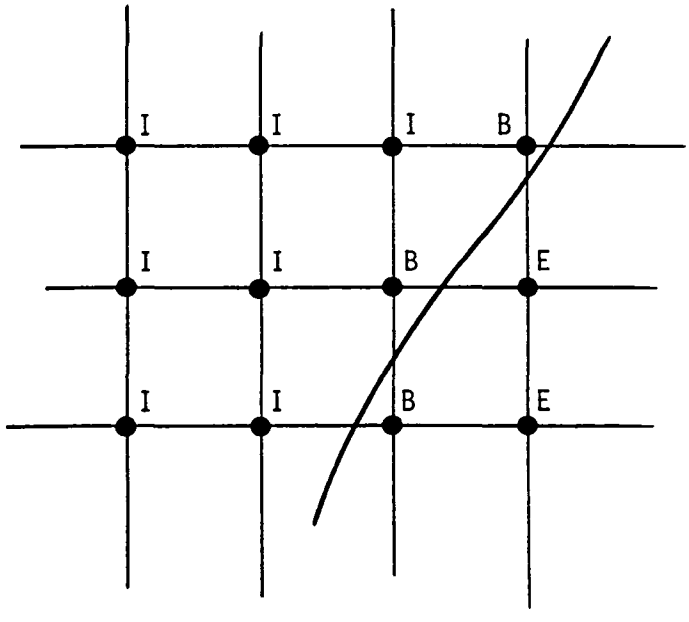

(b)

FIGURE 6. FINITE DIFFERENCE GRID NOMENCLATURE

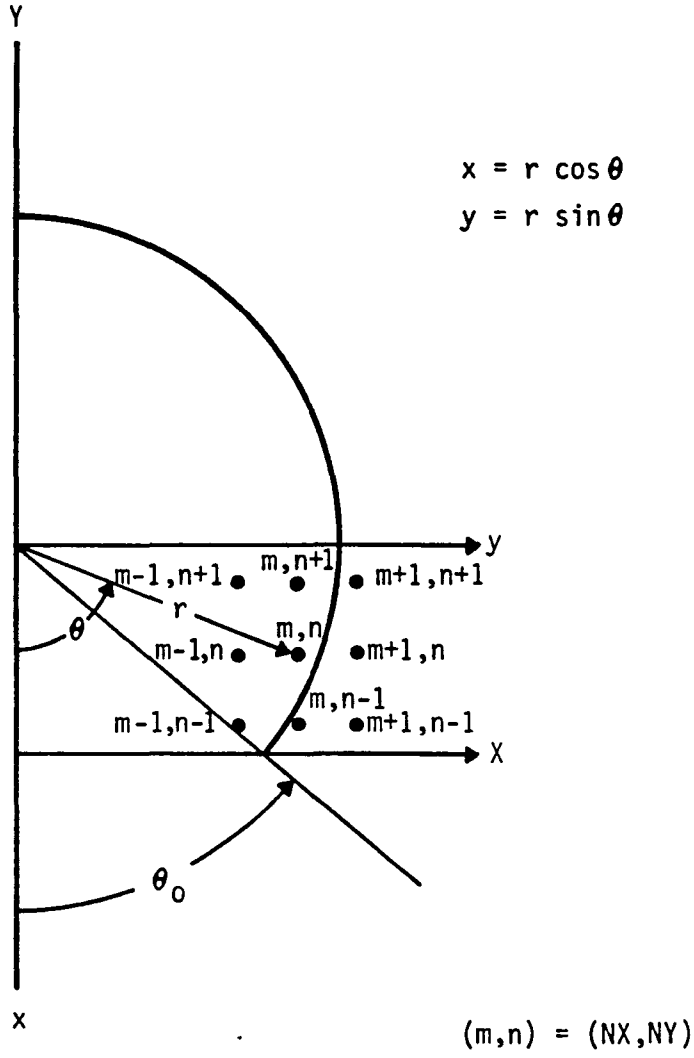

FIGURE 7. GRID COORDINATE SPECIFICATION

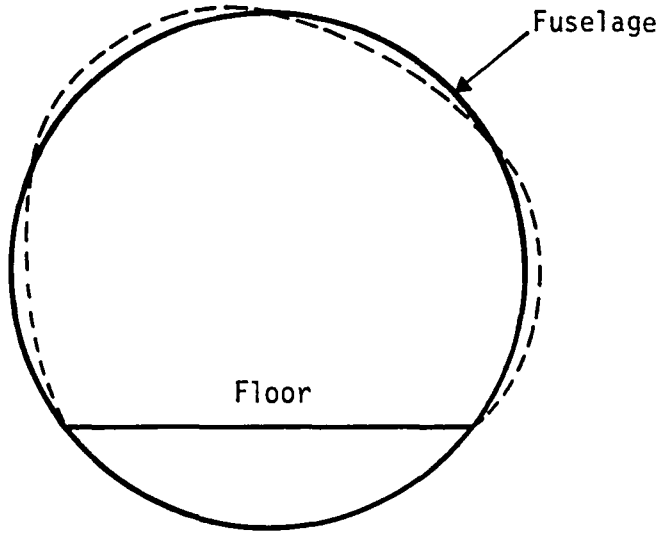

(a)

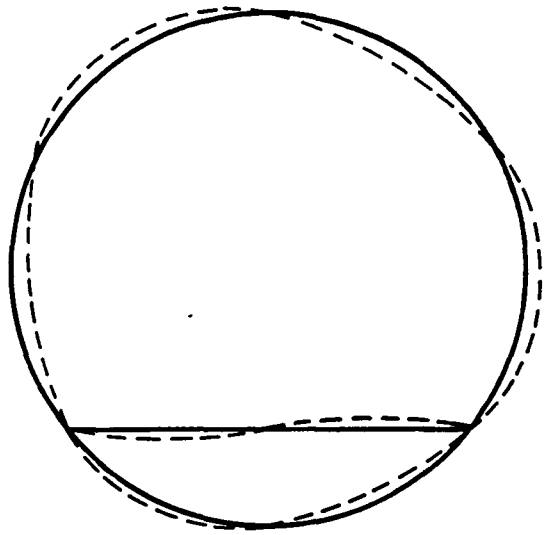

(b)

FIGURE 8. FUSELAGE STRUCTURAL MODELS

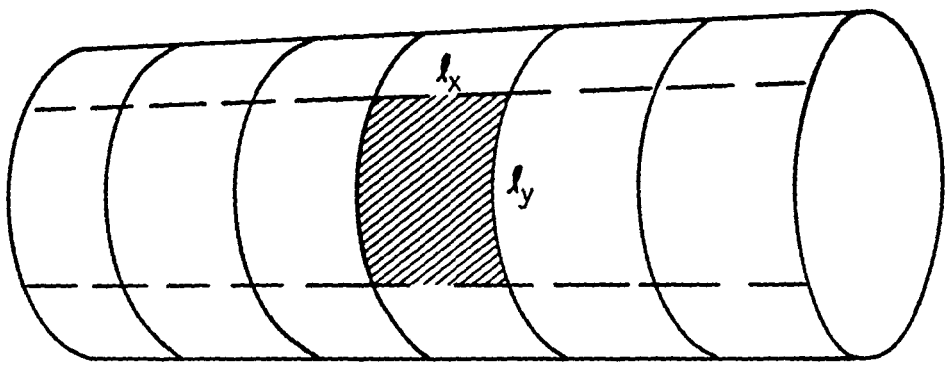

SUBPANEL

ℓ_x = 0.169 m (6.6 in)

ℓ_y = 0.294 m (11.6 in)

h = 0.0005 m (0.02 in)

FIGURE 9. CYLINDER SUBPANEL DIMENSIONS (SKIN ONLY)

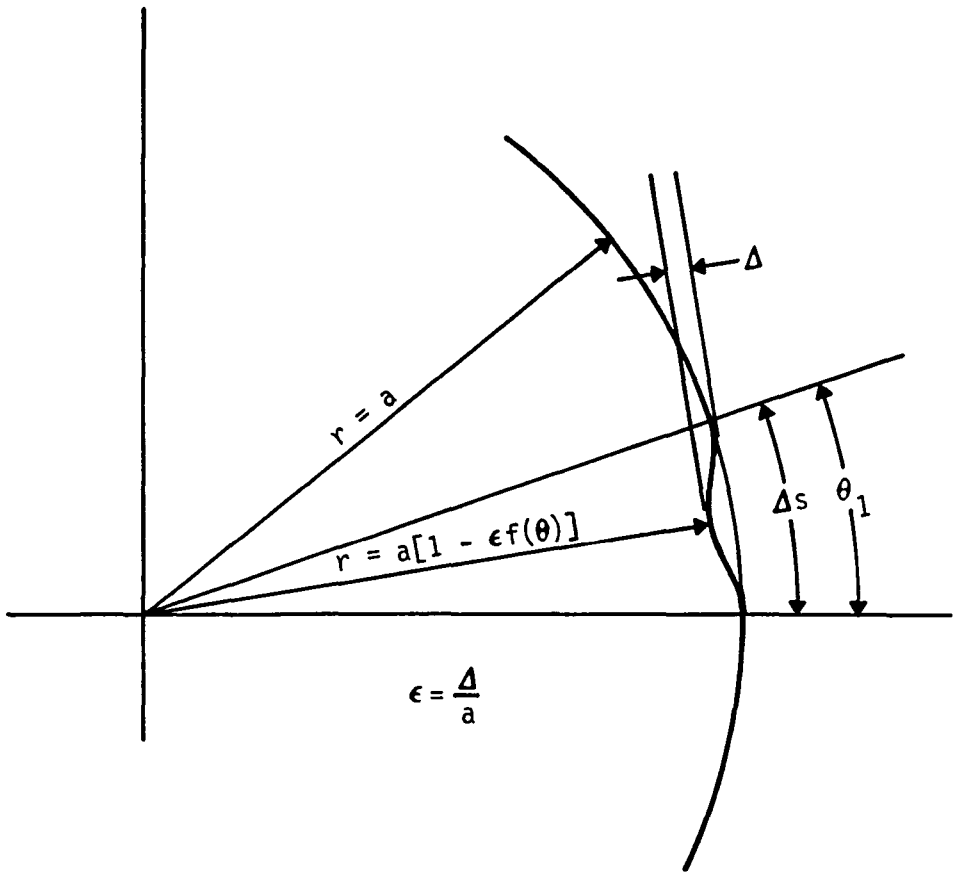

FIGURE 10. CYLINDER IMPERFECTION MODEL

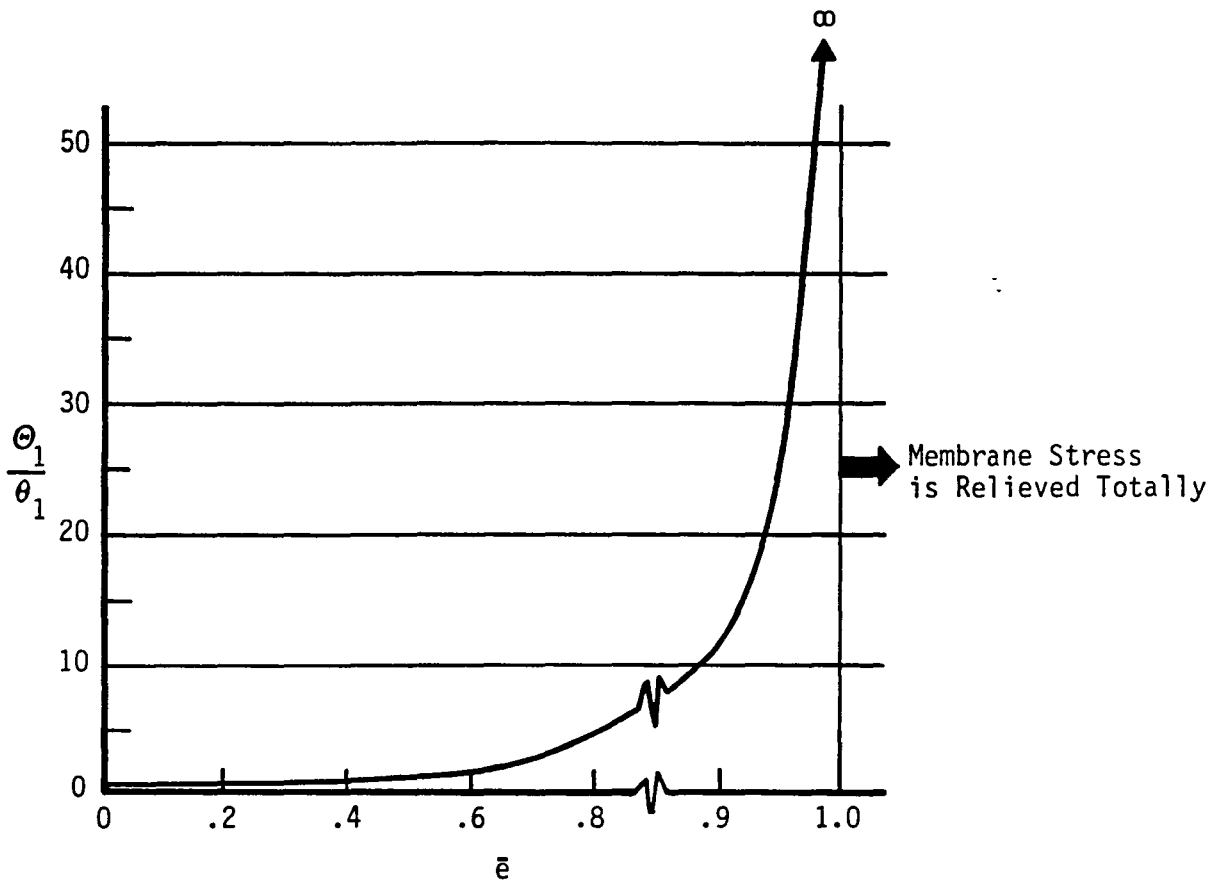

FIGURE 11. RATIO OF THE INTEGRAL Θ_1 TO INTERVAL θ_1 VERSUS ē

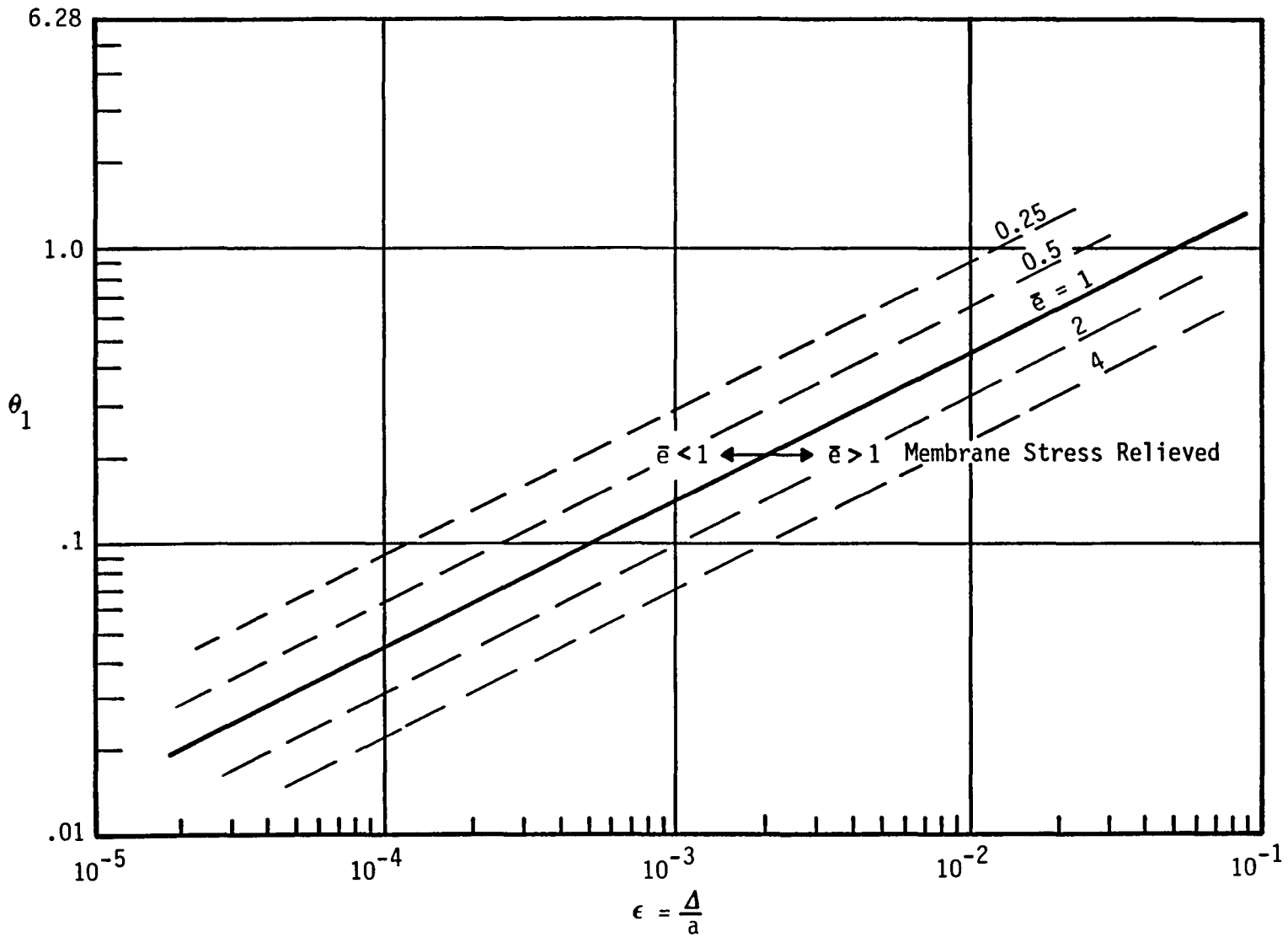

FIGURE 12. APPROXIMATE CRITERIA FOR RELIEF OF MEMBRANE STRESSES

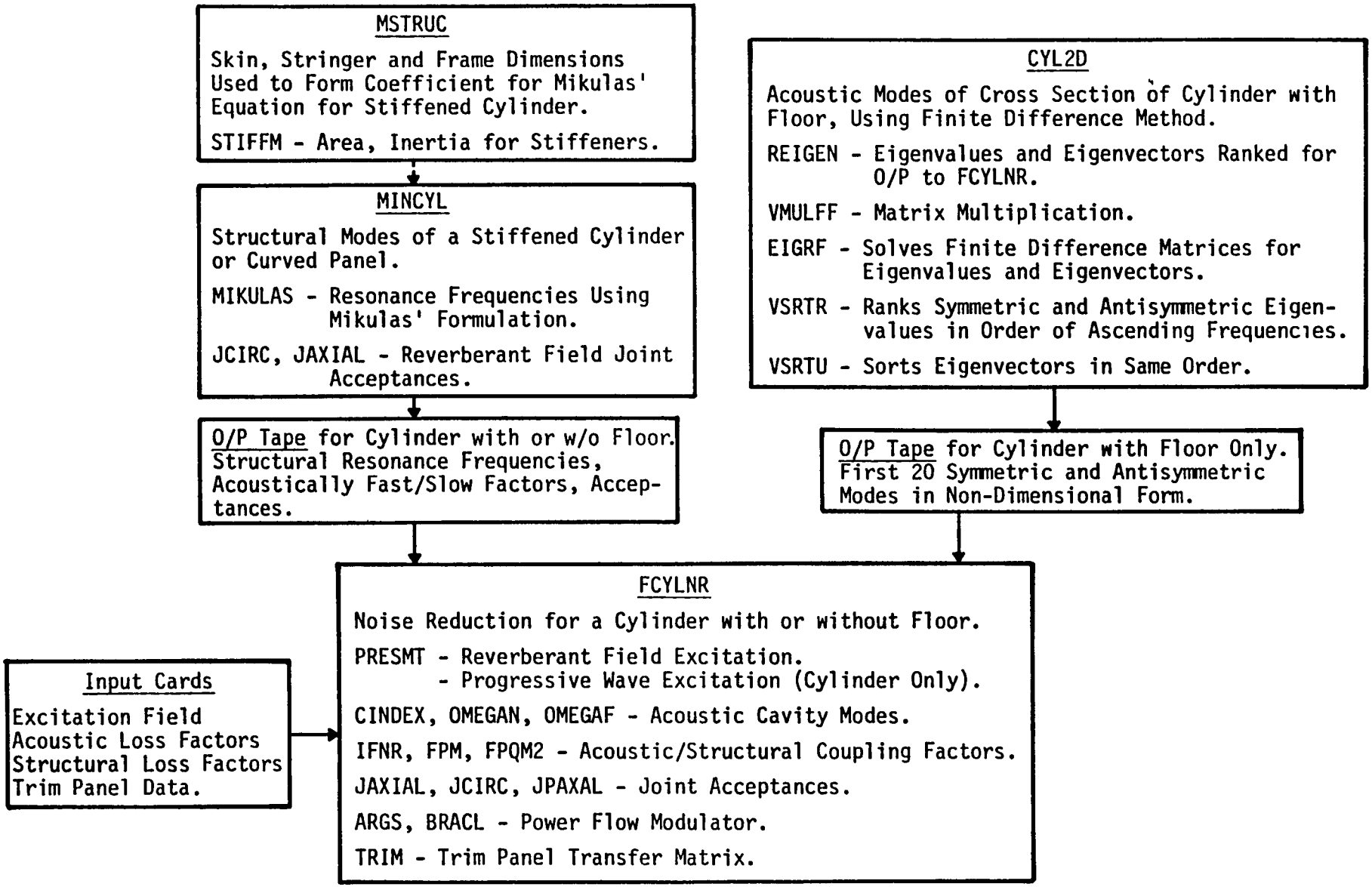

FIGURE 13. STATUS OF CYLINDER NOISE REDUCTION PROGRAM (PHASE II)

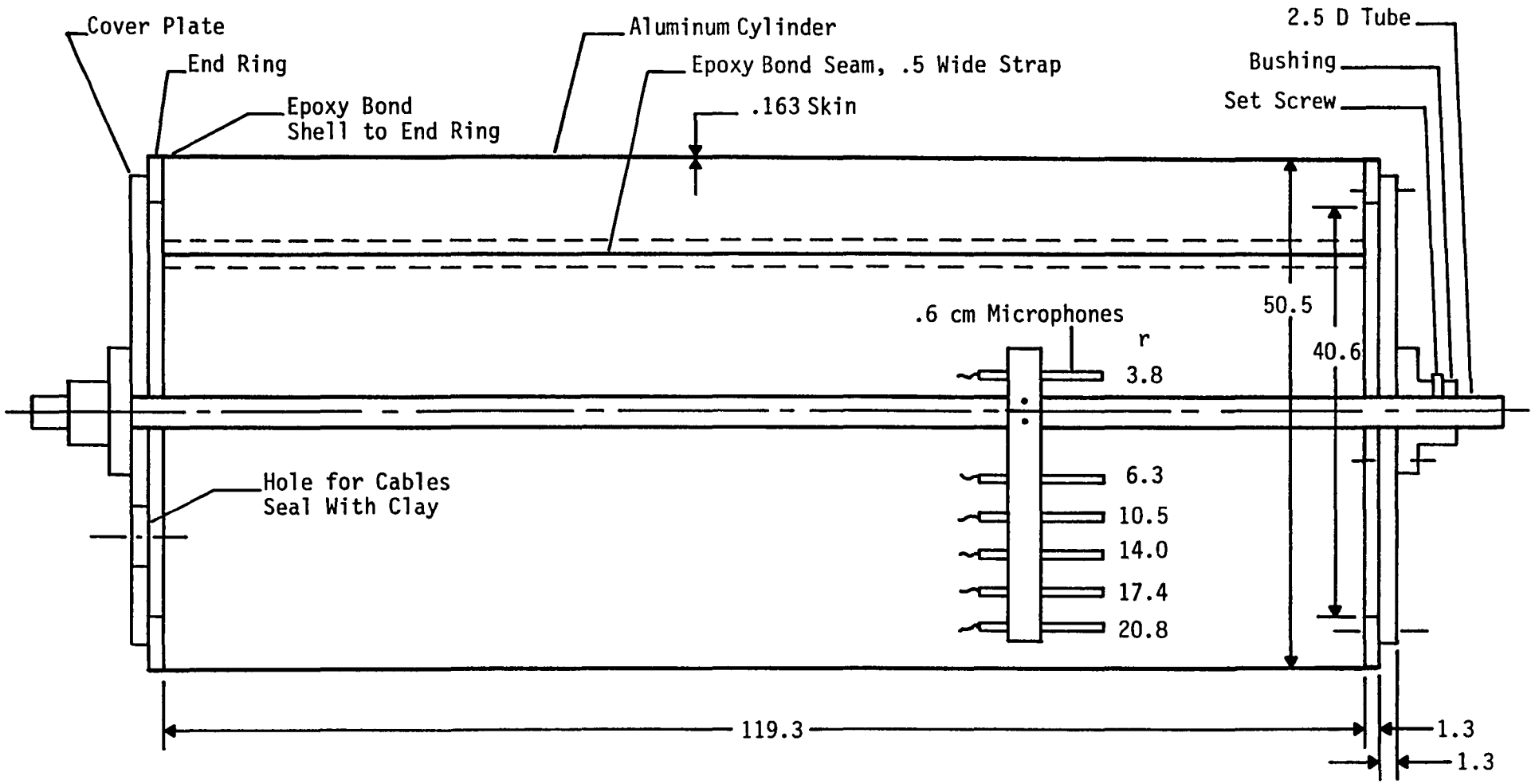

FIGURE 14. UNSTIFFENED CYLINDER - MODEL DETAILS AND MICROPHONE LOCATIONS (DIMENSIONS IN CENTIMETERS)

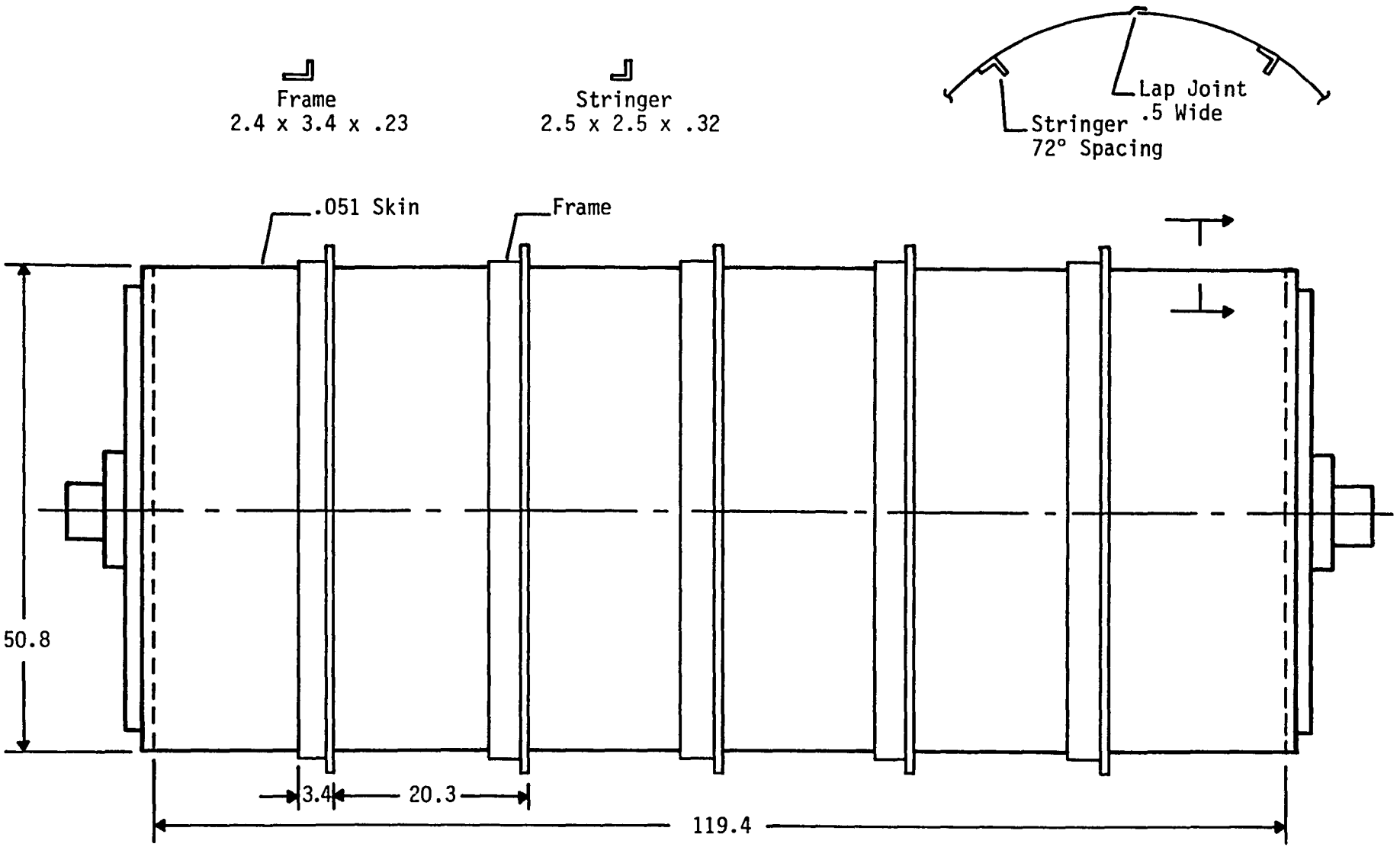

STIFFENED CYLINDER

FIGURE 15. STIFFENED CYLINDER (DIMENSIONS IN CM.)

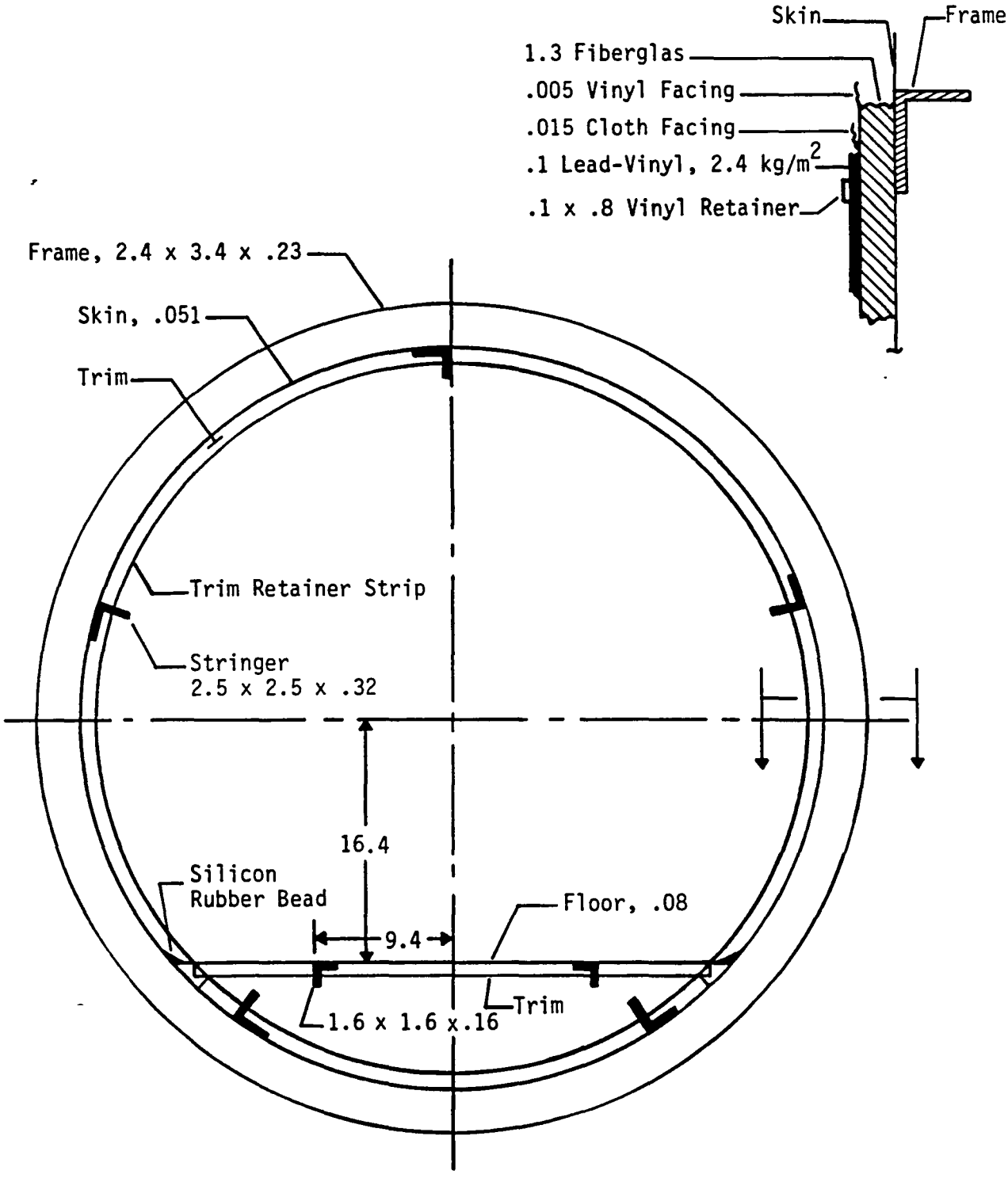

FIGURE 16. CROSS SECTION OF STIFFENED CYLINDER WITH FLOOR

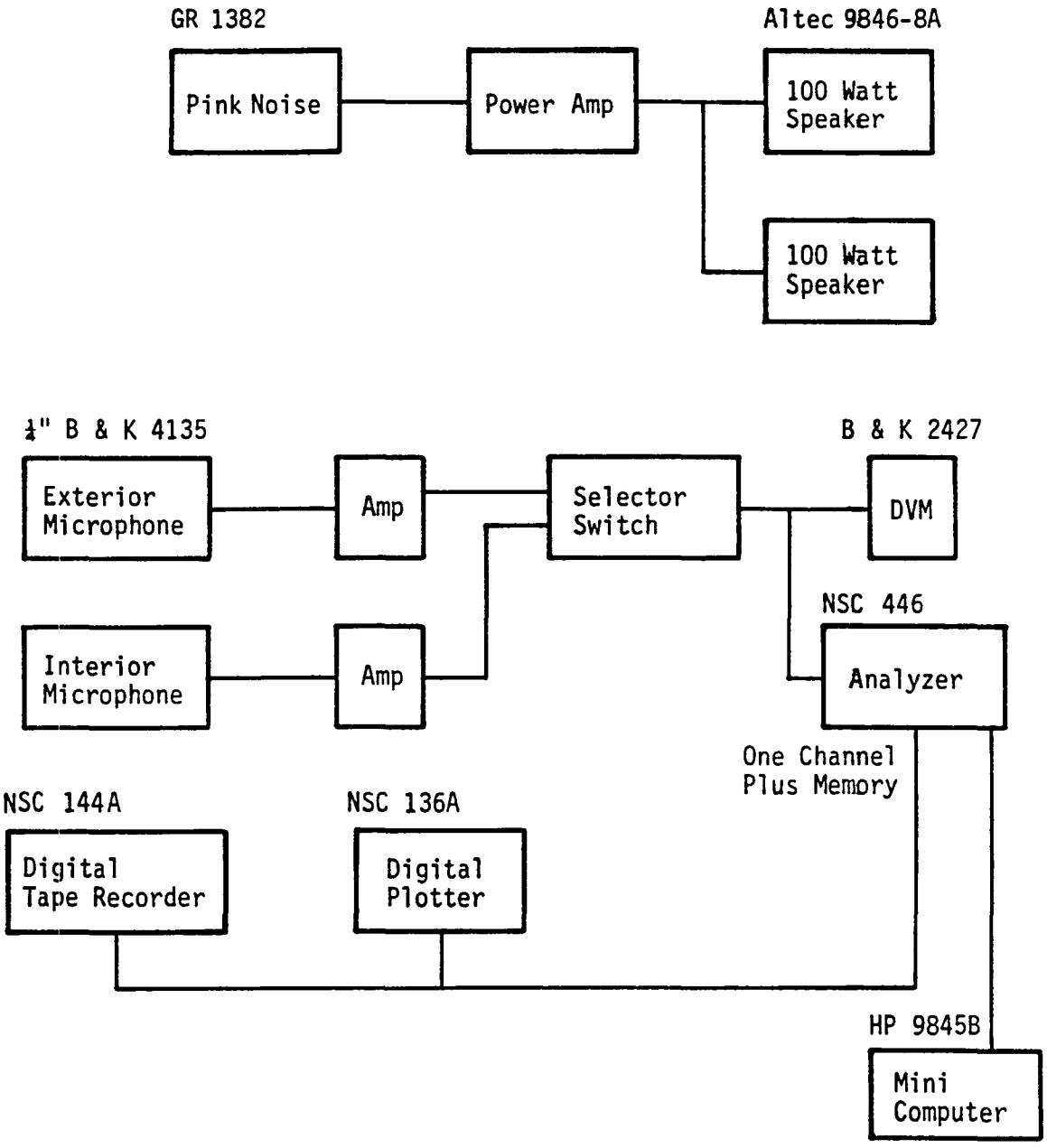

FIGURE 17. NOISE REDUCTION TEST INSTRUMENTATION

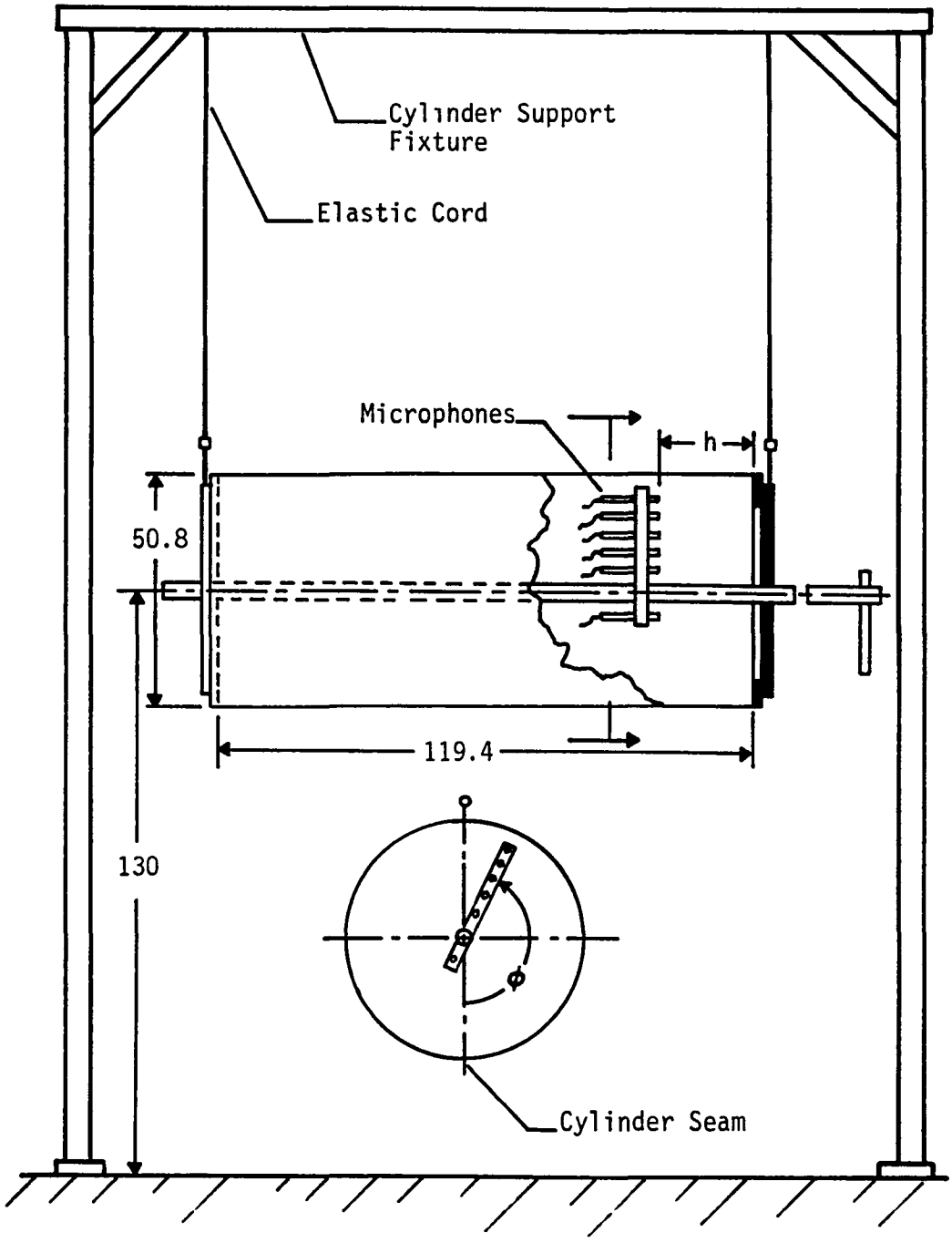

FIGURE 18. ARRANGEMENT OF APPARATUS (DIMENSIONS IN CM.)

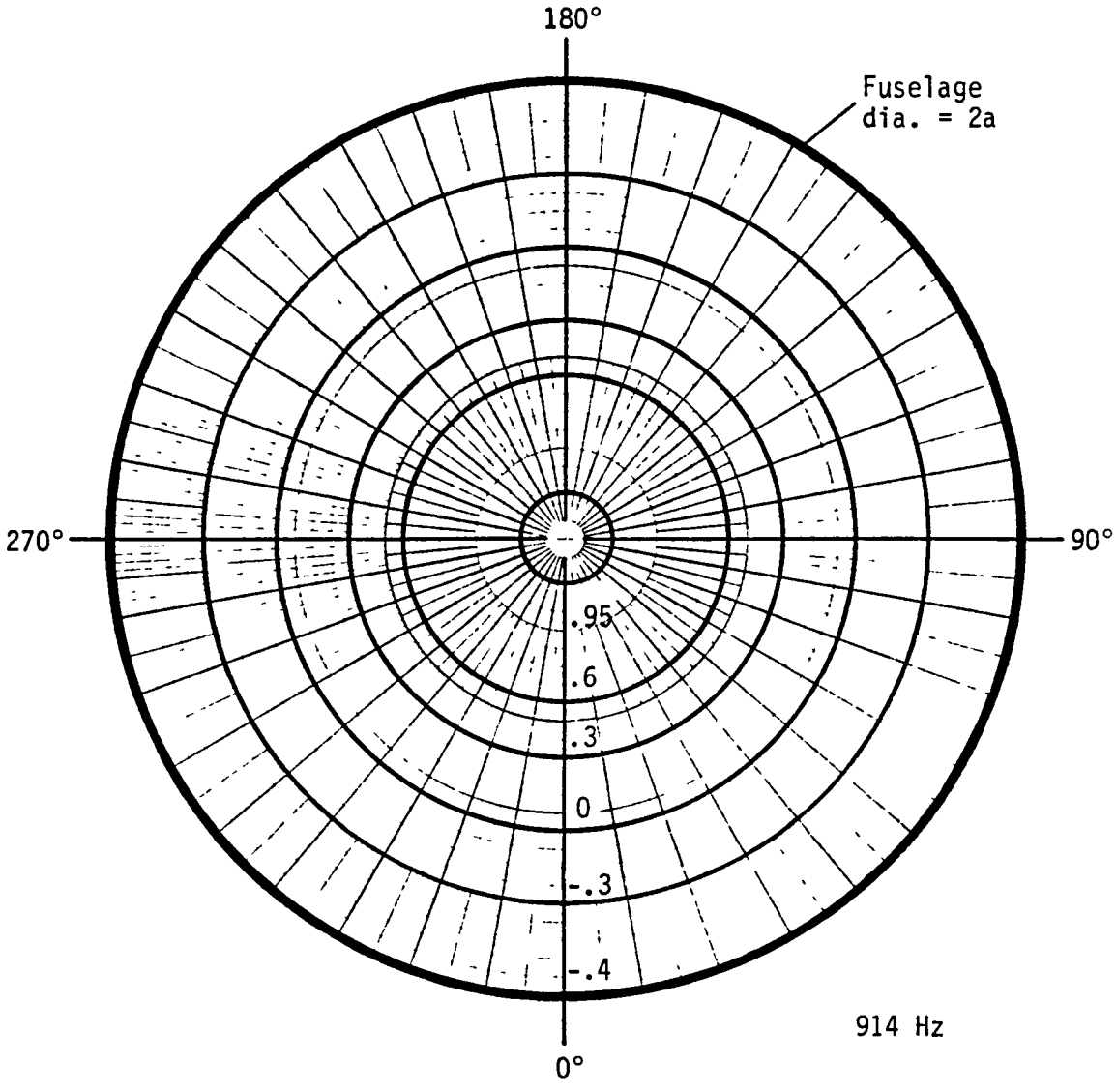

$\theta_0 = 0$

$\phi_{0,0,2}$

FIGURE 19. MODAL PATTERN FOR THE (0,0,2) MODE

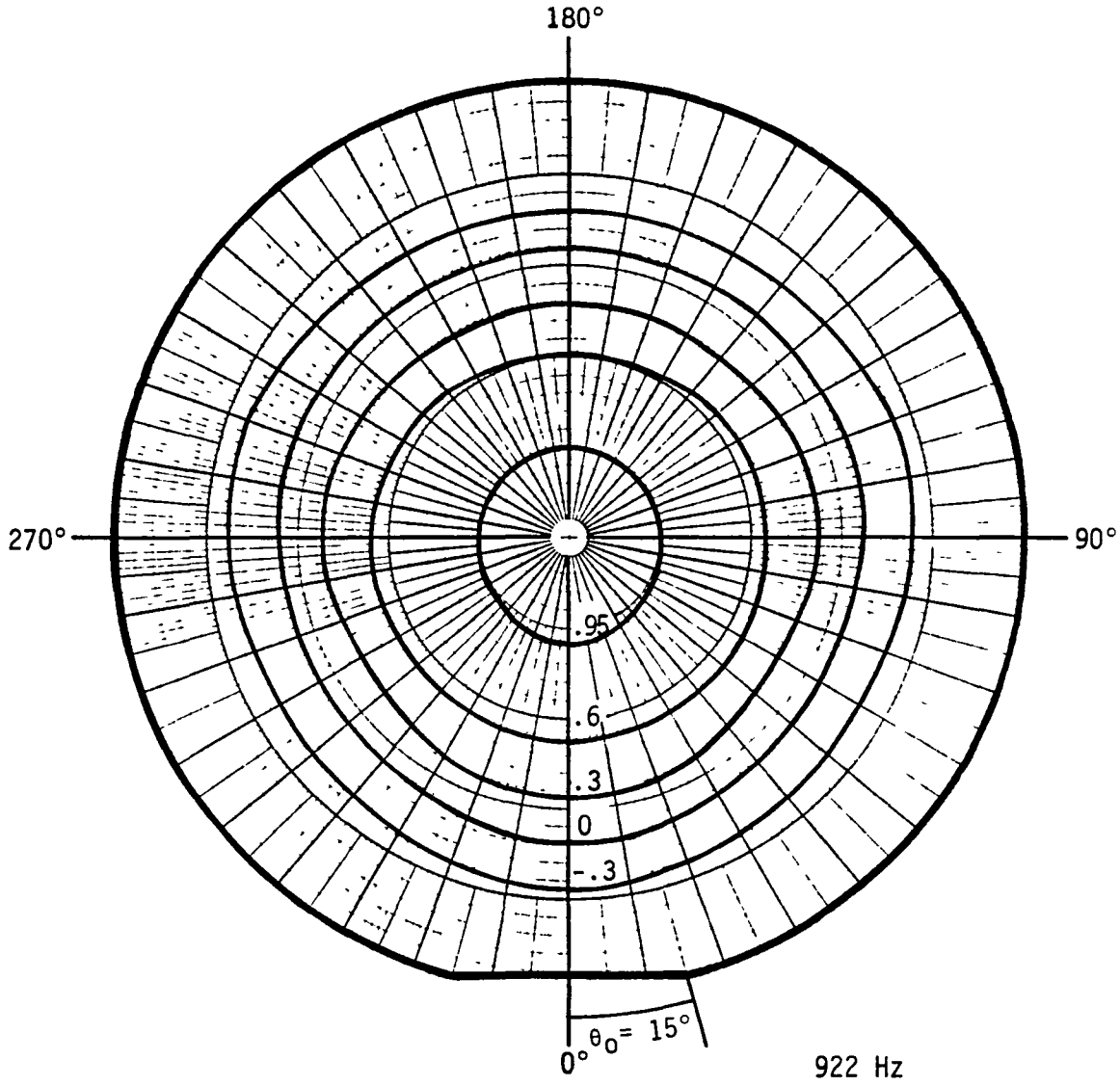

FIGURE 20. MODAL PATTERN FOR A 15° FLOOR

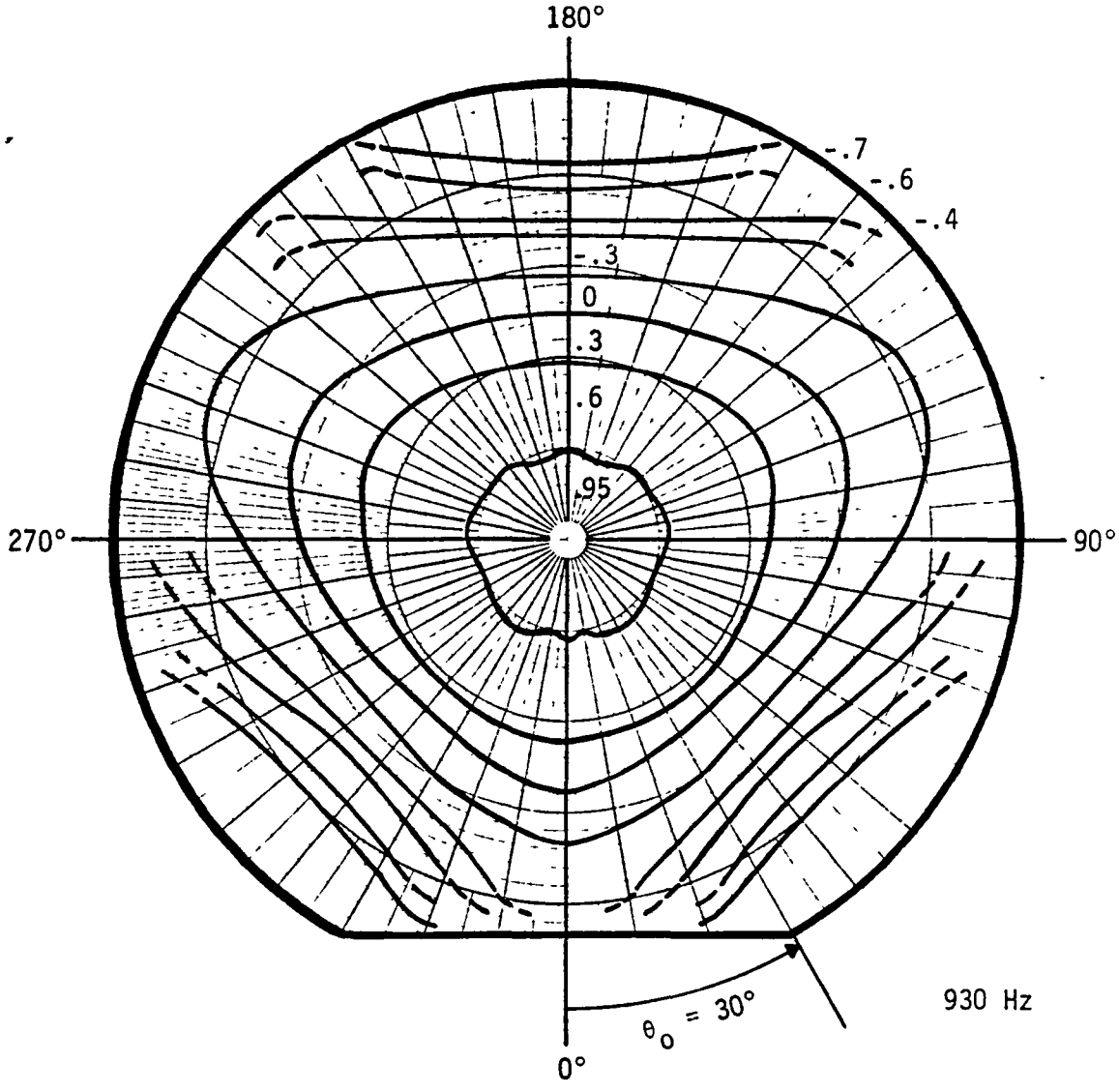

FIGURE 21. MODAL PATTERN FOR A 30° FLOOR

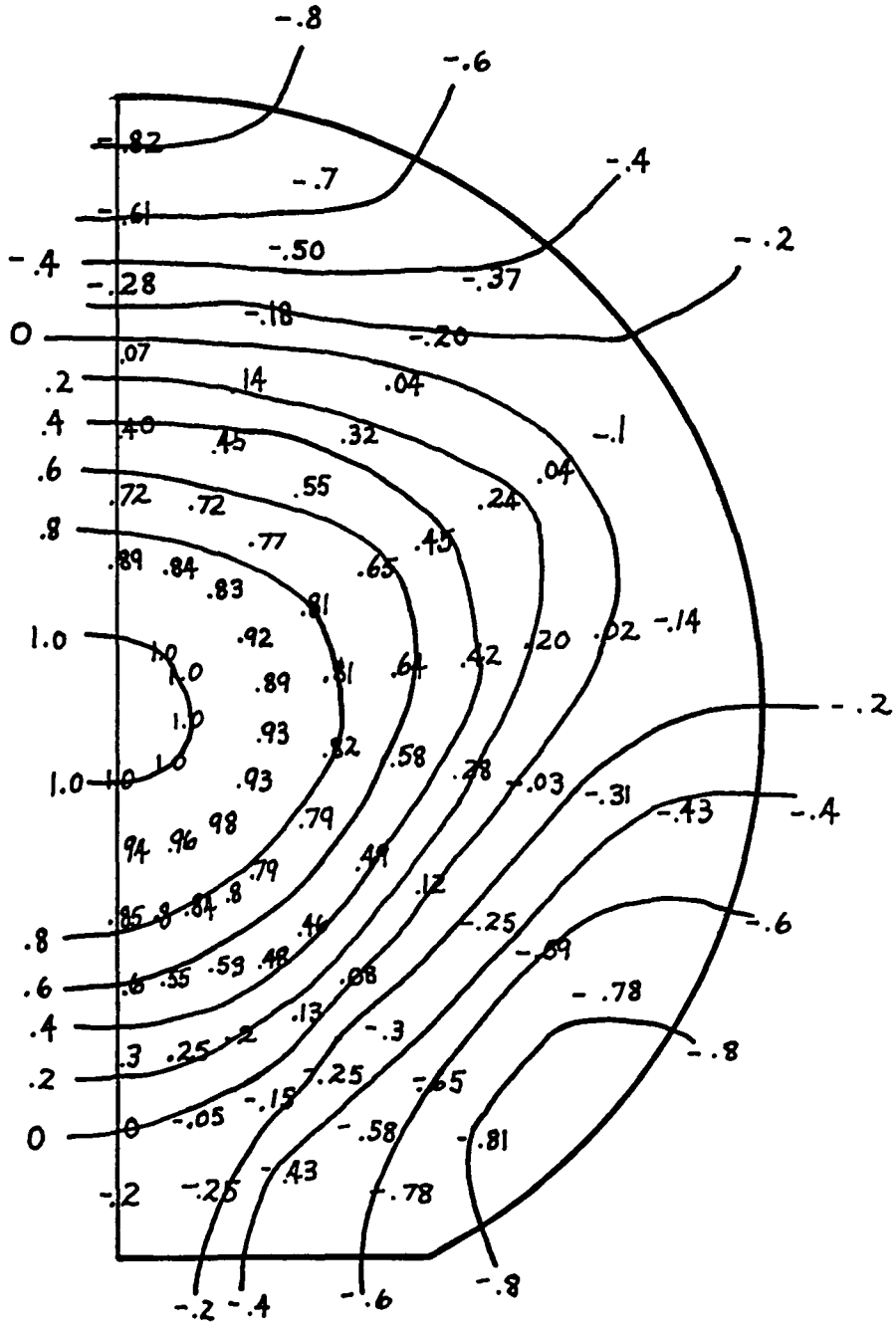

FIGURE 22. DETAILS OF THE 30° FLOOR MEASUREMENT

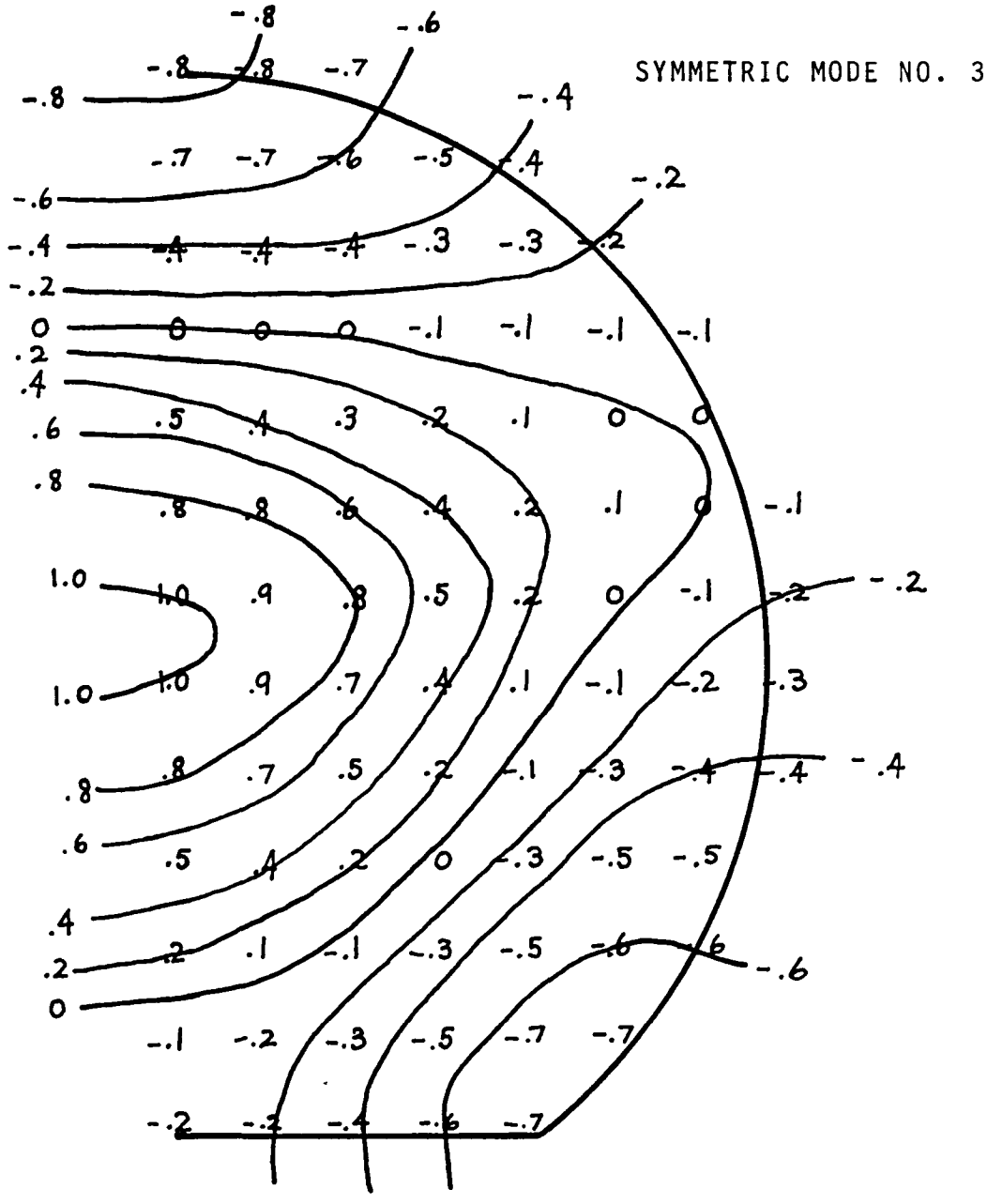

FIGURE 23. FINITE DIFFERENCE CALCULATION (40° FLOOR)

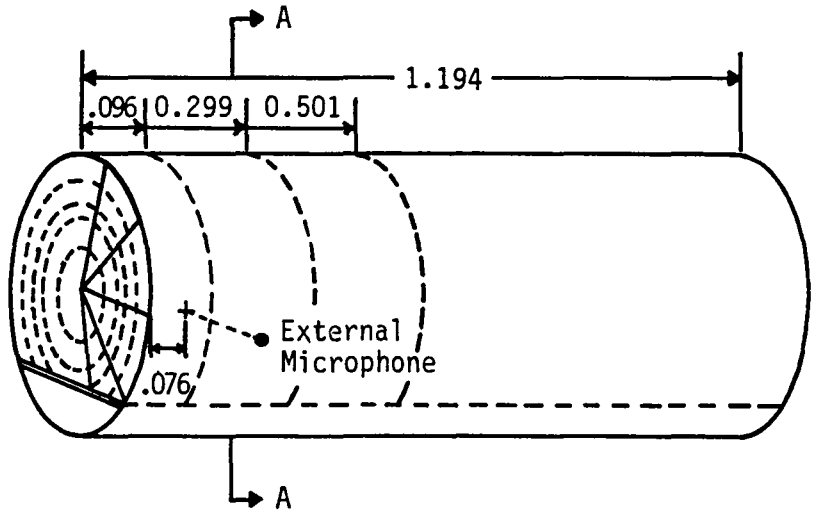

SKETCH OF 3 CYLINDER MEASUREMENT PLANES

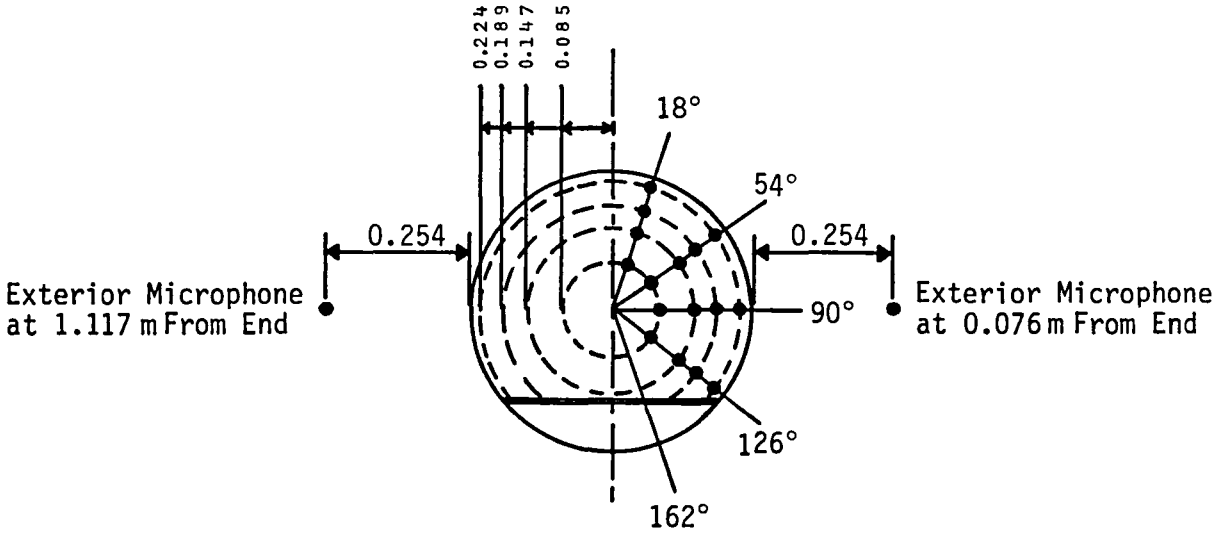

SECTION A-A. MEASUREMENT LOCATIONS AT EACH OF 3 AXIAL SECTIONS

FIGURE 24. EQUAL VOLUME SAMPLING SCHEME

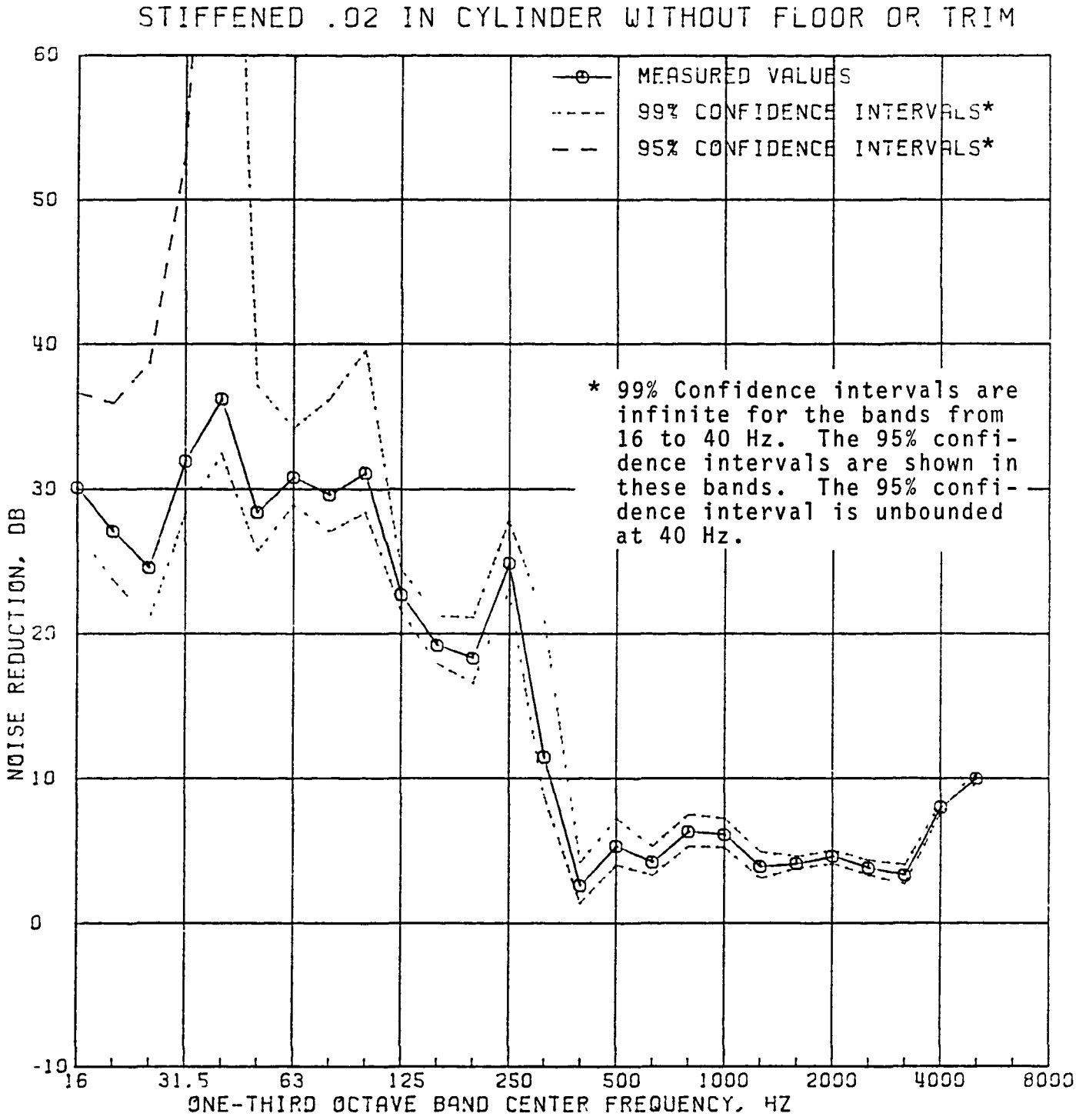

FIGURE 25. MEASURED NOISE REDUCTION OF THE BARE 0.020 IN. RING-STRINGER STIFFENED CYLINDER

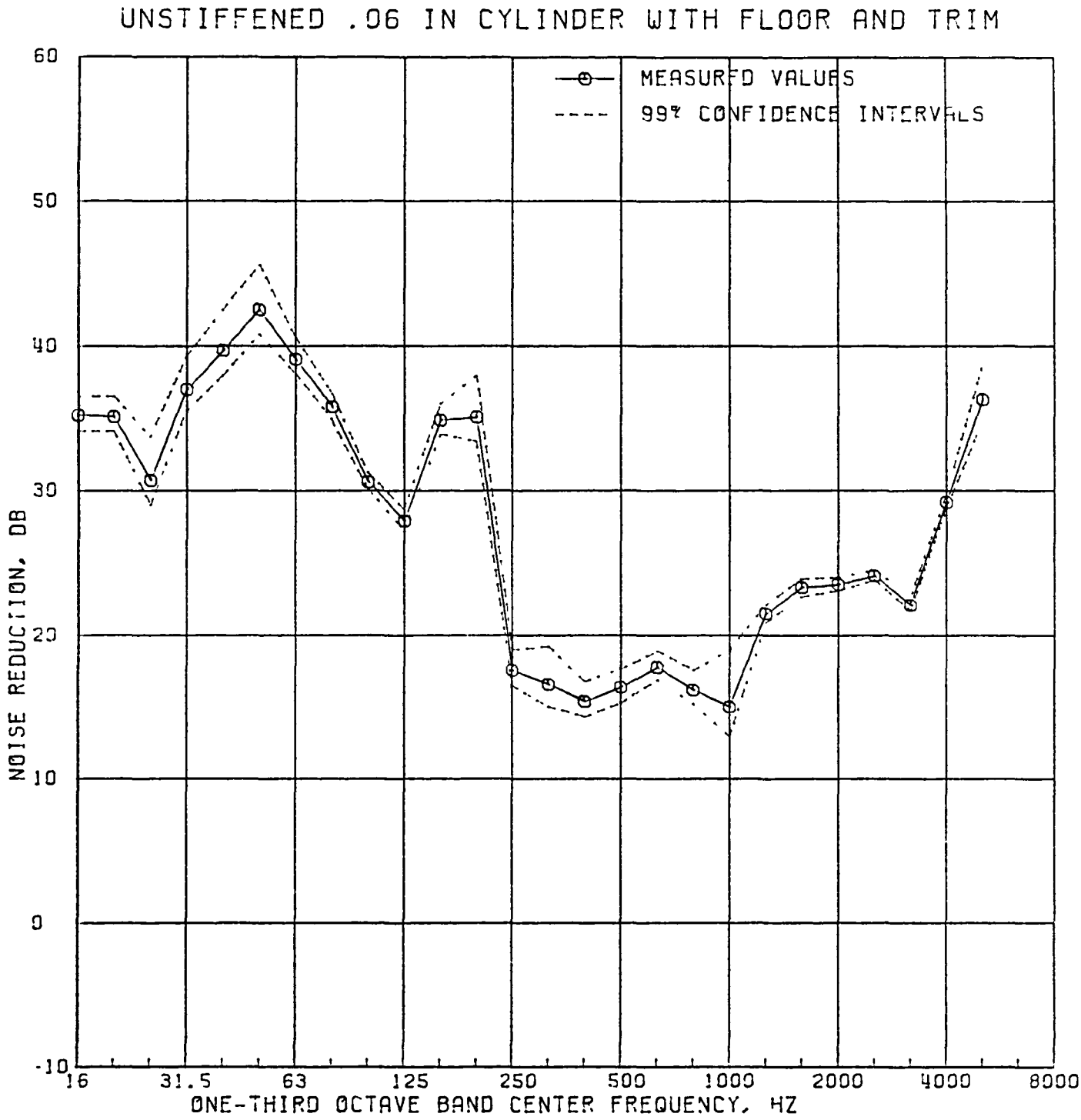

FIGURE 26. MEASURED NOISE REDUCTION OF THE 0.063 IN. UNSTIFFENED CYLINDER WITH FLOOR AND INSULATION

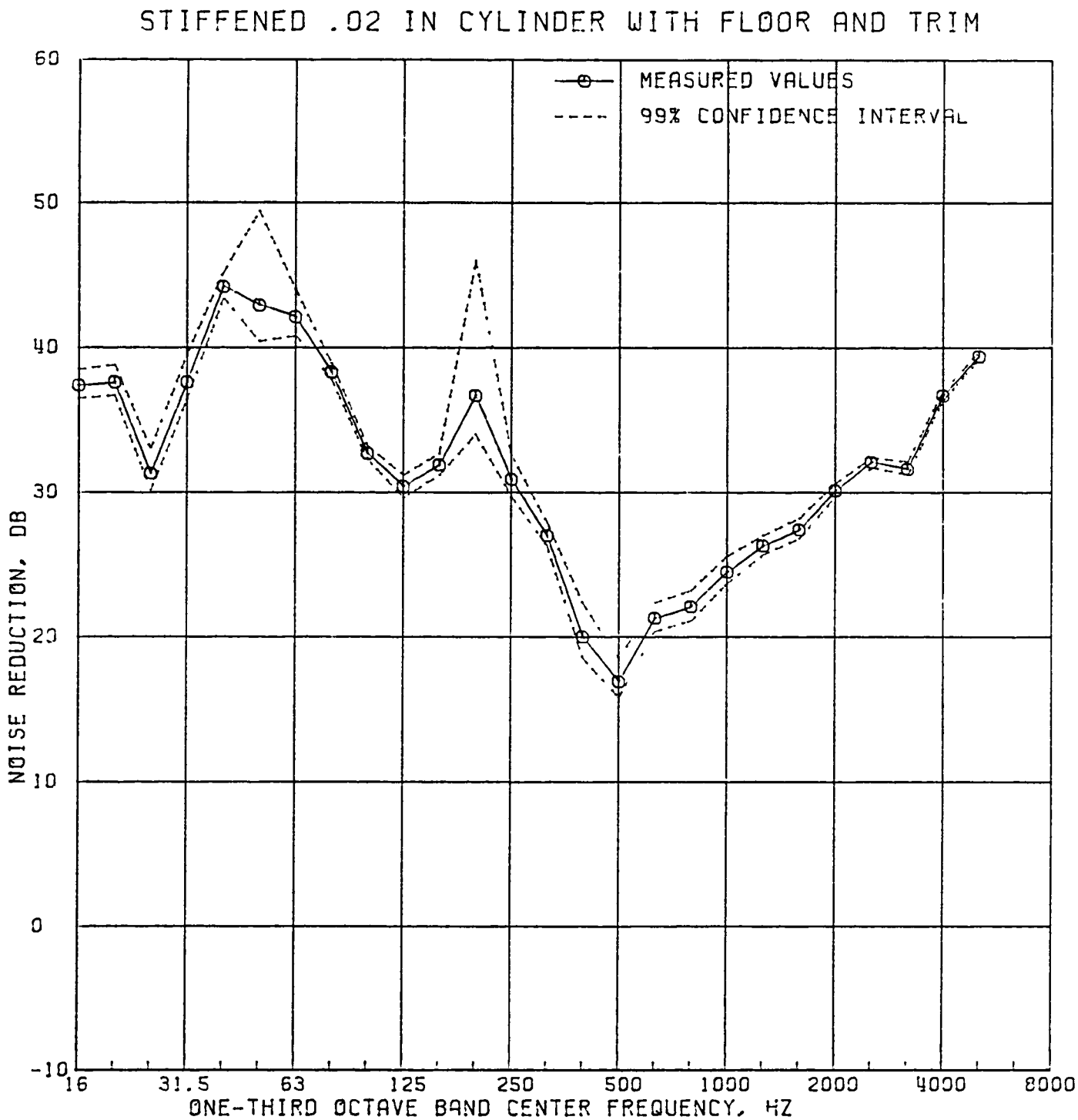

FIGURE 27. MEASURED NOISE REDUCTION OF THE 0.020 IN. RING-STRINGER STIFFENED CYLINDER WITH FLOOR AND TRIM

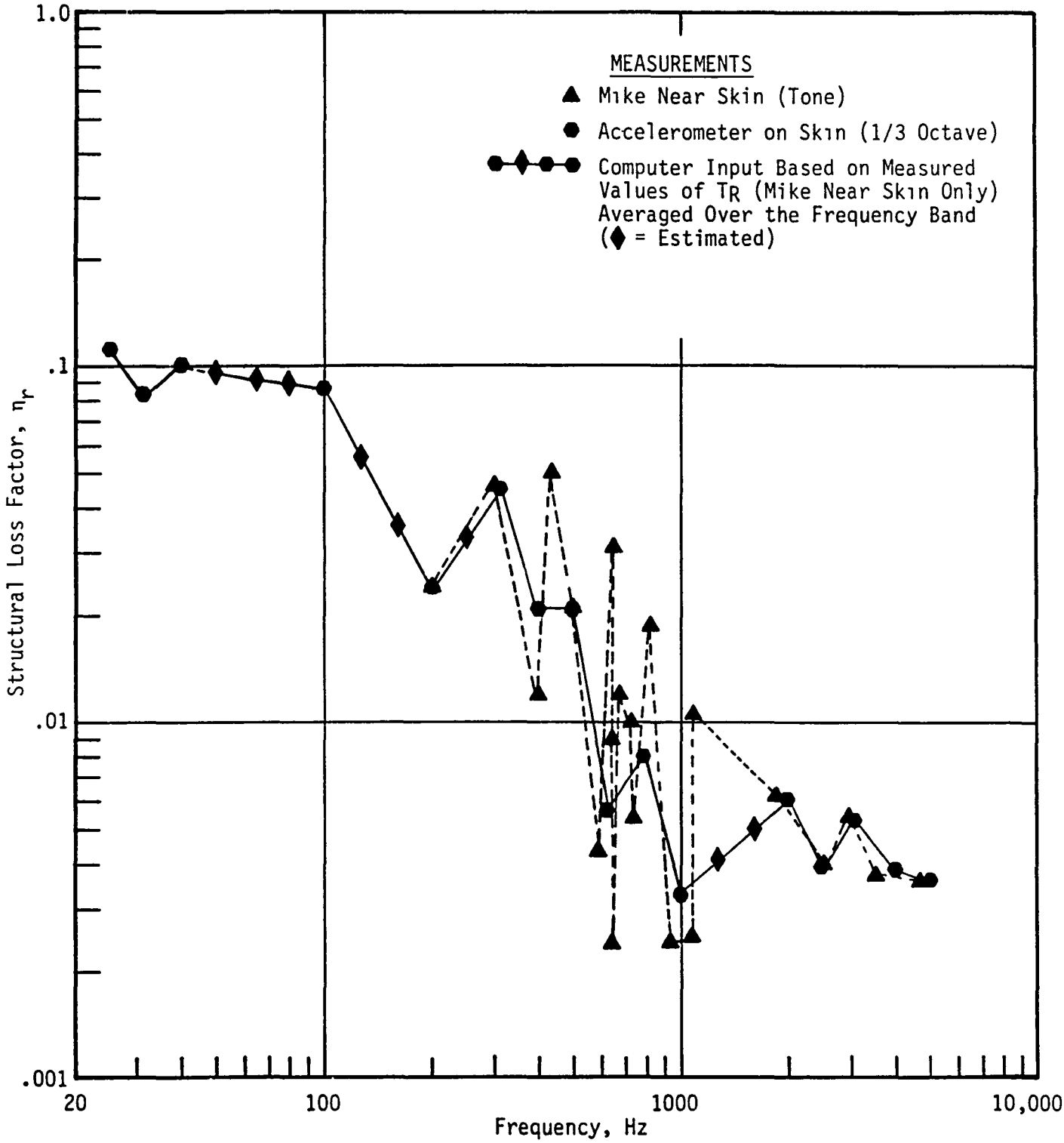

FIGURE 28. STRUCTURAL LOSS FACTORS OF THE STIFFENED CYLINDER WITHOUT FLOOR

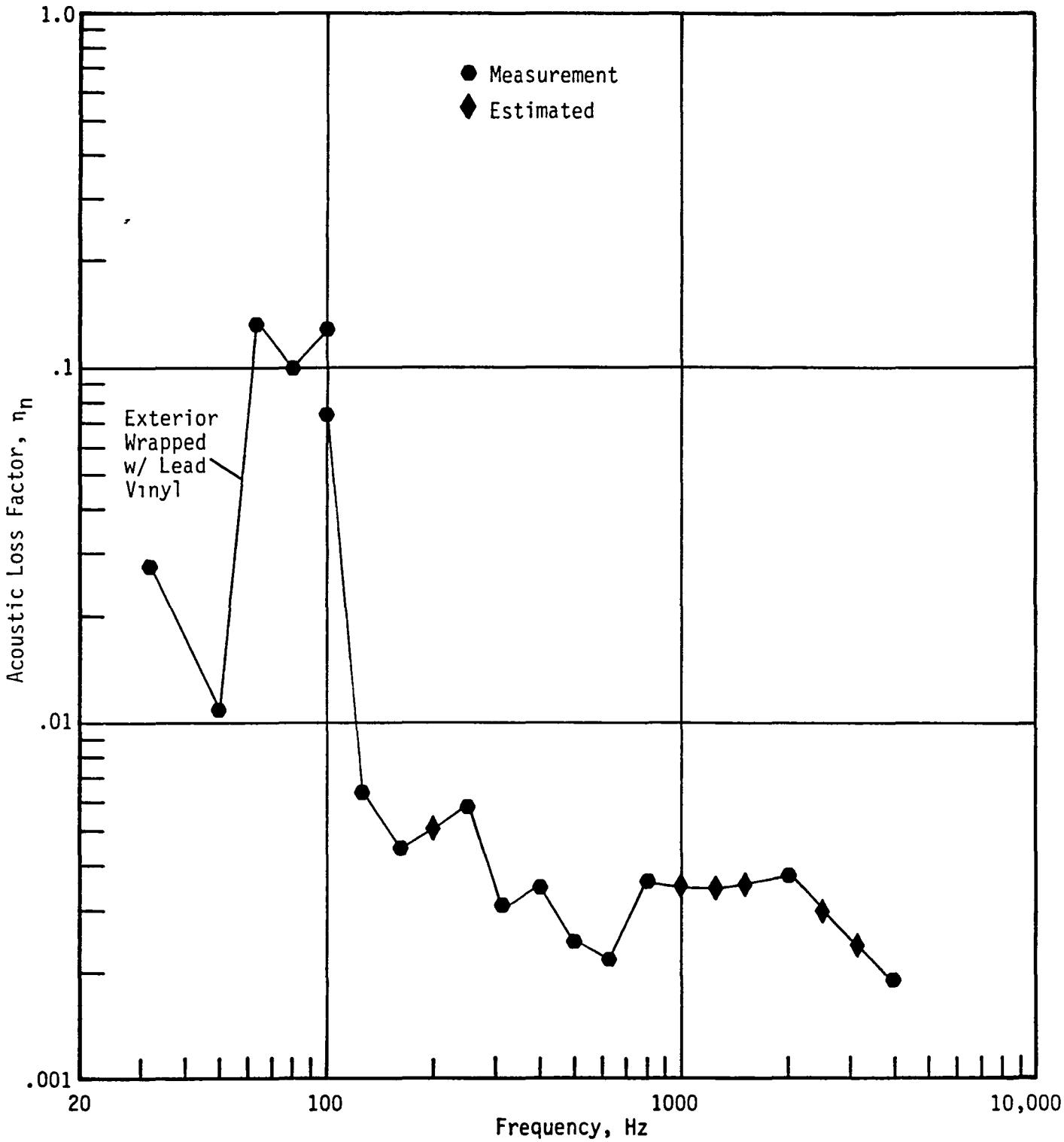

FIGURE 29. ACOUSTIC LOSS FACTORS OF THE STIFFENED CYLINDER WITHOUT FLOOR

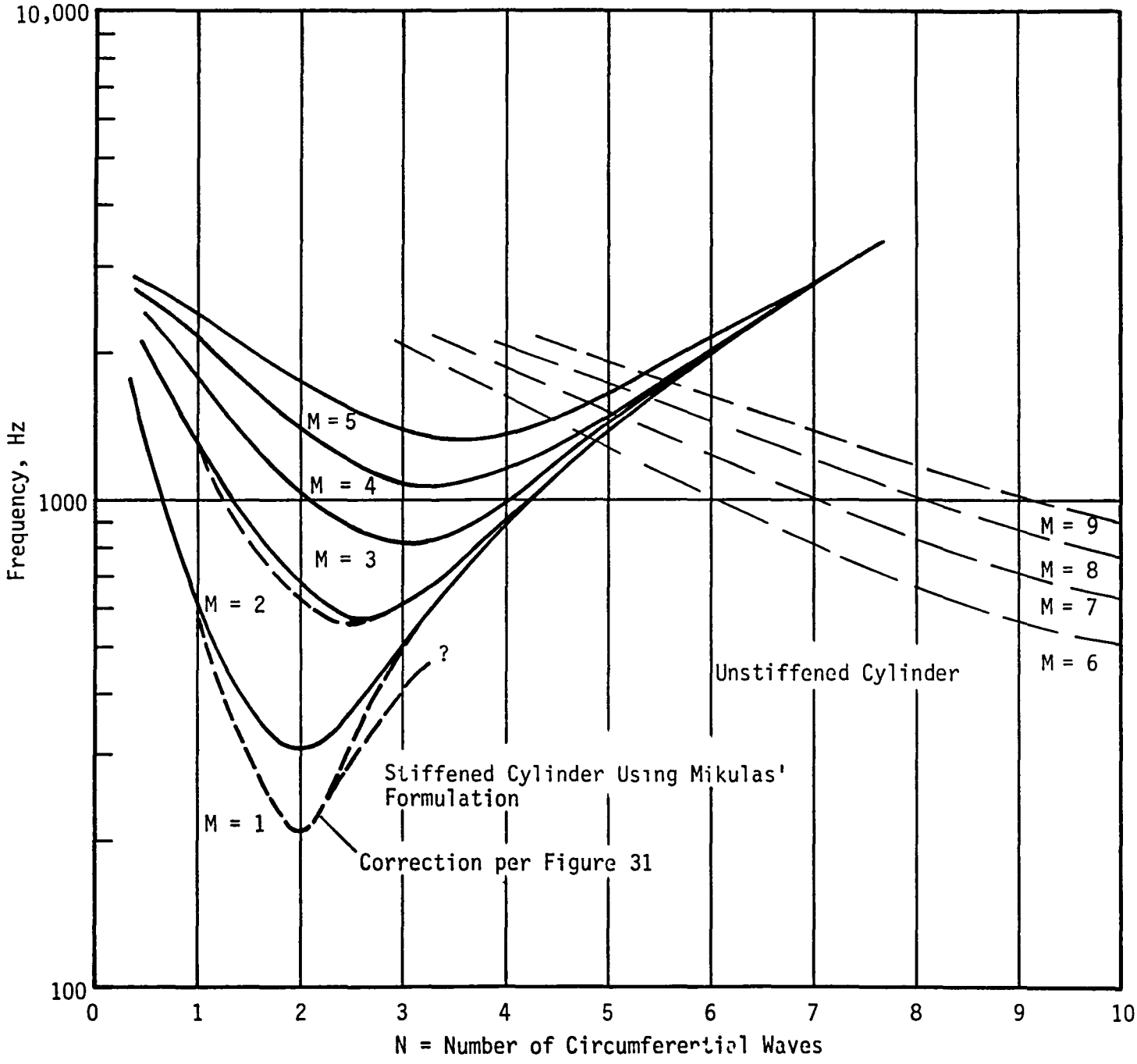

FIGURE 30. MODES OF THE STIFFENED CYLINDER COMPUTED WITH THE MIKULAS AND McELMAN EQUATION

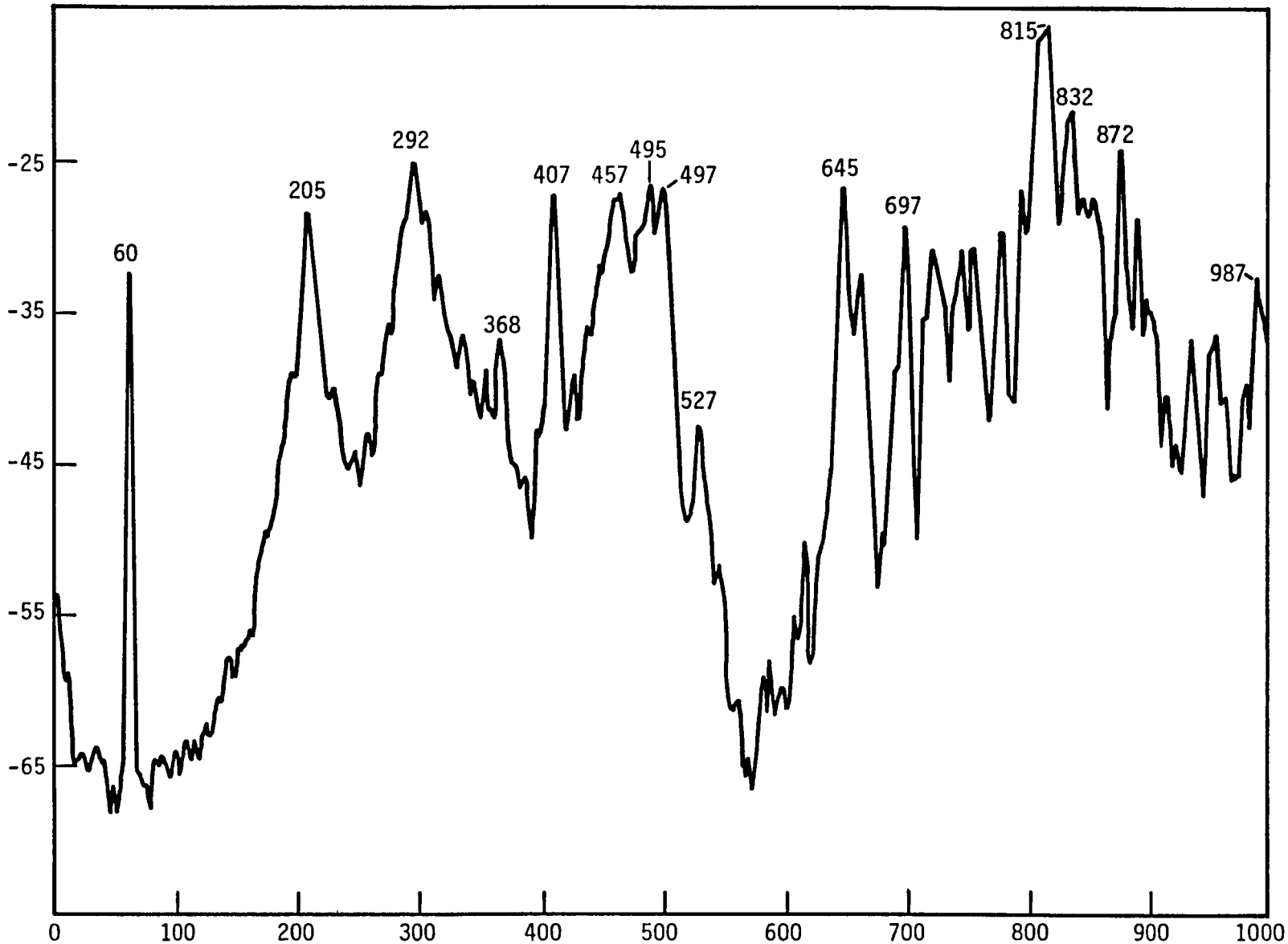

FIGURE 31. RESPONSE OF THE CYLINDER SKIN TO BROAD BAND SHAKER INPUT

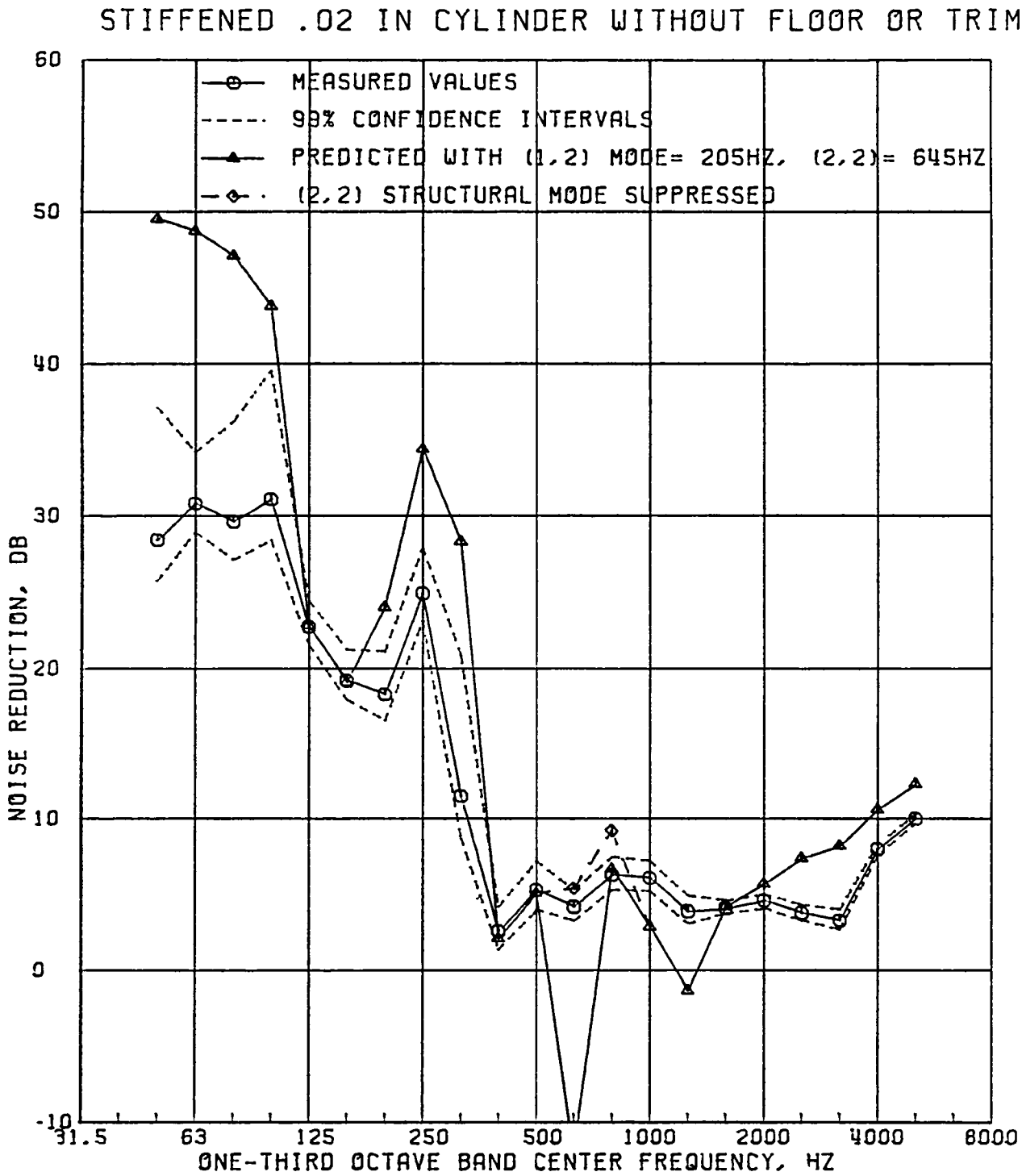

FIGURE 32. COMPARISON OF PREDICTED AND MEASURED NOISE REDUCTIONS, 0.02 IN. STIFFENED CYLINDER WITHOUT FLOOR OR TRIM

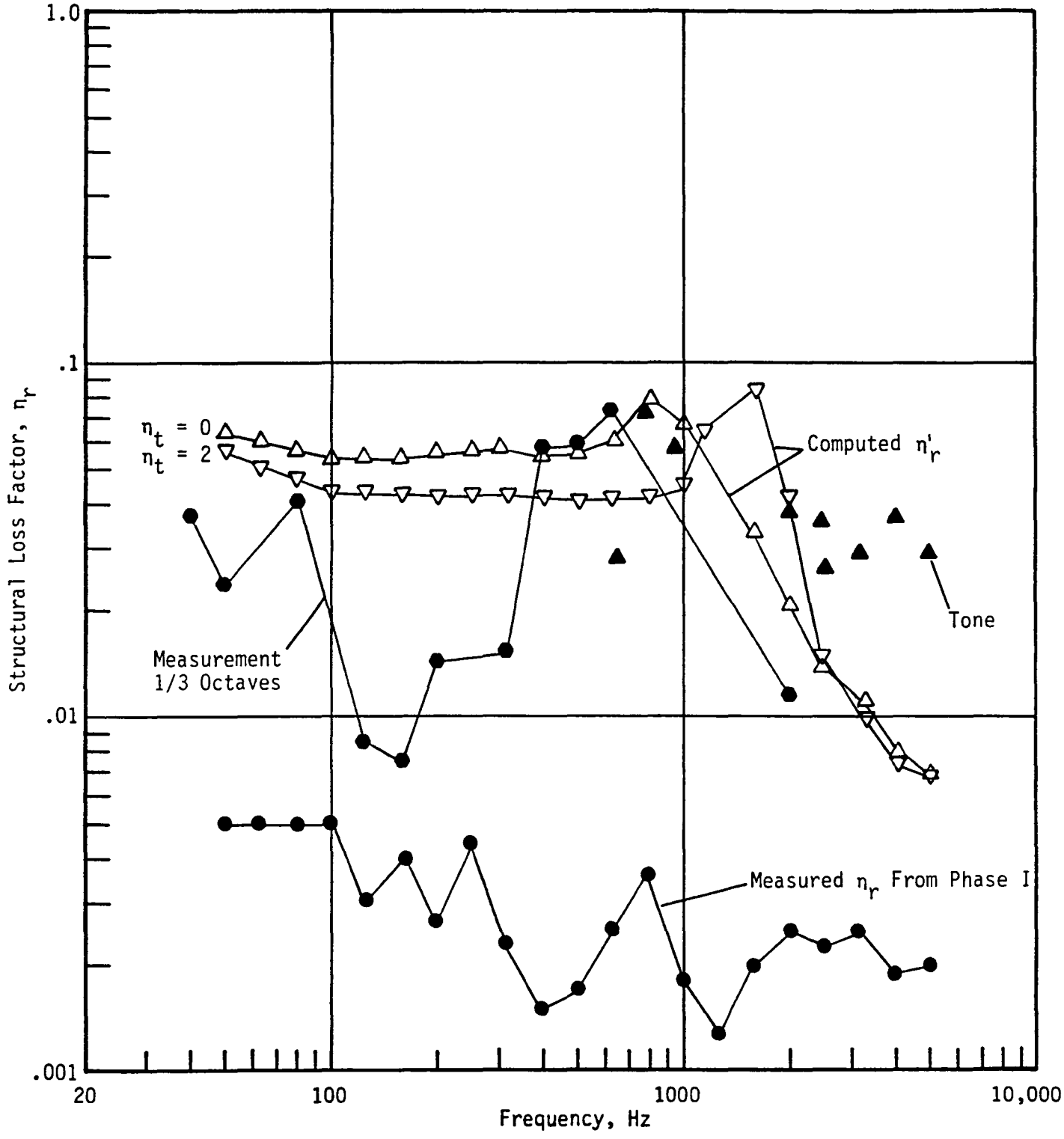

FIGURE 33. STRUCTURAL LOSS FACTORS OF THE UNSTIFFENED CYLINDER WITH FLOOR AND INSULATION

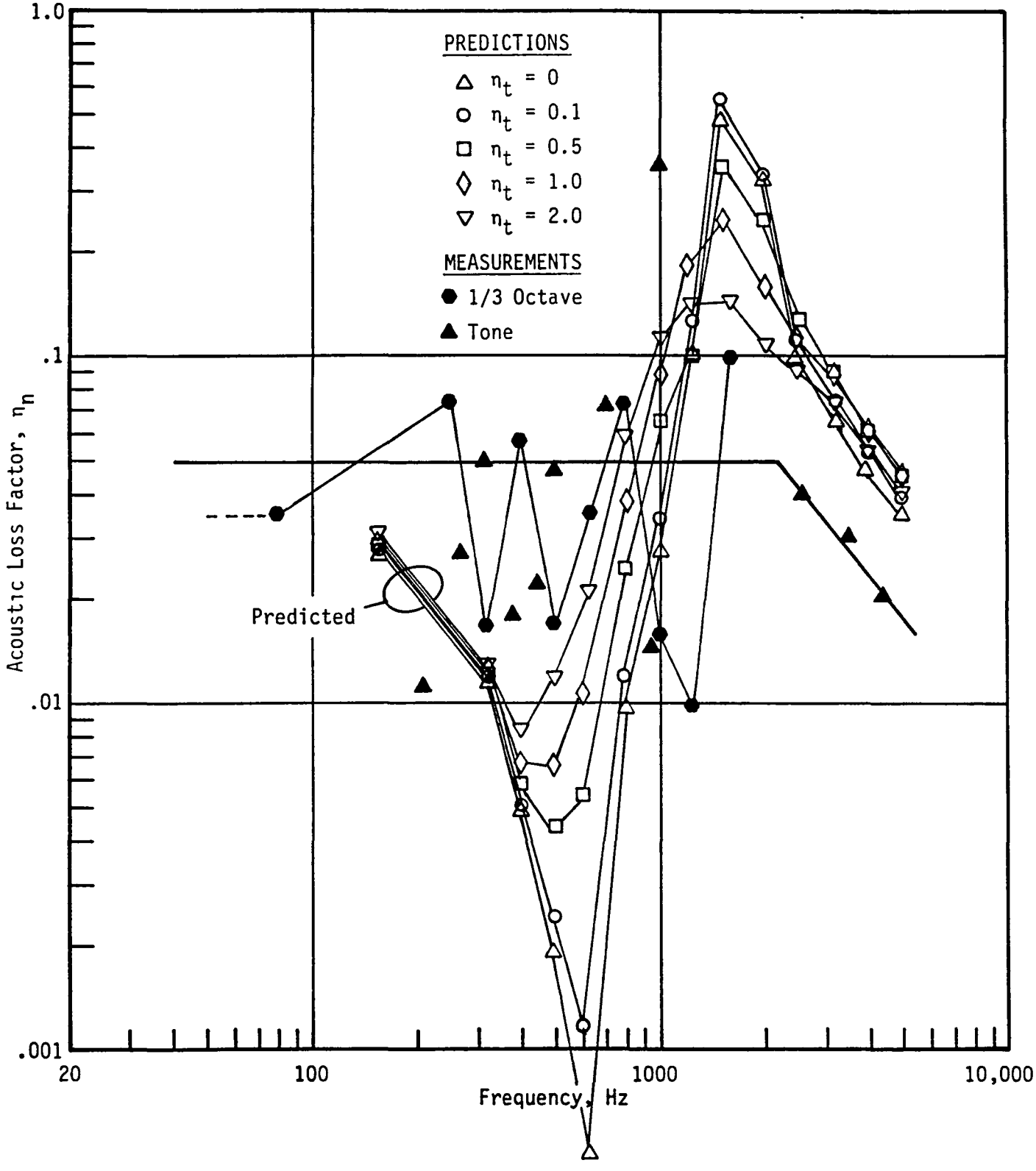

FIGURE 34. ACOUSTIC LOSS FACTORS OF THE UNSTIFFENED CYLINDER WITH FLOOR AND INSULATION

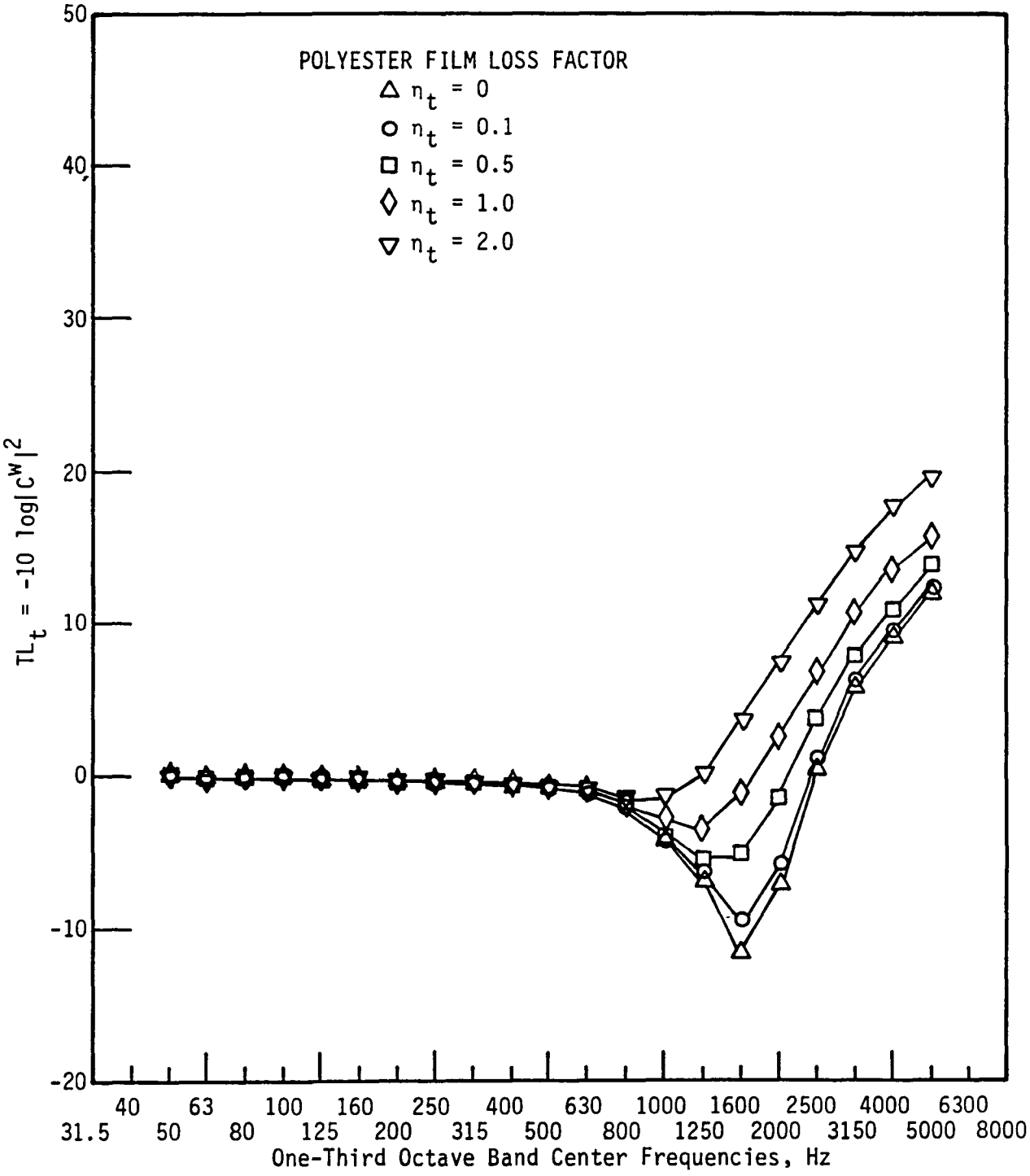

FIGURE 35. TRIM TRANSFER COEFFICIENT FOR THE UNSTIFFENED CYLINDER WITH FLOOR AND INSULATION

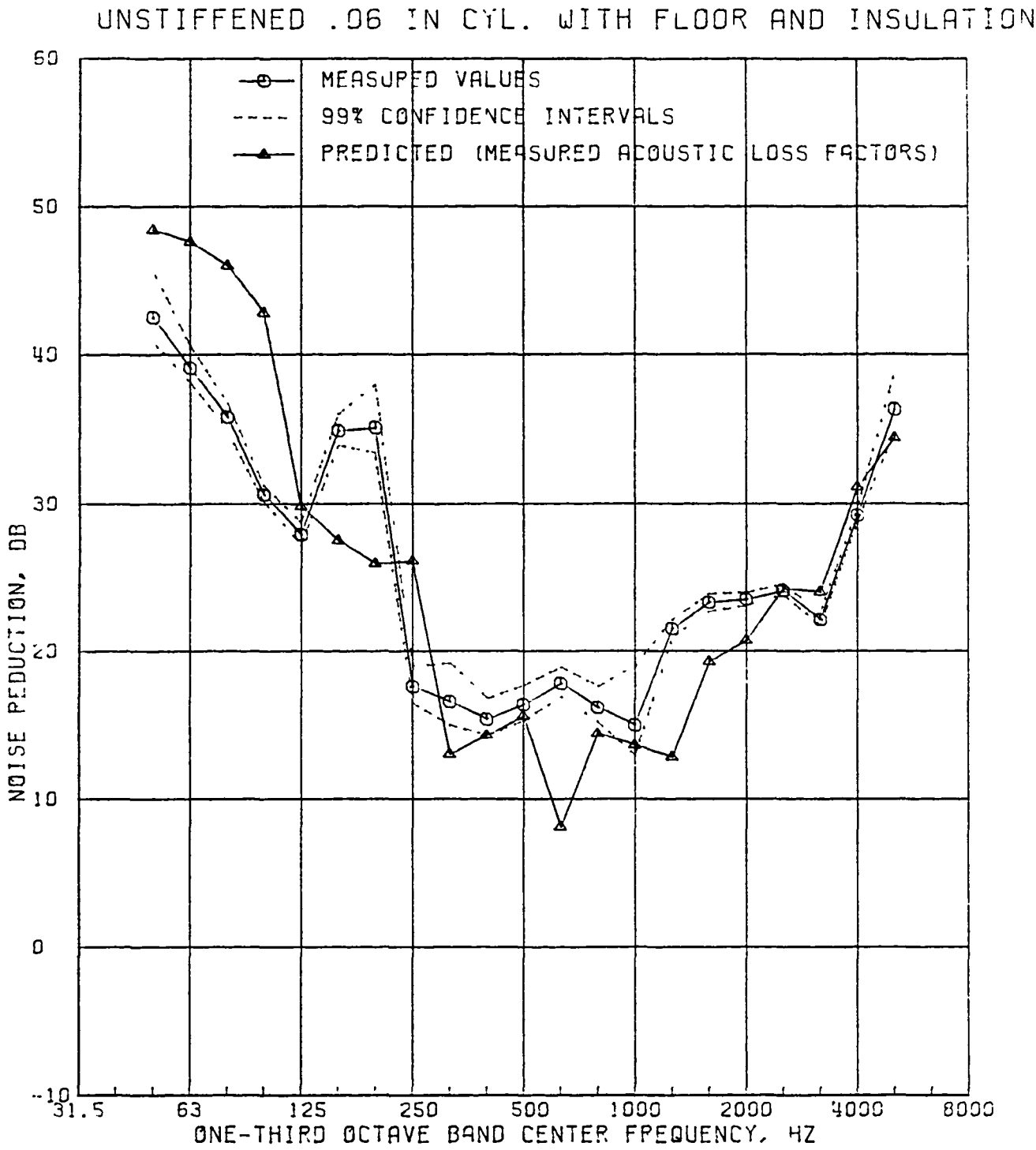

FIGURE 36. COMPARISON OF PREDICTED AND MEASURED NOISE REDUCTIONS, 0.063 IN. UNSTIFFENED CYLINDER WITH FLOOR AND INSULATION

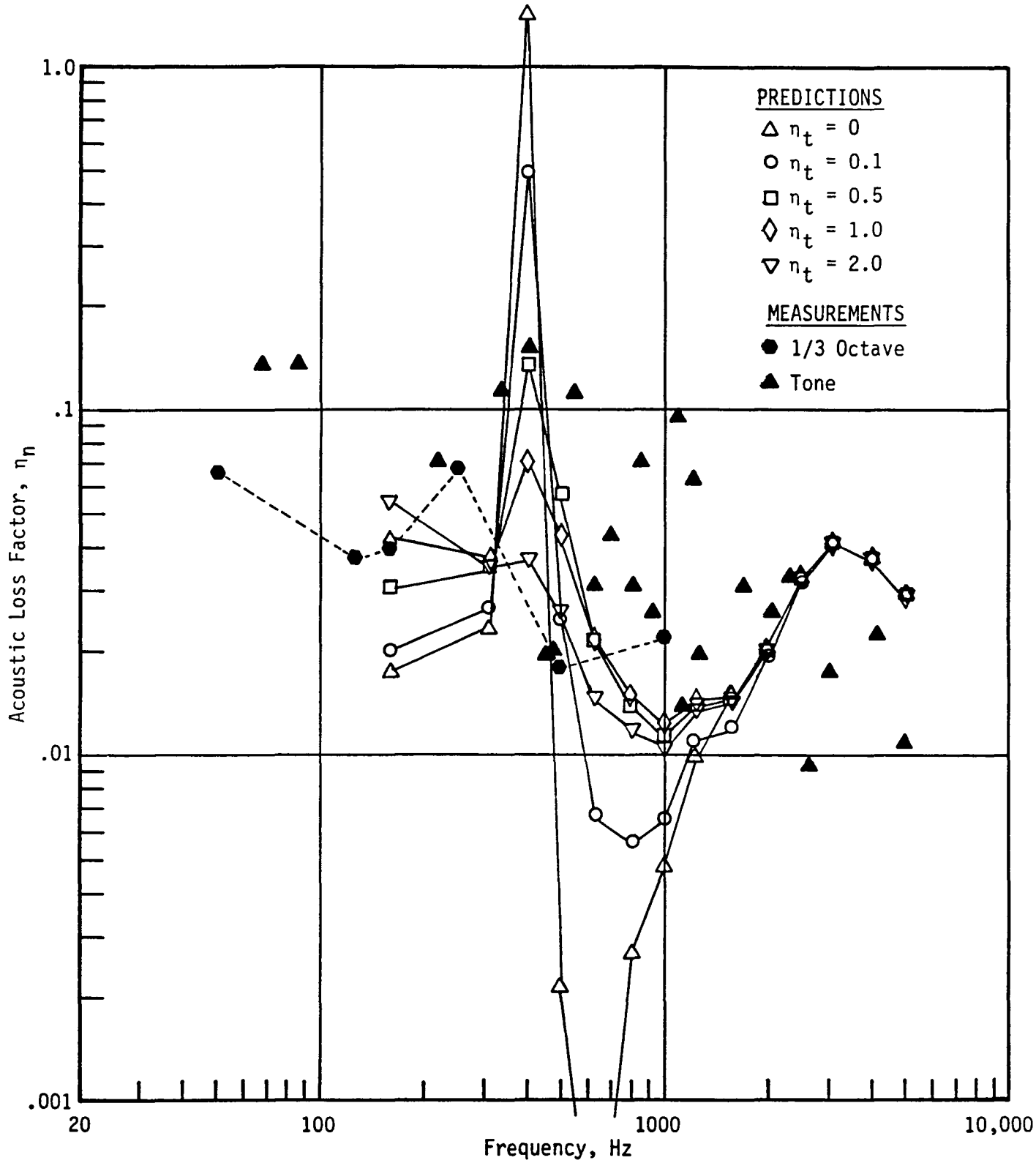

FIGURE 37. ACOUSTIC LOSS FACTORS OF THE STIFFENED CYLINDER WITH FLOOR AND TRIM

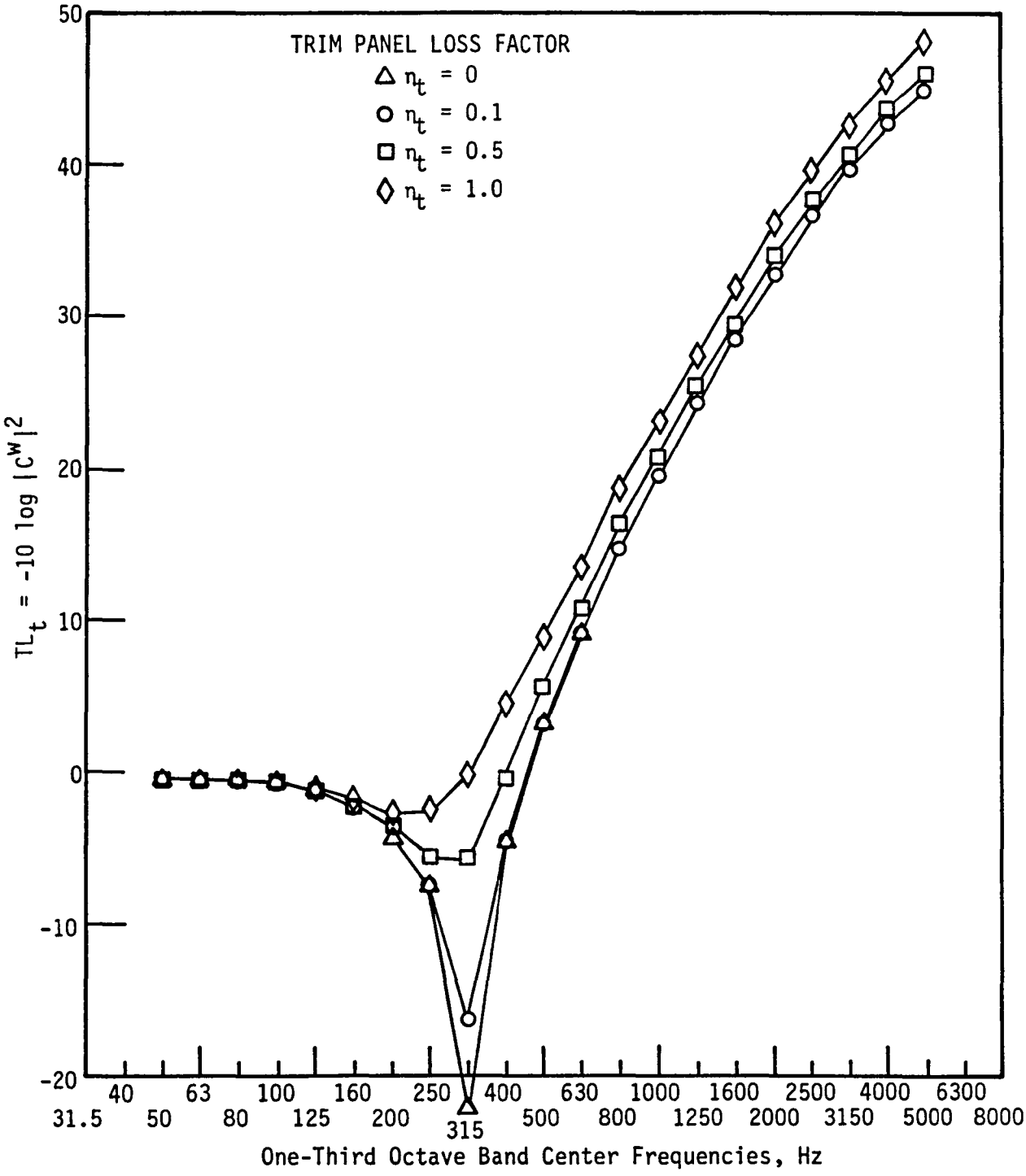

FIGURE 38. TRANSFER COEFFICIENT FOR THE STIFFENED CYLINDER WITH FLOOR AND TRIM

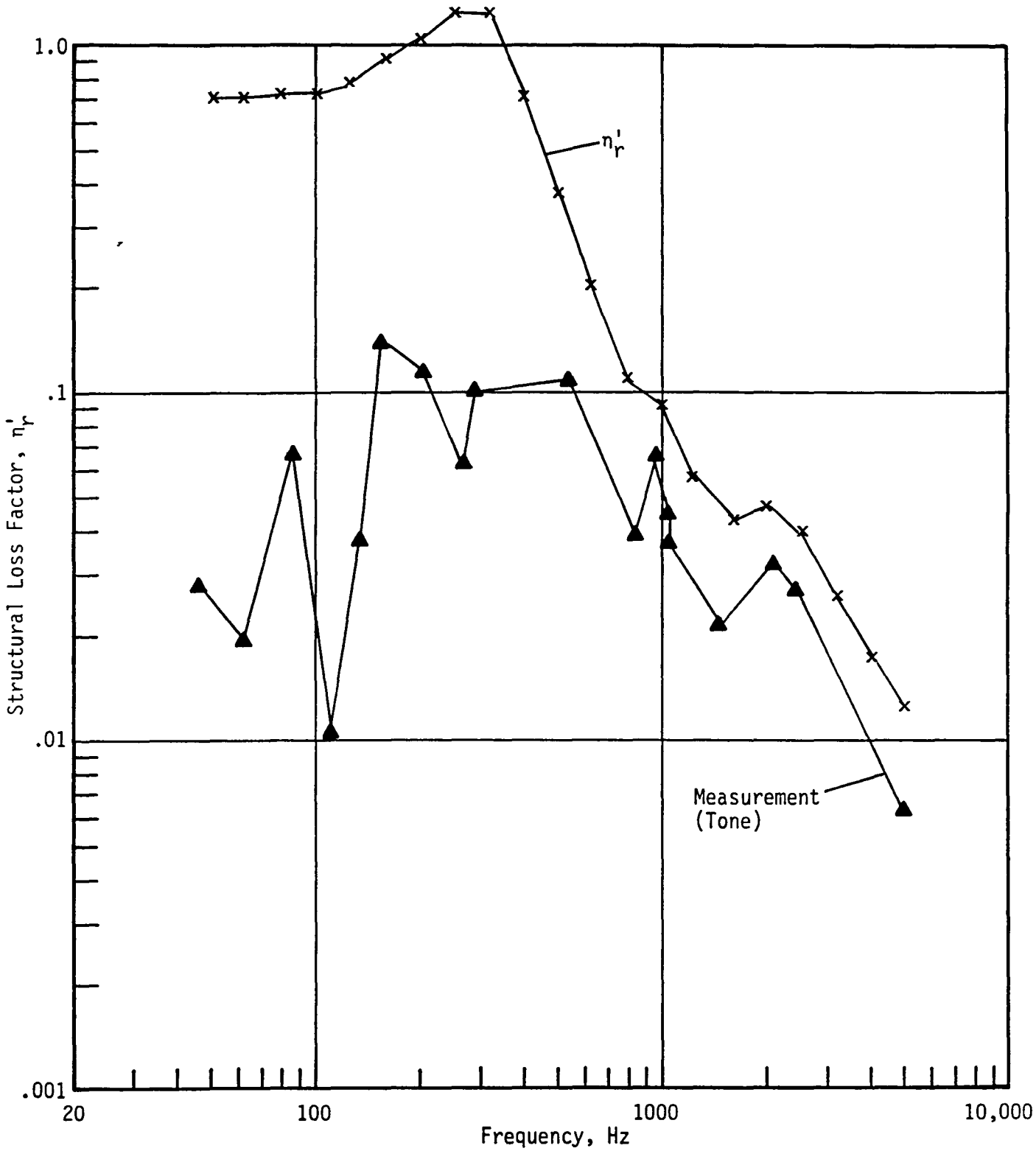

FIGURE 39. STRUCTURAL LOSS FACTORS FOR THE STIFFENED CYLINDER WITH FLOOR AND TRIM

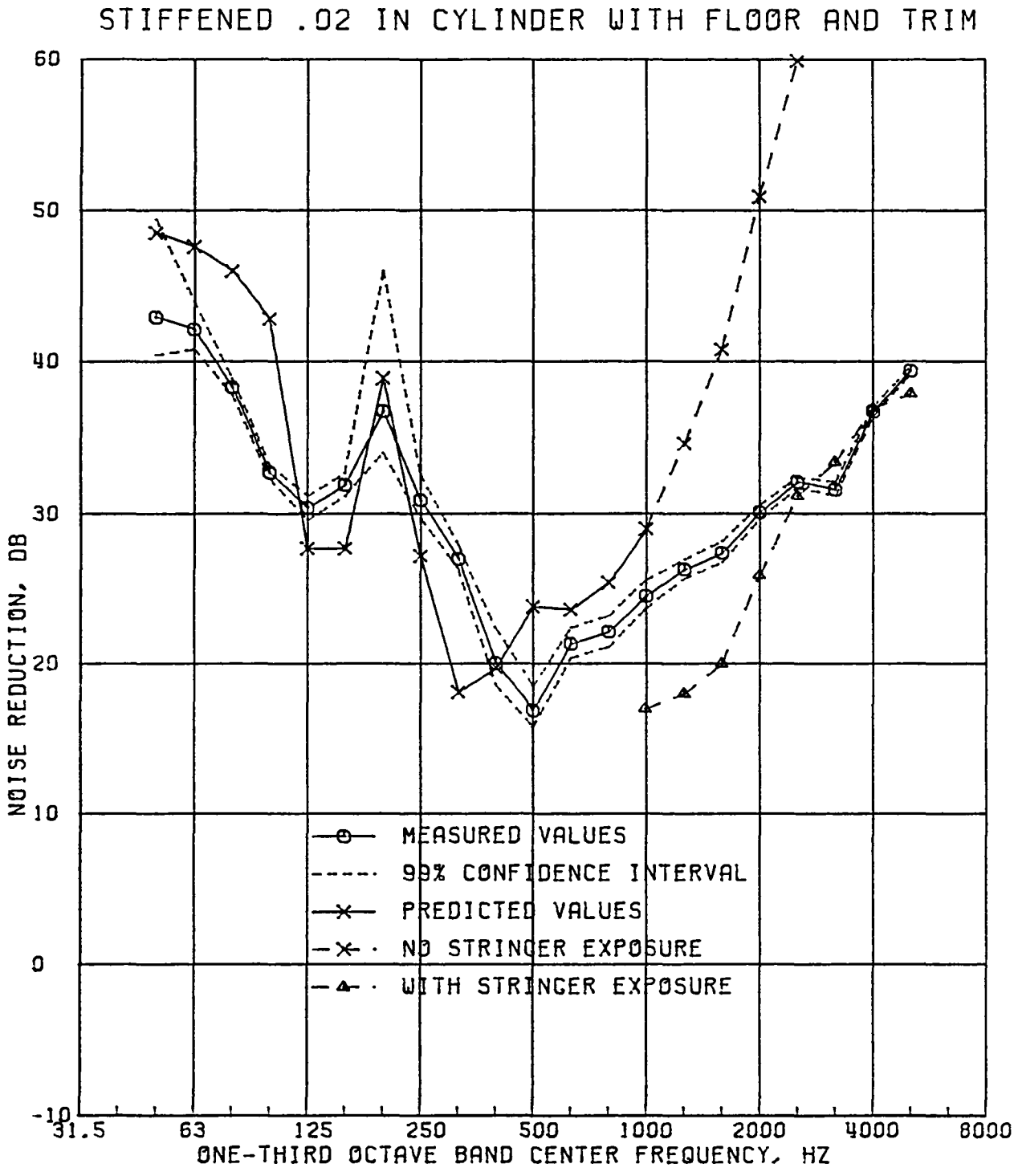

FIGURE 40. COMPARISON OF PREDICTED AND MEASURED NOISE REDUCTIONS, 0.020 IN. STIFFENED CYLINDER WITH FLOOR AND TRIM (STRINGERS EXPOSED)

NASA Contractor Report 165869

Distribution List
NAS1-15782

	No. Copies
NASA Langley Research Center Hampton, VA 23665 Attn: Report and Manuscript Control Office, Mail Stop 180A	1
Technology Utilization Office, Mail Stop 139A	1
William H. Mayes, Mail Stop 463	20
NASA Ames Research Center Moffett Field, CA 94035 Attn: Library, Mail Stop 202-3	1
NASA Dryden Flight Research Center P.O. Box 273 Edwards, CA 93523 Attn: Library	1
NASA Goddard Space Flight Center Greenbelt, MD 20771 Attn: Library	1
NASA Lyndon B. Johnson Space Center 2101 Webster Seabrook Road Houston, TX 77058 Attn: JM5/Library	1
NASA Marshall Space Flight Center Marshall Space Flight Center, AL 35812 Attn: Library, AS61L	1
Jet Propulsion Laboratory 4800 Oak Grove Drive Pasadena, CA 91103 Attn: Library, Mail Code 111-113	1
NASA Lewis Research Center 21000 Brookpark Road Cleveland, OH 44135 Attn: Library, Mail Stop	1
NASA John F. Kennedy Space Center Kennedy Space Center, FL 32899 Attn: Library, NWSI-D	1
National Aeroanutics and Space Administration Washington, DC 20546 Attn: RTE-6	1

	No. Copies
Dr. Rimas Vaicaitis Columbia University Dept. of Civil Engineering and Engineering Mechanics New York, NY 10027	1
Prof. Earl H. Dowell 2 Aero Lab School of Eng. & Applied Science Dept. of Aerospace Mechanical Science James Forestal Campus Princeton, NJ 08540	1
Dr. Frank D. Hart North Carolina State University Director, Center for Acoustical Studies Box 5801 Raleigh, NC 27607	1
Dr. Malcolm Crocker Purdue University The Ray W. Herrick Laboratories West Lafayette, IN 47907	1
Dr. Jan Roskam Dept. of Aerospace Engineering University of Kansas Lawrence, KA 66044	1
Dr. James Unruh Southwest Research Inst. 8500 Culebra Road San Antonio, TX 78284	1
Dr. Jim D. Revell Dept. 75-40 Bldg. 63 Lockheed-California Company P.O. Box 551 Burbank, CA 91520	1
Mr. Robert E. Pendley Douglas Aircraft Company Dept. 251 Mail Code 123-11 3855 Lakewood Boulevard Long Beach, CA 90846	1
Jack V. O'Keefe Acoustics Group Boeing Commercial Airplane Company P. O. Box 3707 Seattle, WA 98124	1

	No. Copies
NASA Scientific and Technical Information Facility 6571 Elkridge Landing Road Linthicum Heights, MD 21090	30 plus original

1 Report No	2 Government Accession No	3 Recipient's Catalog No
NASA CR-165869		

4 Title and Subtitle	5 Report Date
Analytical Prediction of the Interior Noise for Cylindrical Models of Aircraft Fuselages for Prescribed Exterior Noise Fields - Phase II (see 15. Supplem. Notes)	April 1982
	6 Performing Organization Code
7 Author(s) L. D. Pope and E. G. Wilby	8 Performing Organization Report No 4739
	10 Work Unit No
9 Performing Organization Name and Address Bolt Beranek and Newman Inc. 21120 Vanowen Street Canoga Park, CA 91303	11 Contract or Grant No NAS1-15782
	13 Type of Report and Period Covered Contractor Report
12 Sponsoring Agency Name and Address National Aeronautics and Space Administration Langley Research Center Hampton, Virginia 23665	14 Sponsoring Agency Code

15 Supplementary Notes
Langley Technical Representative of Contracting Office: William H. Mayes
BBN Program Manager: Larry D. Pope
Phase II - Models for Sidewall Trim, Stiffened Structures, and Cabin Acoustics with Floor Partition

16 Abstract

As a part of a NASA Langley Research Center Program to determine the important parameters associated with sound transmission into the interiors of airplanes, and to identify appropriate noise control methods, an airplane interior noise prediction model is being developed. In Phase II, models for sidewall trim, stiffened structures, and cabin acoustics with floor partition are developed. Validation studies are undertaken using three test articles: (1) a ring-stringer stiffened cylinder, (2) an unstiffened cylinder with floor partition, and (3) a ring-stringer stiffened cylinder with floor partition and sidewall trim. The noise reductions of the three test articles are computed using the theoretical models developed in Phases I and II and compared to measured values. A statistical analysis of the comparison data indicates that there is no bias in the predictions although a substantial random error exists so that a discrepancy of more than 5 or 6 dB can be expected for about one out of three predictions. It is felt that this error is the result of inadequate input data for the model.

17 Key Words (Suggested by Author(s))	18 Distribution Statement
Aircraft Interior Noise Cylinder Noise Reduction Acoustic Power Flow	Unclassified - Unlimited

19 Security Classif (of this report)	20 Security Classif (of this page)	21. No of Pages	22 Price
Unclassified	Unclassified	205	

N-305

For sale by the National Technical Information Service, Springfield, Virginia 22161

End of Document